UPPSALA
UNIVERSITET

Digital Comprehensive Summaries of Uppsala Dissertations from the Faculty of Science and Technology 952

Maximal Unitarity at Two Loops

A New Method for Computing Two-Loop Scattering Amplitudes

KASPER J. LARSEN

ACTA
UNIVERSITATIS
UPSALIENSIS
UPPSALA
2012

ISSN 1651-6214
ISBN 978-91-554-8423-1
urn:nbn:se:uu:diva-179203

Dissertation presented at Uppsala University to be publicly examined in Å2001, Ångströmlaboratoriet, Lägerhyddsvägen 1, Uppsala, Friday, September 21, 2012 at 09:15 for the degree of Doctor of Philosophy. The examination will be conducted in English.

Abstract

Larsen, K. J. 2012. Maximal Unitarity at Two Loops: A New Method for Computing Two-Loop Scattering Amplitudes. Acta Universitatis Upsaliensis. *Digital Comprehensive Summaries of Uppsala Dissertations from the Faculty of Science and Technology* 952. 135 pp. ISBN 978-91-554-8423-1.

The study of scattering amplitudes beyond one loop is necessary for precision phenomenology for the Large Hadron Collider and may also provide deeper insights into the theoretical foundations of quantum field theory. In this thesis we develop a new method for computing two-loop amplitudes, based on unitarity rather than Feynman diagrams. In this approach, the two-loop amplitude is first expanded in a linearly independent basis of integrals. The process dependence thereby resides in the coefficients of the integrals. These expansion coefficients are then the object of calculation.

Our main results include explicit formulas for a subset of the integral coefficients, expressing them as products of tree-level amplitudes integrated over specific contours in the complex plane. We give a general selection principle for determining these contours. This principle is then applied to obtain the coefficients of integrals with the topology of a double box. We show that, for four-particle scattering, each double-box integral in the two-loop basis is associated with a uniquely defined complex contour, referred to as its master contour. We provide a classification of the solutions to setting all propagators of the general double-box integral on-shell. Depending on the number of external momenta at the vertices of the graph, these solutions are given as a chain of pointwise intersecting Riemann spheres, or a torus. This classification is needed to define master contours for amplitudes with arbitrary multiplicities.

We point out that a basis of two-loop integrals with as many infrared finite elements as possible allows substantial technical simplications, in terms of obtaining the coefficients of the integrals, as well as for the analytic evaluation of the integrals themselves. We compute two such integrals at four points, obtaining remarkably compact expressions. Finally, we provide a check on a recently developed recursion relation for the all-loop integrand of the amplitudes of $\mathcal{N}=4$ supersymmetric Yang-Mills theory, examining the two-loop six-gluon MHV amplitude and finding agreement. The validity of the approach to two-loop amplitudes developed in this thesis extends to all four-dimensional gauge theories, in particular QCD. The approach is suited for obtaining compact analytical expressions as well as for numerical implementations.

Keywords: Amplitudes, NNLO calculations, Quantum Chromodynamics, Unitarity

Kasper J. Larsen, Uppsala University, Department of Physics and Astronomy, Box 516, SE-751 20 Uppsala, Sweden
and Institut de Physique Théorique, CEA-Saclay, F-91191 Gif-sur-Yvette cedex, France

ISSN 1651-6214
ISBN 978-91-554-8423-1
urn:nbn:se:uu:diva-179203 (http://urn.kb.se/resolve?urn=urn:nbn:se:uu:diva-179203)

"One of the most remarkable discoveries in elementary particle physics has been that of the existence of the complex plane."

Julian Schwinger

List of papers

This thesis is based on the following papers, which are referred to in the text by their Roman numerals.

I D. A. Kosower and K. J. Larsen, *Maximal Unitarity at Two Loops*, *Phys. Rev.* **D85** (2012) 045017, [arXiv:1108.1180].

II K. J. Larsen, *Global Poles of the Two-Loop Six-Point $\mathcal{N} = 4$ SYM integrand*, arXiv:1205.0297. [Accepted by Phys. Rev. D]

III S. Caron-Huot and K. J. Larsen, *Uniqueness of Two-Loop Master Contours*, arXiv:1205.0801. [Submitted to JHEP]

IV H. Johansson, D. A. Kosower and K. J. Larsen, *Two-Loop Maximal Unitarity with External Masses*, arXiv:1208.1754.

Reprints were made with permission from the publishers.

Contents

1. Introduction

With the announced finding on July 4, 2012 of a Higgs-boson-like particle with a mass around 125-126 GeV by the ATLAS and CMS collaborations [1, 2], these are truly exciting times to be working in particle physics. No less tantalizing are the possible hints of new physics suggested by the excess of di-photon Higgs-candidate decays observed by both groups.

At least until very recently, the Standard Model of particle physics has been an extremely successful theory, accounting for all observed phenomena in particle collider experiments. It dictates that all matter is composed of quarks (the building blocks of protons and neutrons) and leptons (such as electrons and neutrinos) which can interact through three fundamental forces: the electromagnetic, the weak and the strong interactions. The laws of these interactions are governed by two quantum gauge theories, the electroweak theory and quantum chromodynamics.

The electroweak theory describes the electromagnetic and weak force in a unified way. It has an $SU(2) \times U(1)$ gauge symmetry which is associated with four particles $\gamma, W^{\pm}, Z^0$ that mediate the electroweak force during interactions of elementary particles. At energies below a scale of around 250 GeV, the $SU(2) \times U(1)$ gauge symmetry is spontaneously broken to a $U(1)$ subgroup through the Higgs-mechanism, giving masses to the carriers of the weak force $W^{\pm}, Z^0$, whereas the photon γ, mediating the electromagnetic force, remains massless. The Higgs-mechanism, in addition, gives masses to all elementary particles.

Quantum chromodynamics (QCD) is the theory of interactions between the constituents of protons and neutrons, namely the quarks. The interactions are mediated through the exchange of eight different particles called gluons g which are associated with the gauge group $SU(3)$. Unlike photons, the gluons interact among themselves, leading to the curious phenomenon that as one attempts to pull the quarks in a proton away from each other, the strength of their mutual attraction rapidly increases, keeping them permanently confined within a radius of about 10^{-15} m.

Despite its successes, it is clear that the Standard Model cannot be a complete theory of particle physics. Indeed, discrepancies between the observed velocities of stars in galactic orbit and those predicted by the directly observable matter points to the existence of unobserved dark matter, estimated to constitute 84% of the matter of the universe. As none of the particles of the Standard Model are viable dark matter candidates, some extension of the model is clearly necessary.

A more speculative, but nonetheless very attractive idea is that of grand unification in which the theories of electroweak and strong interactions at some appropriate energy scale become parts of a grand unified theory (GUT) with a larger gauge group, for example $SU(5)$. The breaking of this enhanced gauge symmetry down to the $SU(3) \times SU(2) \times U(1)$ gauge symmetry of the Standard Model is believed to be similar to the Higgs-mechanism. Beyond the elegance of accounting for all fundamental interactions in a single unified theory, the $SU(5)$ GUT consistently explains the fractional electric charges of the quarks in terms of their charge under the $SU(3)$ gauge group: in a nutshell, quarks carry $1/3$ of the lepton charge because they have three colors. GUT theories may also be able to explain the smallness of neutrino masses through the seesaw-mechanism. Nevertheless, unification of the electromagnetic, weak and strong couplings is only close, but not exact, within the Standard Model itself.

A particularly elegant scenario is offered by supersymmetric extensions of the Standard Model. Such extensions contain dark matter candidates, achieve grand unification and stabilize the Higgs mass against large radiative corrections. Moreover, supersymmetry (SUSY) seems an important ingredient in finite theories of quantum gravity. A particular paradigm of supersymmetric model building which does not appear to be under pressure by current LHC data is that of split supersymmetry. Here, the SUSY breaking scale is high, around the GUT scale of 10^{16} GeV, and all supersymmetric scalars are ultraheavy. This naturally suppresses unwanted side effects such as proton decay and flavor-changing neutral currents which would be mediated by these scalars. On the other hand, the supersymmetric fermions can remain light, protected by chiral symmetry. Among these fermions, the lightest electrically neutral ones may be dark matter candidates whereas the lightest electrically charged ones may couple to the final-state photons in the Higgs decay, enhancing the rate. A recent analysis [3] shows that if the diphoton excess survives further scrutiny, split SUSY requires the existence of a new charged fermion around 115-150 GeV.

Although many of the above ideas may turn out to have nothing to do with nature, we outlined them here to suggest that new physics may well be within the reach of the LHC. Thus, the purpose of the Large Hadron Collider is twofold. One, which at the time of writing seems very likely to have been fulfilled, is the discovery of the Higgs boson. The other is (hopefully) the discovery of new physics beyond that of the Standard Model.

The LHC is a hadron collider. This in turn means that there is a large QCD background present in the experiments, accounting for more than 99% of the events. Identifying signal processes therefore requires a quantitative understanding of the background which must first in a sense be subtracted from the collected data. Figure 1.1 below illustrates a typical example of a signal process and a background process.

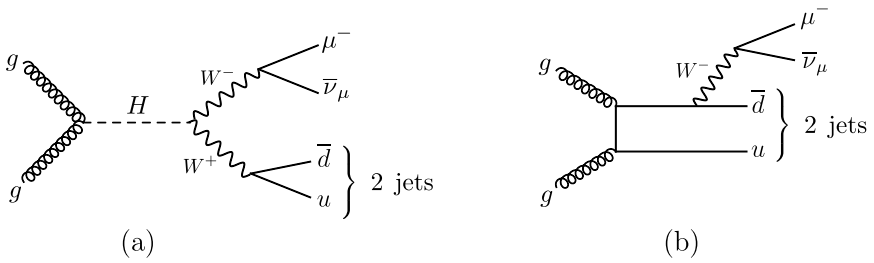

Figure 1.1. An example of (a) a signal process and (b) a background process.

In precise terms, an understanding of the QCD background amounts to the knowledge of the cross-sections of all relevant Standard Model processes to some sufficiently high precision. An important ingredient, but by no means the only one, needed for computing cross-sections are the scattering amplitudes of processes.

Traditionally, scattering amplitudes have been computed by means of Feynman diagrams, and very impressive calculations have been performed by their use. Nevertheless, this approach inevitably runs out of steam at some point, owing to the explosive growth of the number and complexity of the Feynman diagrams contributing to the amplitudes. Efficient methods for computing tree-level amplitudes have emerged more recently, including most notably the BCFW-recursion relations [4].

More powerful methods for calculating loop-level amplitudes were developed in the mid-1990's exploiting the unitarity of the S-matrix along with an ansatz for one-loop amplitudes involving simpler integrals than those appearing in Feynman diagram calculations. Exploiting the analytic structure of the loop-integrand it is then possible to determine the coefficients of these integrals in terms of tree-level amplitudes. This approach is known as the unitarity method. It has proven very successful at one loop where it has rendered a number of amplitude calculations possible, in particular of processes with many partons in the final state. One-loop unitarity also exists in an even more recent form, called generalized unitarity. Here the analytic structure of the loop-integrand is probed by a larger number of on-shell constraints, leading to formulas of the integral coefficients in terms of tree amplitudes without the need for performing algebra at intermediate stages.

The subject of this thesis is the development of a systematic approach for computing two-loop amplitudes based on generalized unitarity. Such an extension of the unitarity method is necessary for an efficient numerical implementation, but it is very likely that such a formalism will also produce extremely compact analytical results for scattering amplitudes, obtained in a simple and straightforward way. It should be emphasized that generalized unitarity has certainly

been applied beyond one loop, primarily in the calculation of amplitudes of $\mathcal{N} = 4$ supersymmetric Yang-Mills (SYM) theory and $\mathcal{N} = 8$ supergravity. However, the first step in these calculations is to construct a suitable ansatz for the amplitude of interest in terms of a craftily chosen set of integrals. It is therefore fair to say that no *systematized* use of generalized unitarity exists beyond one loop.

Two-loop amplitudes are needed for quantitative estimates of the QCD background at the LHC. For example, there are processes (such as $gg \to \gamma\gamma$ and $gg \to W^+W^-$) whose amplitudes start at one loop, and whose differential cross sections therefore begin not at $\mathcal{O}(\alpha_s^0)$ but rather at $\mathcal{O}(\alpha_s^2)$. The next-to-leading order (NLO) cross section therefore receives contributions from the interference of one- and two-loop amplitudes. (The process $gg \to \gamma\gamma$ is effectively NLO as the suppression from the extra powers of α_s compared to $q\bar{q} \to \gamma\gamma$ are roughly compensated by the large density of gluons at small x.) Moreover, any calculation at NNLO will require two-loop amplitudes as input. The practical uses of NNLO calculations involve providing theory for precision measurements (beyond the processes $e^+e^- \to 3$ jets, $gg \to H$ and W, Z production, which have already been computed), providing uncertainty estimates on NLO calculations, and further reducing the dependence on the choice of renormalization scale in, for example, $gg \to W + n$ jets.

Although outside of the main focus of this thesis, it is worth mentioning that the past 8-9 years have witnessed astounding progress in $\mathcal{N} = 4$ SYM amplitudes, uncovering dualities with Wilson loops and correlators of local operators; an integrable structure leading to an all-loop solution; and an all-loop recursion relation for the integrand à la BCFW. No less spectacular is a reformulation of the theory's S-matrix as a contour integral on a Grassmannian manifold, allowing a notion of particle scattering without manifest spacetime. The hope raised by some of these advances is that the study of scattering amplitudes may ultimately teach us something fundamental about quantum field theory, or even spacetime itself.

This thesis is organized as follows. In Chapter 2 we give a pedagogical introduction to unitarity at one loop, explaining its origin in the analytic S-matrix program of the 1960's, its modern revival in the 1990's and finally its present-day incarnation in the form of generalized unitarity. In Chapter 3 we take the first steps in developing a systematic extension of generalized unitarity to two loops. In this approach, the two-loop amplitude is expanded in a basis of integrals. The expansion coefficents are obtained by integrating products of tree amplitudes along contours in the complex plane. We give a selection principle for determining contours that are guaranteed to produce correct results for amplitudes in any gauge theory, including QCD. In Chapter 4 we explain how the double-box integrals in the two-loop integral basis are each associated with a uniquely defined contour producing their coefficient. In Chapter 5 we identify a class of basis integrals which are likely to simplify unitarity calcula-

tions substantially at two loops, and moreover analytically evaluate two such integrals at four points. Chapter 6 falls somewhat outside the mainstream of purpose and method in this thesis. Here we provide a check on a recently developed BCFW-like recursion relation [5, 6] for the integrand of $\mathcal{N} = 4$ SYM amplitudes, investigating the two-loop six-gluon maximally helicity violating (MHV) integrand. In Chapter 7 we give our conclusions and suggest many open directions of future research. In Appendix A we specify conventions and notation used throughout the thesis.

2. One-loop unitarity

In this chapter we give a pedagogical review of the unitarity method at one loop, a modern alternative to the more traditional Feynman-diagrammatic approach to scattering amplitudes. We follow the development of this method through its rise and fall with the analytic S-matrix program in the 1960's into its modern revival in the 1990's by Bern, Dixon and Kosower, culminating in its present-day form known as generalized unitarity.

2.1 Unitarity in the 1960's

2.1.1 Unitarity of the S-matrix

The basic process in a particle collider is one where a number of particles approach each other from a macroscopic distance and collide in a microscopic interaction region, after which the products of the interaction travel out to a macroscopic distance. The probability amplitude for the transition from some initial state $|\Psi_\alpha^+\rangle$ (characterized by spins, flavor, eletroweak and color charges etc.) to some final state $|\Psi_\beta^-\rangle$ is the inner product

$$S_{\alpha\beta} \equiv \langle \Psi_\alpha^+ \,|\, \Psi_\beta^- \rangle \tag{2.1}$$

which defines an element of the *S-matrix*. The S-matrix may be decomposed into two parts

$$S = \mathbf{1} + iT \tag{2.2}$$

according to the respective possibilities that the particles either pass by each other with no interactions, or interact. Factoring a momentum-conservation delta function out of the T-matrix defines the *scattering amplitude* $\mathscr{A}_{\alpha\beta}$ of the process,

$$T_{\alpha\beta} = (2\pi)^4 \delta\Big(\sum_{i\in\alpha} p_i + \sum_{i\in\beta} p_i\Big)\, \mathscr{A}_{\alpha\beta}\,. \tag{2.3}$$

Conservation of probability requires the S-matrix to be unitary. This is easily seen to be the case: for example,

$$(S^\dagger S)_{\alpha\gamma} = \int d\beta\, S^*_{\beta\alpha} S_{\beta\gamma} = \int d\beta\, \langle \Psi_\alpha^- \,|\, \Psi_\beta^+ \rangle \langle \Psi_\beta^+ \,|\, \Psi_\gamma^- \rangle = \langle \Psi_\alpha^- \,|\, \Psi_\gamma^- \rangle \tag{2.4}$$

$$= \delta(\alpha - \gamma)\,, \tag{2.5}$$

and similarly one can show that $SS^\dagger = \mathbf{1}$.

Using the decomposition in eq. (2.2), the unitarity of the S-matrix implies for the T-matrix that

$$-i(T - T^\dagger) = T^\dagger T\,. \tag{2.6}$$

As explained, for example, in Section 7.3 of ref. [7], this equation immediately implies the optical theorem. This theorem relates the imaginary part of any *forward* scattering amplitude (i.e., one in which the outgoing momenta are some permutation of the incoming momenta) to the total cross section of the process. Looking beyond forward amplitudes, in Section 2.1.2 we will see how a careful analysis of a generic one-loop Feynman diagram allows one to prove a more refined version of the optical theorem, known as the Cutkosky rules. For now, we restrict ourselves to show how eq. (2.6) relates higher-loop amplitudes to lower-loop amplitudes.

To this end, expand the T-matrix perturbatively in the coupling g,

$$T = \sum_{n=4}^{\infty} g^{n-2}\big(T_n^{(0)} + g^2 T_n^{(1)} + g^4 T_n^{(2)} + \cdots\big) \tag{2.7}$$

where $T_n^{(0)}, T_n^{(1)}, T_n^{(2)}, \ldots$ correspond to the contributions from n-point tree-level, one-loop, two-loop etc. Feynman diagrams. Inserting this expansion into eq. (2.6) one obtains, for example,

$$\text{at order } g^4\text{:} \quad -i\big(T_4^{(1)} - T_4^{(1)\dagger}\big) = T_4^{(0)\dagger} T_4^{(0)} \tag{2.8}$$

$$\text{at order } g^6\text{:} \quad -i\big(T_4^{(2)} - T_4^{(2)\dagger}\big) = T_4^{(0)\dagger} T_4^{(1)} + T_4^{(1)\dagger} T_4^{(0)} + T_5^{(0)\dagger} T_5^{(0)}\,. \tag{2.9}$$

These relations are illustrated schematically in figure 2.1. Implicit in the products of T-matrices on the right hand sides is a sum over all possible states that can propagate across the dashed vertical lines, as dictated by the Feynman rules.

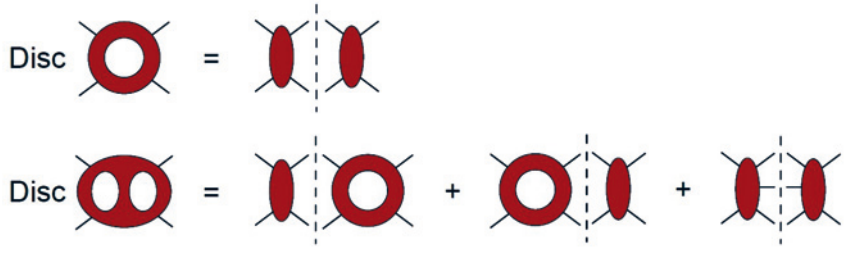

Figure 2.1. The unitarity of the S-matrix implies relations between amplitudes across loop orders, here illustrated in the case of four-particle scattering. The number of holes in a blob indicates the number of loops in the corresponding amplitude. This figure was taken from ref. [8].

2.1.2 The Cutkosky rules

The Cutkosky rules provide a quantitative statement on the relations discussed above between scattering amplitudes across loop orders. This theorem relates the discontinuity of a one-loop amplitude in any of its kinematic channels to the product of the tree-level amplitudes arising in the on-shell factorization on the channel in question.

In order to prove this theorem, let us first introduce the notation

$$K \equiv k_1 + \cdots + k_j \tag{2.10}$$

$$s \equiv K^2 \tag{2.11}$$

$$D \equiv 4 - 2\overline{\varepsilon}\,. \tag{2.12}$$

A generic Feynman diagram contributing to the one-loop amplitude is illustrated in figure 2.2.

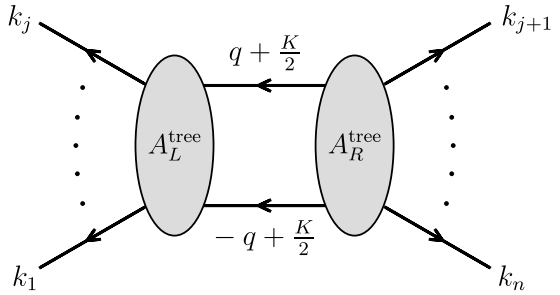

Figure 2.2. A generic one-loop Feynman diagram. The loop integrand is essentially the product of the tree-level amplitudes indicated by the gray blobs, times the two propagators bridging them.

The Feynman rules tell us that the integrand of the diagram consists of the two highlighted propagators times two factors which are essentially tree amplitudes,

$$\begin{aligned}\mathscr{M}^{(1)}(s) = \int \frac{d^D q}{(2\pi)^D} \frac{1}{\big(K/2-q\big)^2 - m_r^2 + i\varepsilon} \frac{1}{\big(K/2+q\big)^2 - m_r^2 + i\varepsilon} \\ \times \widetilde{A}_L^{\text{tree}}\big(k_1,\ldots,k_j,q+K/2\big)\widetilde{A}_R^{\text{tree}}\big(k_{j+1},\ldots,k_n,-q+K/2\big)\end{aligned} \tag{2.13}$$

keeping in mind that the states traveling along the propagators are not on-shell, hence the tildes. In the following theorem we calculate the discontinuity in the s-channel of the *diagram* illustrated in figure 2.2. However, applying eq. (2.16) below to every term in the Feynman diagram expansion of the one-loop amplitude, one arrives at the result alluded to above: the discontinuity of the amplitude equals the sum over all possible ways in which to factor the contributing one-loop diagrams into on-shell tree amplitudes.

Theorem 1 (Cutkosky rules)**.** *The s-channel discontinuity of the diagram in eq.* (2.13) *is computed by replacing the two propagators according to the rule*

$$\frac{1}{\big(K/2\pm q\big)^2-m_r^2+i\varepsilon}\longrightarrow -2\pi i\delta^{(+)}\big(\big(K/2\pm q\big)^2-m_r^2\big) \tag{2.14}$$

where

$$\delta^{(+)}(\cdots)\equiv\theta(K^0)\delta(\cdots) \tag{2.15}$$

with θ denoting the Heaviside step function. In other words, the s-channel discontinuity is given by

$$\begin{aligned}\underset{s}{\mathrm{Disc}}\,\mathscr{M}^{(1)}(s)=\int\frac{d^Dq}{(2\pi)^D}\delta^{(+)}\big(\big(K/2-q\big)^2-m_r^2\big)\delta^{(+)}\big(\big(K/2+q\big)^2-m_r^2\big)\\ \times(-2\pi i)^2A_L^{\text{tree}}\big(k_1,\ldots,k_j,q+K/2\big)A_R^{\text{tree}}\big(k_{j+1},\ldots,k_n,-q+K/2\big)\,.\end{aligned} \tag{2.16}$$

Proof. [1] It is convenient to work in the center-of-momentum frame where $K^\mu=(K^0,\mathbf{0})$. In this frame, the propagator denominators in eq. (2.13) take the form

$$\begin{aligned}\big(K/2\pm q\big)^2-m_r^2+i\varepsilon&=\big(K^0/2\pm q^0\big)^2-|\mathbf{q}|^2-m_r^2+i\varepsilon &(2.17)\\ &=\big(K^0/2\pm q^0\big)^2-(E_r-i\varepsilon)^2\,, &(2.18)\end{aligned}$$

where we redefined ε in eq. (2.18). Thus, in the center-of-momentum frame, the one-loop diagram takes the form

$$\begin{aligned}\mathscr{M}^{(1)}=\int\frac{d^3\mathbf{q}}{(2\pi)^4}\int_{-\infty}^{\infty}dq^0\frac{1}{\big(K^0/2-q^0\big)^2-(E_r-i\varepsilon)^2}\frac{1}{\big(K^0/2+q^0\big)^2-(E_r-i\varepsilon)^2}\\ \times\widetilde{A}_L^{\text{tree}}\big(k_1,\ldots,k_j,q+K/2\big)\widetilde{A}_R^{\text{tree}}\big(k_{j+1},\ldots,k_n,-q+K/2\big)\,.\end{aligned} \tag{2.19}$$

We observe that the integrand under the $\int_{-\infty}^{\infty}dq^0(\cdots)$ integral has four poles, located at the points $q^0=\frac{K^0}{2}\pm(E_r-i\varepsilon)$ and $q^0=-\frac{K^0}{2}\pm(E_r-i\varepsilon)$. Let us now perform the q^0 integration, closing the integration contour in the upper half of the complex plane, as illustrated in figure 2.3. The integral will then receive contributions from the poles at $q^0=\pm\frac{K^0}{2}-E_r+i\varepsilon$, with residues $\mathrm{Res}=-\frac{1}{2E_r}\frac{1}{K^0(K^0\mp 2E_r)}$, producing

$$\begin{aligned}\mathscr{M}^{(1)}=-2\pi i\int\frac{d^3\mathbf{q}}{(2\pi)^4}\left(\frac{1}{2E_r}\frac{1}{K^0(K^0+2E_r)}+\frac{1}{2E_r}\frac{1}{K^0(K^0-2E_r)}\right)\\ \times\widetilde{A}_L^{\text{tree}}\big(k_1,\ldots,k_j,q+K/2\big)\widetilde{A}_R^{\text{tree}}\big(k_{j+1},\ldots,k_n,-q+K/2\big)\,.\end{aligned} \tag{2.20}$$

[1] Please note that this proof is a (heavily augmented) version of that appearing in Section 7.3 of ref. [7].

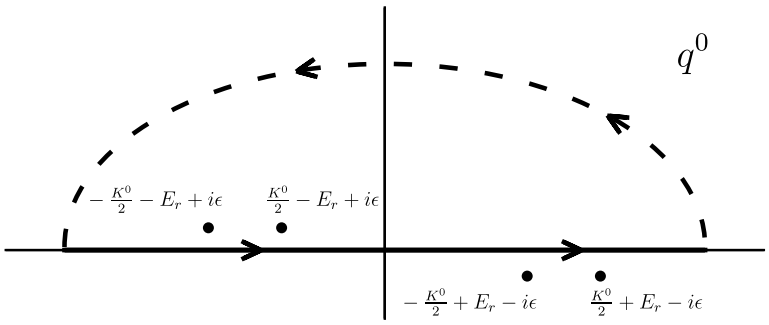

Figure 2.3. The poles of the integrand of eq. (2.19) are located slightly above and below the real axis in the q^0-plane. The integration contour is taken along the real axis and closed in the upper half of the complex plane, as indicated by the dashed semicircle.

At this point, let us pause to make an important observation: as one can directly verify, the expression in eq. (2.20) also results from making the replacement

$$\frac{1}{\big(K/2+q\big)^2-m_r^2+i\varepsilon}\longrightarrow -2\pi i\delta^{(+)}\big(\big(K/2+q\big)^2-m_r^2\big) \tag{2.21}$$

in the integrand of eq. (2.13) and integrating out this delta function (indeed, the two terms in the $(\cdots)$ part of the integrand of eq. (2.20) correspond to the two points in the support of $\delta\big((q^0+K^0/2)^2-E_r^2\big)$).

Let us now go back to the intermediate result in eq. (2.20) and change the integration variables into polar coordinates. As the integrand only depends on the norm of $\mathbf{q}$, the angular integrations will simply produce a factor of 4π. Further changing the resulting integration measure $|\mathbf{q}|^2 d|\mathbf{q}| \longrightarrow |\mathbf{q}|E_r dE_r$, one then finds

$$\begin{aligned}\mathscr{M}^{(1)} = -2\pi i\frac{4\pi}{(2\pi)^4}\int_{m_r}^{\infty} dE_r E_r|\mathbf{q}|\left(\frac{1}{2E_r}\frac{1}{K^0(K^0+2E_r)}+\frac{1}{2E_r}\frac{1}{K^0(K^0-2E_r)}\right)\\ \times\widetilde{A}_L^{\text{tree}}(k_1,\ldots,k_j,q+K/2)\widetilde{A}_R^{\text{tree}}(k_{j+1},\ldots,k_n,-q+K/2)\,.\end{aligned} \tag{2.22}$$

The integrand has poles at $E_r=\pm\frac{K^0}{2}$. When $K^0<2m_r$, the pole does not lie on the integration contour, so $\mathscr{M}^{(1)}$ is manifestly real. When $K^0>2m_r$, however, the pole lies just above or below the contour of integration, depending upon whether K^0 is given a small positive or negative imaginary part; that is, depending on whether we are evaluating $\mathscr{M}^{(1)}(s+i\varepsilon)$ or $\mathscr{M}^{(1)}(s-i\varepsilon)$.

The one-loop diagram $\mathscr{M}^{(1)}(s)$ thus has a branch cut along the real axis, running from $s=4m_r^2$ to $s=+\infty$. To evaluate the discontinuity $\mathscr{M}^{(1)}(s+i\varepsilon)-\mathscr{M}^{(1)}(s-i\varepsilon)$, we rewrite the integrand of eq. (2.22) using the Sokhatsky-

Weierstrass theorem,

$$\frac{1}{K^0-2E_r\pm i\varepsilon}=PV\frac{1}{K^0-2E_r}\mp\pi i\delta(K^0-2E_r) \tag{2.23}$$

where PV denotes the Cauchy principal value. The discontinuity is thus given by replacing

$$\frac{1}{K^0(K^0-2E_r)}\longrightarrow -2\pi i\delta\big(K^0(K^0-2E_r)\big) \tag{2.24}$$

in the second term in the integrand of eq. (2.22), the first term yielding no contribution to the discontinuity. Recall that the q^0 contour integration producing the former term froze the integration variable to the value $q^0=-\frac{K^0}{2}+E_r-i\varepsilon$, in turn setting $K^0(K^0-2E_r)=(K/2-q)^2-m_r^2$. Thus, the replacement in eq. (2.24) is equivalent to the replacement

$$\frac{1}{\big(K/2-q\big)^2-m_r^2+i\varepsilon}\longrightarrow -2\pi i\delta^{(+)}\big((K/2-q\big)^2-m_r^2\big)\,. \tag{2.25}$$

Alternatively, one can easily check that the expression resulting from applying the replacement (2.24) to the integrand of eq. (2.22) is identical to that resulting from applying the replacements in eqs. (2.21) and (2.25) to the integrand of eq. (2.13). This completes the proof of eq. (2.16). □

In conclusion, the one-loop diagram $\mathscr{M}^{(1)}(s)$ illustrated in figure 2.2 and explicitly given in eq. (2.13) has a branch cut along the real axis, running from $s=4m_r^2$ to $s=+\infty$. The associated discontinuity $\mathscr{M}^{(1)}(s+i\varepsilon)-\mathscr{M}^{(1)}(s-i\varepsilon)$ is computed by replacing the two propagators in eq. (2.13) by delta functions according to the replacements in eq. (2.14). These replacements are often referred to as *unitarity cuts* or as *cutting the propagators*.

Stated differently, the discontinuity arises from the region of the d^4q integration in which the two propagators in figure 2.2 are put simultaneously on-shell. This region is referred to as *Lorentz invariant phase space*. Labeling the propagator momenta as

$$p_1=q+\frac{K}{2}\,,\qquad p_2=-q+\frac{K}{2}\,, \tag{2.26}$$

the measure over Lorentz invariant phase space implicit in eq. (2.16) takes the form

$$\begin{aligned}d\mathrm{LIPS}(p_1,p_2)\equiv\frac{d^4p_1}{(2\pi)^4}\frac{d^4p_2}{(2\pi)^4}(2\pi)^4\delta^{(4)}(p_1+p_2-K)\\ \times(-2\pi i)^2\delta^{(+)}(p_1^2-m_r^2)\delta^{(+)}(p_2^2-m_r^2)\,.\end{aligned} \tag{2.27}$$

This way of writing the measure makes its interpretation clear: the integration is over all possible propagator momenta p_1,p_2 that satisfy momentum conservation $p_1+p_2=K$ and put the two propagators simultaneously on-shell.

Employing this notation and now applying eq. (2.16) to all Feynman diagrams contributing to the one-loop amplitude we conclude that

$$\operatorname*{Disc}_s A^{(1)}(s) = \sum_{\substack{\text{intermediate}\\ \text{states}}} \int d\text{LIPS}(p_1,p_2) A_L^{\text{tree}}\big(k_1,\ldots,k_j,p_1\big) \times A_R^{\text{tree}}\big(k_{j+1},\ldots,k_n,p_2\big) \tag{2.28}$$

where the summation runs over all possible ways in which to factor the contributing one-loop diagrams into on-shell tree amplitudes.

2.1.3 Dispersion integrals and bootstrapping

As shown in the previous section, the one-loop diagram $\mathscr{M}^{(1)}(s)$ (illustrated in figure 2.2) has a branch cut along the real axis, running from $s = 4m_r^2$ to $s = +\infty$. The finite branch point $s_0 = (2m_r)^2$ has a clear physical meaning: it is the threshold energy for production of a two-particle state. For real s below s_0, the two intermediate states cannot go on-shell whereby the Feynman $i\varepsilon$-prescription becomes irrelevant and $\mathscr{M}^{(1)}(s)$ is real. However, at $s = s_0$, the propagator denominators vanish, and at this point the diagram acquires an imaginary part.

Now, since $\mathscr{M}^{(1)}(s)$ is meromorphic in the upper half of the s-plane and real on the real axis for $\operatorname{Re} s < s_0$, the Schwarz reflection principle dictates that $\mathscr{M}^{(1)}(s)$ can be analytically continued to the lower half plane with

$$\mathscr{M}^{(1)}(s) = \big(\mathscr{M}^{(1)}(s^*)\big)^* . \tag{2.29}$$

Near the real axis for $s > s_0$, eq. (2.29) implies

$$\operatorname{Re}\mathscr{M}^{(1)}(s+i\varepsilon) = \operatorname{Re}\mathscr{M}^{(1)}(s-i\varepsilon) \tag{2.30}$$

$$\operatorname{Im}\mathscr{M}^{(1)}(s+i\varepsilon) = -\operatorname{Im}\mathscr{M}^{(1)}(s-i\varepsilon) . \tag{2.31}$$

In particular, the discontinuity across the branch cut is

$$\operatorname*{Disc}_s \mathscr{M}^{(1)}(s) = 2i \operatorname{Im}\mathscr{M}^{(1)}(s+i\varepsilon) . \tag{2.32}$$

At this point, let us remind ourselves of the content of the Cutkosky rule in eq. (2.16): the discontinuity of $\mathscr{M}^{(1)}(s)$ can be obtained by integrating the two tree-level amplitudes arising in the on-shell factorization over relativistic phase space. The knowledge of this tree-level data therefore suffices to determine the imaginary part of $\mathscr{M}^{(1)}(s)$.

Assuming $\mathscr{M}^{(1)}(s)$ has no poles in the upper half of the s-plane[2], this is enough to determine the function completely. Namely, the real part can then

[2]This is for example the case for supersymmetric gauge theories. In contrast, QCD and $\mathscr{N} = 0$ SYM amplitudes contain terms which are rational functions of the external momenta (often referred to as *rational terms*). These terms give rise to poles in the complex s-plane, in addition to the branch cuts discussed above.

be found by means of the Kramers-Kronig relation

$$\mathrm{Re}\mathscr{M}^{(1)}(s) = \frac{1}{\pi}\mathrm{PV}\int_{-\infty}^{\infty} ds' \, \frac{\mathrm{Im}\mathscr{M}^{(1)}(s')}{s'-s}\,. \tag{2.33}$$

Here again PV refers to the Cauchy principal value prescription. The integral in eq. (2.33) is known as a *dispersion integral*[3].

To summarize what we have found in this section: assuming the dispersion integral in eq. (2.33) can be performed, any *one-loop* diagram can be explicitly reconstructed from the *tree-level* amplitudes arising in the on-shell factorization on its various kinematic channels. This was the philosophy of the unitarity bootstrap approach: to determine the S-matrix iteratively in the loop order, starting from tree amplitudes.

As alluded to in the previous paragraph, the difficulty of carrying out the required dispersion integrals, along with the ambiguity arising from rational contributions to the amplitude, led to a breakdown of the analytic S-matrix program in the late 1960's. However, as we shall see in the next section, the program experienced a dramatic revival in the 1990's.

2.2 Unitarity in the 1990's

The crucial insight that led to the resurrection of the unitarity approach came from Bern, Dixon and Kosower in the 1990's [9–13]. Rather than trying to reconstruct a one-loop amplitude directly from its discontinuities à la eq. (2.33), in their approach one exploits that the basic algebraic structure of the one-loop integrand is already known from the sum over all Feynman diagrams. Indeed, as we shall see in Section 2.2.1, this sum can be expressed as a linear combination of a small set of one-loop basis integrals.[4] Taking discontinuities of this basis decomposition in all possible channels then relates the basis coefficients to tree amplitudes through the Cutkosky rule (2.28), allowing one to unambiguously determine the coefficients, and in turn the amplitude.

2.2.1 Integral reductions and integral bases

The generic one-loop Feynman diagram is an integral over an arbitrary number of propagators, multiplied by powers of the loop momentum ℓ in the numerator. In particular, the integrand of an n-point amplitude in Yang-Mills theory may contain up to n propagators and rank n tensors in ℓ^μ, owing to the three-gluon vertex. Such integrals cannot be evaluated directly, and instead one uses integral reductions to express the desired integral as a sum of simpler integrals.

[3] The integral transform in eq. (2.33) is known as a Hilbert transform.

[4] As already mentioned above, the amplitude will in general also have contributions from functions which are rational in the external momenta.

To illustrate how such reductions are performed, let us start with an n-gon integral of the form described above, assuming all propagators to be massless,

$$I_{n-\text{gon}}[P(\ell^\mu)] \equiv \int \frac{d^D\ell}{(2\pi)^D} \frac{P(\ell^\mu)}{\ell^2(\ell-K_1)^2\cdots(\ell-K_{n-1})^2} \tag{2.34}$$

where the K_i denote sums of external momenta attached to the vertices of the n-gon and the numerator insertion $P(\ell^\mu)$ represents an arbitrary polynomial in ℓ^μ. We will refer to the special case $P(\ell^\mu) = 1$ as a *scalar* integral, and the generic case as a *tensor* integral (irrespective of whether the Lorentz indices are contracted or not). As we will now outline, the integrals (2.34) can be iteratively reduced to scalar n-gons with $n = 1,2,3,4$. Please note that the presentation below is based on Section 4.2 in ref. [14].

First, if $n \geq 5$, four independent momenta $K_1,\ldots,K_4$ are available. These can be used to define dual momenta,

$$\begin{aligned} v_1^\mu &= \varepsilon(\mu,2,3,4), & v_2^\mu &= \varepsilon(1,\mu,3,4) \\ v_3^\mu &= \varepsilon(1,2,\mu,4), & v_4^\mu &= \varepsilon(1,2,3,\mu) \\ v_i\cdot K_j &= \varepsilon(1,2,3,4)\delta_{ij}, \end{aligned} \tag{2.35}$$

in terms of which the loop momentum can be expanded as,[5]

$$\ell^\mu = \frac{1}{\varepsilon(1,2,3,4)} \sum_{i=1}^4 v_i^\mu \; \ell\cdot K_i \tag{2.36}$$

$$= \frac{1}{2\varepsilon(1,2,3,4)} \sum_{i=1}^4 v_i^\mu \left(\ell^2 - (\ell-K_i)^2 + K_i^2\right). \tag{2.37}$$

Now, inserting eq. (2.37) into the degree p polynomial $P(\ell^\mu)$ in eq. (2.34), the first two terms will collapse propagators, thus producing $(n-1)$-gon integrals with numerator polynomials of degree $p-1$, while the last term remains an n-gon integral, also of degree $p-1$. Iterating this procedure, n-gon integrals may be reduced to box integrals plus scalar n-gon integrals.

Furthermore, all scalar n-gons with $n \geq 6$ can be reduced into scalar polygons with fewer sides. Namely, for $n \geq 6$ we have an additional independent momentum K_5. Dotting this momentum into eq. (2.36), the resulting equation can be rewritten in the form

$$1 = a_0\ell^2 + \sum_{i=1}^5 a_i(\ell-K_i)^2. \tag{2.38}$$

[5]Please note that eq. (2.37) is only a valid identity for the four-dimensional part of the loop momentum, and care must be taken when applying it to a D-dimensional loop momentum. However, in practice, loop momenta typically appear dotted into (strictly four-dimensional) external momenta or polarization vectors.

Inserted into the numerator of eq. (2.34), we see that this equation allows us to write, for example, a scalar hexagon integral as a sum of six scalar pentagons. Furthermore, in strictly four dimensions, a Gram determinant identity is available which reduces the scalar pentagon to a sum of five boxes.

Finally, tensor n-gons with $n = 4, 3, 2, 1$ can be reduced into scalar n-gons with $n = 4, 3, 2, 1$ using either Passarino-Veltman reduction, or using dual vectors in analogy with the steps above, but we omit the details here. In conclusion, any one-loop Feynman diagram can be expressed as a linear combination of scalar boxes, triangles, bubbles and tadpoles.

Applying integral reductions to the Feynman diagram expansion of any n-point one-loop amplitude—which we take to *define* the amplitude—we conclude that the amplitude can be expressed as a linear combination of the following basis integrals,[6]

$$A_n^{(1)} = \sum_{\text{boxes}} c_{\square} I_{\square} + \sum_{\text{triangles}} c_{\triangle} I_{\triangle} + \sum_{\text{bubbles}} c_{\circ} I_{\circ} + \sum_{\text{tadpoles}} c_{-\circ} I_{-\circ} + \text{rational terms} \tag{2.39}$$

with a priori unknown coefficients, and where the summations run over all possible ways of distributing the n (cyclically ordered) external momenta at the vertices of the integrals. The definition of these integrals can be read off from figure 2.4 which also serves to restate the basis decomposition of the one-loop amplitude schematically.

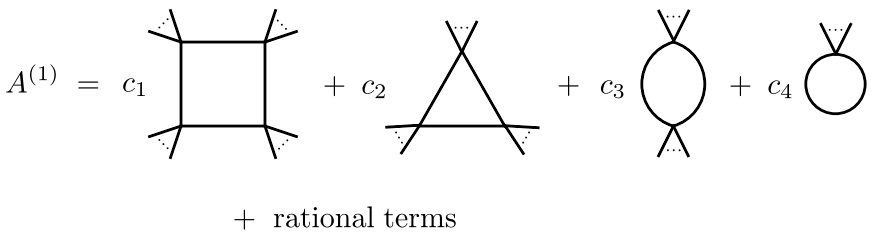

Figure 2.4. Schematic representation of the decomposition of a generic one-loop amplitude into the basis of one-loop integrals. The $\cdots$ at each vertex represent the presence of an arbitrary number of external legs. Implicit here is a summation over all possible ways of distributing the (cyclically ordered) legs at the vertices.

The box and triangle integrals are classified according to which of their external momenta are massless. Triangles exist in zero-mass through three-mass configurations (0m, 1m, 2m, 3m) while boxes exist in zero-mass through four-mass configurations. Here the two-mass case contains two distinct subclasses

[6] Although massless tadpoles vanish in dimensional regularization, we include them here to accomodate the general case of massive propagators.

referred to as two-mass-easy (2me) and two-mass-hard (2mh), corresponding to the massless corners of the box being opposite and adjacent, respectively.

2.2.2 Example: the one-loop n-gluon MHV amplitude in $\mathcal{N}=4$ SYM theory

We briefly outlined the basic ideas of the modern unitarity method in the introduction of Section 2.2. To give an example of how this method is used in practice, we sketch here the computation of the one-loop n-gluon MHV amplitude in $\mathcal{N}=4$ super Yang-Mills theory. The presentation here is inspired by Section 4.4 of ref. [14].

Expressed in the integral basis of Section 2.2.1, this amplitude is known to only contain boxes, as the triangle and bubble coefficients vanish due to supersymmetric cancelations. Thus, we can write

$$A^{(1)}_{n,\mathrm{MHV}}(i^-,j^-) = \sum_{a\in\text{boxes}} c_a I_a \,. \tag{2.40}$$

Let us define

$$K_{j_1,j_2} \equiv \left(k_{j_1}+\cdots+k_{j_2}\right) \tag{2.41}$$

$$s_{j_1,j_2} \equiv \left(k_{j_1}+\cdots+k_{j_2}\right)^2 . \tag{2.42}$$

Using the Cutkosky rule in eq. (2.28), the discontinuity in the s_{j_1,j_2}-channel of the left hand side of eq. (2.40) evaluates to

$$\begin{aligned}\underset{s_{j_1,j_2}}{\mathrm{Disc}} A^{(1)}_{n,\mathrm{MHV}}(i^-,j^-) = \sum_{h,h'}\int d\mathrm{LIPS}(p_1,p_2) A^{\mathrm{tree}}_L\left(k_{j_1},\ldots,k_{j_2},p_1^h,p_2^{h'}\right) \\ \times A^{\mathrm{tree}}_R\left(k_{j_2+1},\ldots,k_{j_1-1},p_1^h,p_2^{h'}\right)\end{aligned} \tag{2.43}$$

where the sum over helicities h,h' indicates that we are to sum over all states that can propagate along the cut propagators. Depending on the cut under consideration, the two negative-helicity external states i and j can appear in two possible configurations, as illustrated in figure 2.5: either a) they are involved in the same tree-level amplitude, in which case only gluons can propagate in the cut loop; or b) they are not involved in the same tree-level amplitude, in which case the entire $\mathcal{N}=4$ supermultiplet of states can propagate in the cut loop.

The amplitudes involved in the summation over the $\mathcal{N}=4$ multiplet are related to gluonic amplitudes through a supersymmetric Ward identity [15, 16]. Direct calculation shows that the integrand of eq. (2.43) in both cases a) and b) yields the same result,

$$A^{\mathrm{tree}}_{n,\mathrm{MHV}}(i^-,j^-)\frac{\langle j_1-1,\,j_1\rangle\langle p_1\,p_2\rangle}{\langle j_1-1,\,p_1\rangle\langle p_1\,j_1\rangle}\frac{\langle j_2,\,j_2+1\rangle\langle p_2\,p_1\rangle}{\langle j_2\,p_2\rangle\langle p_2,\,j_2+1\rangle}\,. \tag{2.44}$$

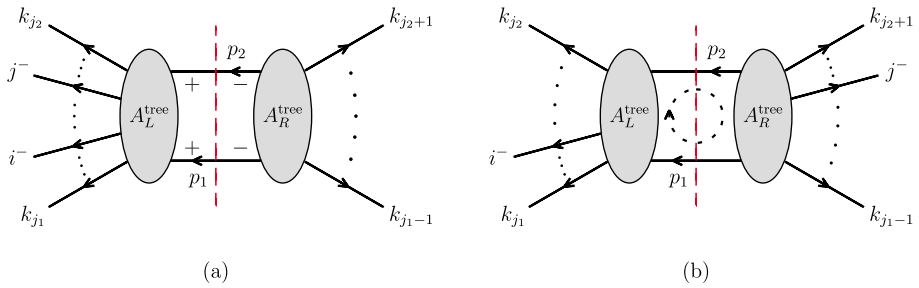

Figure 2.5. The s_{j_1,j_2}-channel discontinuity of the one-loop n-gluon MHV amplitude in $\mathcal{N}=4$ super Yang-Mills theory. The Cutkosky rule relates this discontinuity to the product of tree-level amplitudes separated by the dashed red line, illustrating the cut. Depending on the cut, the two negative-helicity external states may appear in (a) the same tree amplitude, in which case only gluons can propagate along the cut propagators (as indicated by the assigned internal helicities); or (b) in distinct tree amplitudes, in which case the entire $\mathcal{N}=4$ supermultiplet of states can propagate (as indicated by the dashed circle).

After some algebra (we refer to eqs. (103)-(107) in ref. [14] for details), this can be rewritten as

$$\frac{A^{\text{tree}}_{n,\text{MHV}}(i^-,j^-)}{2}\left(\frac{s_{j_1,j_2}s_{j_1-1,j_2+1}-s_{j_1-1,j_2}s_{j_1,j_2+1}}{(p_1+k_{j_1-1})^2(p_2+k_{j_2+1})^2}\right.$$
$$+\frac{s_{j_1,j_2-1}s_{j_1-1,j_2}-s_{j_1-1,j_2-1}s_{j_1,j_2}}{(p_1+k_{j_1-1})^2(p_2-k_{j_2})^2}$$
$$+\frac{s_{j_1+1,j_2}s_{j_1,j_2+1}-s_{j_1,j_2}s_{j_1+1,j_2+1}}{(p_1-k_{j_1})^2(p_2+k_{j_2+1})^2}$$
$$\left.+\frac{s_{j_1+1,j_2-1}s_{j_1,j_2}-s_{j_1,j_2-1}s_{j_1+1,j_2}}{(p_1-k_{j_1})^2(p_2-k_{j_2})^2}\right) \tag{2.45}$$

plus terms that vanish after integration.

In summary, we have expressed the s_{j_1,j_2}-channel discontinuity of the one-loop amplitude as the phase space integral (2.43), with the $A_L^{\text{tree}}(\cdots)A_R^{\text{tree}}(\cdots)$ integrand explicitly given in eq. (2.45). Let us now go back to eq. (2.40) and consider how this discontinuity may be produced by the right hand side. Recalling the cut propagators $\delta^{(+)}(p_1^2)\delta^{(+)}(p_2^2)$ implicit in the phase space measure (see eq. (2.27)), the explicit propagators in eq. (2.45) allow us to directly read off the relevant box integrals. That is, the terms on the right hand side of eq. (2.40) producing the discontinuity are of the form $\int \frac{d^D\ell}{(2\pi)^D}(\cdots)$ where the integrand is obtained by multiplying eq. (2.45) by $1/(p_1^2p_2^2)$ and then

replacing $(p_1, p_2) \longrightarrow (\ell, K_{j_1,j_2} - \ell)$,

$$\begin{aligned}
&\underset{s_{j_1,j_2}}{\text{Disc}} A^{(1)}_{n,\text{MHV}}(i^-, j^-) = \frac{A^{\text{tree}}_{n,\text{MHV}}(i^-, j^-)}{2} \times \\
&\underset{s_{j_1,j_2}}{\text{Disc}} \Bigg[\Big(s_{j_1,j_2} s_{j_1-1,j_2+1} - s_{j_1-1,j_2} s_{j_1,j_2+1} \Big) I^{\text{2me}}_{\square}\big(k_{j_1-1},\, K_{j_1,j_2},\, k_{j_2+1},\, -K_{j_1-1,j_2+1}\big) \\
&\quad + \Big(s_{j_1,j_2-1} s_{j_1-1,j_2} - s_{j_1-1,j_2-1} s_{j_1,j_2} \Big) I^{\text{2me}}_{\square}\big(k_{j_1-1},\, K_{j_1,j_2-1},\, k_{j_2},\, -K_{j_1-1,j_2}\big) \\
&\quad + \Big(s_{j_1+1,j_2} s_{j_1,j_2+1} - s_{j_1,j_2} s_{j_1+1,j_2+1} \Big) I^{\text{2me}}_{\square}\big(k_{j_1},\, K_{j_1+1,j_2},\, k_{j_2+1},\, -K_{j_1,j_2+1}\big) \\
&\quad + \Big(s_{j_1+1,j_2-1} s_{j_1,j_2} - s_{j_1,j_2-1} s_{j_1+1,j_2} \Big) I^{\text{2me}}_{\square}\big(k_{j_1},\, K_{j_1+1,j_2-1},\, k_{j_2},\, -K_{j_1,j_2}\big) \Bigg] \qquad (2.46)
\end{aligned}$$

where the notation $I^{\text{2me}}_{\square}$ denotes that the box integrals are of the two-mass-easy type (as defined at the end of Section 2.2.1).

Summing over all possible and independent kinematic channels, one finds the following result for the one-loop n-gluon MHV amplitude in $\mathcal{N} = 4$ super Yang-Mills theory,[7]

$$A^{(1)}_{n,\text{MHV}} = (\mu^2)^{\varepsilon} \frac{\Gamma(1+\varepsilon)\Gamma^2(1-\varepsilon)}{(4\pi)^{2-\varepsilon}\Gamma(1-2\varepsilon)} A^{\text{tree}}_{n,\text{MHV}}\, V_n \,. \qquad (2.47)$$

Here the function V_n takes the form

$$V_{2m+1} = \sum_{j=1}^{m-1} \sum_{i=1}^{n} f_{i,j} \qquad (2.48)$$

$$V_{2m} = \sum_{j=1}^{m-2} \sum_{i=1}^{n} f_{i,j} + \sum_{i=1}^{n/2} f_{i,m-1} \,, \qquad (2.49)$$

with the two-mass-easy box functions given by

$$\begin{aligned}
f_{i,j} = &-\frac{1}{\varepsilon^2}\Big[\big(-s_{i-1,i+j-1}\big)^{-\varepsilon} + \big(-s_{i,i+j}\big)^{-\varepsilon} - \big(-s_{i,i+j-1}\big)^{-\varepsilon} - \big(-s_{i-1,i+j}\big)^{-\varepsilon} \Big] \\
&+ \text{Li}_2\left(1 - \frac{s_{i,i+j-1}}{s_{i-1,i+j-1}}\right) + \text{Li}_2\left(1 - \frac{s_{i,i+j-1}}{s_{i,i+j}}\right) + \text{Li}_2\left(1 - \frac{s_{i-1,i+j}}{s_{i-1,i+j-1}}\right) \\
&+ \text{Li}_2\left(1 - \frac{s_{i-1,i+j}}{s_{i,i+j}}\right) - \text{Li}_2\left(1 - \frac{s_{i,i+j-1}\, s_{i-1,i+j}}{s_{i-1,i+j-1}\, s_{i,i+j}}\right) + \frac{1}{2}\log^2\left(\frac{s_{i-1,i+j-1}}{s_{i,i+j}}\right) .
\end{aligned} \qquad (2.50)$$

We note that the result given in eqs. (2.47)-(2.50) has been shown to pass independent consistency checks; in particular, it has the correct collinear limits.

[7] Please note that from this point on, we drop the bar on the dimensional regulator ε introduced in eq. (2.12), used above to distinguish it from that of the Feynman $i\varepsilon$-prescription.

It is remarkable that a compact result for an all-multiplicity one-loop amplitude can be obtained through a small number of steps. This clearly shows the power of the unitarity approach.

2.3 Generalized unitarity

One-loop amplitudes in generic Yang-Mills theories have nonzero contributions from triangle and bubble integrals in the basis decomposition (2.39). In the presence of these additional integrals, the unitarity approach described in Section 2.2.2 can still be used to determine all the respective coefficients, but the procedure is in practice somewhat cumbersome. Schematically, the result of applying a cut in the s_{j_1,j_2}-channel to eq. (2.39) is,

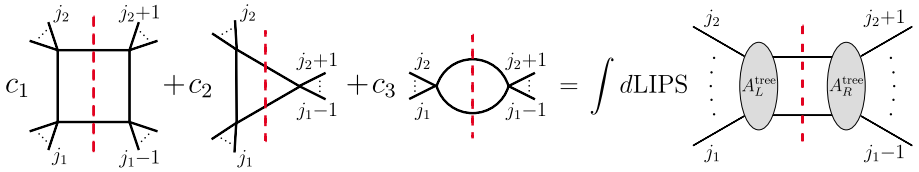

Figure 2.6. The result of applying a cut in the s_{j_1,j_2}-channel to eq. (2.39). It is implied that, on the left hand side, one should sum over all possible box, triangle and bubble integrals containing the propagators being put on-shell; similarly for the Feynman diagrams on the right hand side.

That is, all integrals containing the propagators being put on-shell will enter on the left hand side, and a nontrivial amount of algebra is required to disentangle their respective coefficients.

One conceivable way to cut down the required algebra would be to put several propagators on-shell simultaneously. Assuming this is a valid operation, putting four propagators on-shell would leave on the left hand side in figure 2.6 only the particular box integral containing these propagators, and no disentangling is necessary to find its coefficient. Moreover, extracting the coefficient of a particular triangle integral would be done by putting its three propagators on-shell: the only other contributions on the left hand side in figure 2.6 would come from box integrals containing one propagator in addition to the three being put on-shell. At this stage, some disentangling would be needed to determine the triangle coefficient, but the prior knowledge of the contaminating box coefficients makes this task comparatively straightforward.

As we shall see in the following sections, not only is the operation of putting more than two propagators on-shell valid, there are further refinements available in which the box, triangle and bubble coefficients can be obtained directly, with no need for disentangling their respective coefficients.

2.3.1 Quadruple cuts: direct extraction of box coefficients

In this section we examine what happens to the one-loop equation (2.39) when four propagators are put on-shell and how the resulting equation enables us to obtain box coefficients directly from tree-level data. This is essentially a review of the BCF quadruple-cut method [17], though the phrasing in terms of multidimensional contour integrals presented here owes to the mathematically rigorous viewpoint taken in refs. [18–21] and Paper I.

Let us consider a specific box integral with massless propagators,[8]

$$I_{\square}(K_1,K_2,K_3,K_4) = \int_{\mathbb{R}^D} \frac{d^D\ell}{(2\pi)^D} \frac{1}{\ell^2(\ell-K_1)^2(\ell-K_1-K_2)^2(\ell+K_4)^2} \quad (2.51)$$

illustrated in figure 2.7,

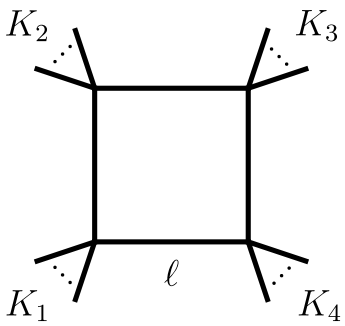

Figure 2.7. The general one-loop box integral. The $\cdots$ dots at each vertex represent the presence of an arbitrary number of massless legs. The vertex momenta K_i are sums of these momenta.

and the associated quadruple cut in which the propagators are replaced by delta functions solving the on-shell constraints

$$p_1^2 \equiv \ell^2 = 0 \quad (2.52)$$
$$p_2^2 \equiv (\ell-K_1)^2 = 0 \quad (2.53)$$
$$p_3^2 \equiv (\ell-K_1-K_2)^2 = 0 \quad (2.54)$$
$$p_4^2 \equiv (\ell+K_4)^2 = 0\,. \quad (2.55)$$

This is a system of one quadratic and three linear equations (as one can see by subtracting eq. (2.52) from eq. (2.53), eq. (2.53) from eq. (2.54) etc.), and thus has two distinct solutions.

What is perhaps not immediately obvious is that the solutions of eqs. (2.52)-(2.55) are generically complex, $\ell \in \mathbb{C}^4$. A special case in which this is easy to see arises when one of the external momenta, for example K_1, is lightlike. With

[8] Note that we suppress the Feynman $i\varepsilon$-prescription as it is irrelevant here.

the adjacent propagator momenta p_1 and p_2 also being lightlike, momentum conservation $K_1 = p_1 - p_2$ then implies

$$0 = -2p_1 \cdot p_2 = \langle p_1\, p_2\rangle [p_1\, p_2]\,. \tag{2.56}$$

This equation has two solutions: either the holomorphic or the antiholomorphic spinors are proportional [22],

$$\langle p_1\, p_2\rangle = 0 \implies \lambda_{p_1} \propto \lambda_{p_2} \quad \text{or} \quad [p_1\, p_2] = 0 \implies \widetilde{\lambda}_{p_1} \propto \widetilde{\lambda}_{p_2}\,. \tag{2.57}$$

Corresponding to each of these cases we will label the vertex with respectively $\oplus$ or $\ominus$, referred to as the *chirality* of the vertex. These considerations will be important throughout this thesis and are summarized in figure 2.8.

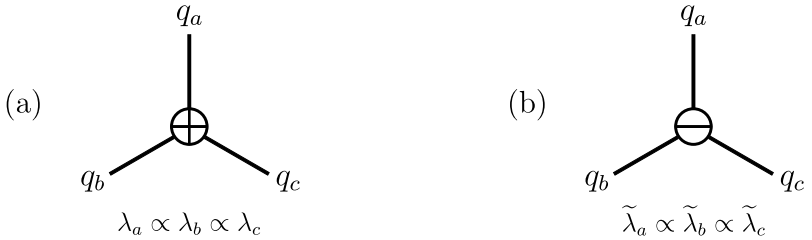

Figure 2.8. Momentum conservation at the massless three-point vertex implies that either (a) the holomorphic spinors are proportional, denoted with $\oplus$; or (b) the antiholomorphic spinors are proportional, denoted with $\ominus$. It should be noted that the labeling of holomorphically-collinear vertices as $\oplus$, and of antiholomorphically-collinear ones as $\ominus$ is not uniform in the literature.

Now, insisting that the momenta p_1, p_2 be real in Minkowski signature implies $\langle p_1\, p_2\rangle^* = -[p_1\, p_2]$, whereby both cases in eq. (2.57) are simultaneously realized, causing the momenta to be proportional, $p_1^\mu = \alpha p_2^\mu$. This would be unacceptable: for example, if in addition K_4 is lightlike, momentum conservation at the vertex containing this external leg would then imply $K_4^\mu \propto K_1^\mu$. To ensure that eqs. (2.52)-(2.55) have solutions for generic external momenta, we must go back and relax the assumptions on p_1, p_2 so that their angle and bracket spinor products are not related by complex conjugation. Two options are available: either allow these momenta to live in $(2,2)$-signature, or allow them to be complex. We will stick to the latter option, $p_1, p_2 \in \mathbb{C}^4$.

To summarize what we have seen so far, the equations (2.52)-(2.55) have two distinct solutions $\{L, L^\bullet\}$, both of which are generically complex, $\{L, L^\bullet\} \subset \mathbb{C}^4$; moreover, they are each other's complex conjugates when the external momenta are real. (Though we have only established this in the special case where at least one external momentum K_i is massless, the conclusion holds true in complete generality.) We will refer to the points $L, L^\bullet$ as the *leading singularities* of the integrand in eq. (2.51).

Keeping these facts in mind, let us now return to the procedure of putting four propagators on-shell in eq. (2.39). Schematically, one would like to perform the replacement

$$\prod_{i=1}^{4} \frac{1}{p_i^2} \;\longrightarrow\; (-2\pi i)^4 \prod_{i=1}^{4} \delta^{\mathbb{C}}(p_i^2) \tag{2.58}$$

where, compared to eq. (2.14), we have dropped the now meaningless restriction to positive-energy states and instead added the superscript $^{\mathbb{C}}$ to indicate that the integration range in eq. (2.51) must necessarily be pushed into $\mathbb{C}^4$ in order to contain the leading singularities.

More accurately, the natural definition of delta functions with complex arguments involves contour integrals – integrating out a variable q in an integrand involving delta functions will fix q to some value q_0; in the language of contour integrals, this corresponds to integrating in the complex q-plane along a small circle centered at q_0. Indeed, as observed in refs. [23, 24], Cauchy's residue theorem implies that the localization property

$$\int dq\, \delta(q-q_0) f(q) \;=\; f(q_0) \tag{2.59}$$

continues to hold if we define $\delta(q-q_0) \equiv -\frac{1}{2\pi i}\frac{1}{q-q_0}$ and take the integral to be a contour integral along a small circle in the complex q-plane centered at q_0. Stated differently, starting from the integral $-\frac{1}{2\pi i}\int_{\mathbb{R}} dq \frac{f(q)}{q-q_0}$, we can think of the operation of "cutting the propagator" in two equivalent ways: as the replacement $\frac{1}{q-q_0} \longrightarrow -2\pi i \delta(q-q_0)$, or as the change of integration contour $\mathbb{R} \longrightarrow C_\varepsilon(q_0)$. (Of course, this equivalence is exactly what is made explicit in the Feynman $i\varepsilon$-prescription by giving the pole q_0 a small imaginary part, as we have already seen in the proof of the Cutkosky rules.)

By analogy, taking the quadruple cut of the box integral (2.51) should really be understood as a change of integration range from $\mathbb{R}^D$ to a surface (of real dimension 4) embedded in $\mathbb{C}^4$ while leaving the integrand in eq. (2.51) unchanged. The quadruple-cut integral is thus a multidimensional contour integral whose contour is a linear combination of the two 4-tori that encircle the leading singularities $L, L^\bullet$, the first of which can be written formally as[9]

$$T_\varepsilon^4(L) = \{\ell \in \mathbb{C}^4 : |p_i^2(\ell)| = \varepsilon_i, \quad i = 1,\ldots,4\}\,. \tag{2.60}$$

At this point it is not clear which linear combinations $\omega_1 T_\varepsilon^4(L) + \omega_2 T_\varepsilon^4(L^\bullet)$ define valid integration contours, and for now we will *assume* that one should simply average over the two contributions; that is, set $\omega_1 = \omega_2 = \frac{1}{2}$. (As we will show in Section 3.2, this choice is indeed valid.)

[9] Using the parametrization of the loop momentum introduced in the next section it is possible to write down these tori explicitly, see eqs. (2.99)-(2.100) as an example.

Thus, we *define* the quadruple cut as the change of contour[10]

$$\int_{\mathbb{R}^D} \frac{d^D\ell}{(2\pi)^D} \frac{\Phi(\ell)}{\prod_{i=1}^4 p_i^2(\ell)} \quad \longrightarrow \quad \frac{1}{2} \sum_{a\in\{L,L^\bullet\}} \int_{T^4_\varepsilon(a)} \frac{d^4\ell}{(2\pi)^4} \frac{\Phi(\ell)}{\prod_{i=1}^4 p_i^2(\ell)} \,. \tag{2.61}$$

Note in particular that the change of contour away from real Minkowski space renders the box integral IR finite, and one may therefore disregard the dimensional regulator part of the measure $d^{-2\overline{\varepsilon}}\ell$ and the $(-2\overline{\varepsilon})$-dimensional components of the loop momentum.

One important respect in which the multidimensional contour integrals do not behave like integrals of delta functions is the transformation formula for changing variables: Given a holomorphic function $f = (f_1, \ldots, f_n) : \mathbb{C}^n \to \mathbb{C}^n$ with an isolated zero[11] at $a \in \mathbb{C}^n$, the residue at a is computed by the integral over the contour $\Gamma_\varepsilon(a) = \{z \in \mathbb{C}^n : |f_i(z)| = \varepsilon_i,\ i = 1, \ldots, n\}$. This contour integral satisfies the transformation formula

$$\frac{1}{(2\pi i)^n} \int_{\Gamma_\varepsilon(a)} \frac{h(z)\, dz_1 \wedge \cdots \wedge dz_n}{f_1(z) \cdots f_n(z)} \;=\; \frac{h(a)}{\det_{i,j} \frac{\partial f_i}{\partial z_j}} \tag{2.62}$$

which, crucially, does not involve taking the absolute value of the inverse Jacobian. This ensures that this factor is analytic in any variables on which it depends, so that further contour integrations can be carried out.

At long last, let us return to what we set out to do, namely to put four propagators $\frac{1}{p_i^2}$ on-shell in eq. (2.39). Changing the contour of integration as prescribed by eq. (2.61) turns this equation into

$$\begin{aligned} &\frac{c_\square}{2} \sum_{a\in\{L,L^\bullet\}} \int_{T^4_\varepsilon(a)} \frac{d^4\ell}{(2\pi)^4} \prod_{i=1}^4 \frac{1}{p_i^2(\ell)} \\ &\quad = \frac{1}{2} \sum_{a\in\{L,L^\bullet\}} \sum_{\substack{\text{helicities,}\\ \text{species}}} \int_{T^4_\varepsilon(a)} \frac{d^4\ell}{(2\pi)^4} \prod_{i=1}^4 \frac{1}{p_i^2(\ell)} A_i^{\text{tree}}\big(p_i(\ell), p_{i+1}(\ell)\big) \,. \end{aligned} \tag{2.63}$$

We observe that the triangle, bubble and tadpole integrals on the right hand side of eq. (2.39) have disappeared: their integrands take the form given in eq. (2.61) where, e.g., in the case of triangles, $\Phi(\ell) = p_j^2(\ell)$. The contour integration freezes the value of ℓ to one of the leading singularities $L, L^\bullet$, and

[10] Please note that all (generalized-)unitarity cuts used in this chapter are taken in strictly four dimensions. The formalism can be usefully extended to $D = 4 - 2\overline{\varepsilon}$ dimensions [25–27] where contributions to the amplitude which are rational in four dimensions gain branch cuts and become obtainable by unitarity cuts [28]. However, this extension of the unitarity formalism will not concern us here.

[11] A function $f = (f_1, \ldots, f_n) : \mathbb{C}^n \to \mathbb{C}^n$ is said to have an isolated zero at $a \in \mathbb{C}^n$ iff by choosing a small enough neighborhood U of a one can achieve $f^{-1}(0) \cap U = \{a\}$.

the residues of a triangle integral thus contain the vanishing factor $\Phi(L^{(\bullet)}) = p_j^2(L^{(\bullet)}) = 0$. Similarly, in the sum over all one-loop Feynman diagrams implicit on the left hand side of eq. (2.39), only the diagrams whose integrands contain the four propagators being put on-shell will contribute to the quadruple cut. In the right hand side of eq. (2.63), the summation over species and helicities refers to this restricted set of diagrams; moreover, we have factored the integrand of any such diagram into the product of the four propagators times the tree-level amplitudes separated by these propagators (see figure 2.9).

Defining the Jacobian[12],

$$\mathscr{J}_{\rm BCF} \equiv \left(\det_{i,\mu} \frac{\partial p_i^2(\ell)}{\partial \ell^\mu} \right)^{-1} \Bigg|_{\ell = L, L^\bullet} \tag{2.64}$$

$$= \frac{1}{4(K_1+K_2)^2(K_4+K_1)^2\sqrt{1-2(t_{13}+t_{24})+(t_{13}-t_{24})^2}}\,, \tag{2.65}$$

where $t_{ij} = \frac{K_i^2 K_j^2}{(K_4+K_1)^2(K_1+K_2)^2}$, we can utilize the transformation formula (2.62) to perform the contour integrations in eq. (2.63), yielding

$$c_\square \mathscr{J}_{\rm BCF} = \frac{1}{2}\mathscr{J}_{\rm BCF} \sum_{a\in\{L,L^\bullet\}} \sum_{\substack{\text{helicities,}\\ \text{species}}} \prod_{i=1}^{4} A_i^{\rm tree}\big(p_i(a), p_{i+1}(a)\big)\,. \tag{2.66}$$

Canceling out the Jacobian factor on both sides we are left with the BCF formula for the box coefficient [17],

$$\boxed{c_\square = \frac{1}{2} \sum_{a\in\{L,L^\bullet\}} \sum_{\substack{\text{helicities,}\\ \text{species}}} \prod_{i=1}^{4} A_i^{\rm tree}\big(p_i(a), p_{i+1}(a)\big)\,.} \tag{2.67}$$

The result is stunningly simple: the coefficient of any one-loop box integral in eq. (2.39) is computed by (essentially) multiplying tree amplitudes arising by literally cutting the propagators of the box graph, as illustrated in figure 2.9. In example 2 below we show how the BCF formula (2.67) may be used to determine box coefficients in practice.

Although the Jacobian $\mathscr{J}_{\rm BCF}$ cancels out on both sides of eq. (2.66), we included it explicitly in this equation for good measure[13]. Namely, as we will

[12] To compute the Jacobian, Wick rotate to Euclidean signature and exploit that, prior to evaluation at the leading singularities, the determinant on the right hand side of eq. (2.64) can be rewritten as $16\det_{i,\mu} p_i^\mu = \pm 16\big(\det_{i,j}(p_i\cdot p_j)\big)^{1/2} = \pm 4\big(\det_{i,j}(p_i^2+p_j^2-(p_i-p_j)^2)\big)^{1/2}$. The first equality uses the fact that both the determinant and the square root of the Gram determinant represent the volume of the parallelotope spanned by the four vectors p_i, up to a sign. This sign, along with any potential factors of i introduced by the Wick rotation, can then be determined numerically. Evaluating at the leading singularities produces $\mathscr{J}_{\rm BCF}^{-1} = 4\big(\det_{i,j}(p_i-p_j)^2\big)^{1/2}$, as given more explicitly in eq. (2.65).

[13] Pun intended.

see in the next section, the Jacobian in general has poles of its own which may be utilized when looking for integration contours that distinguish between the basis integrals in eq. (2.39).

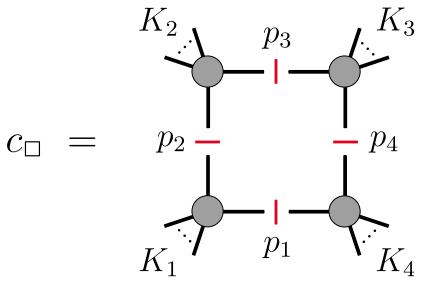

Figure 2.9. Schematic representation of the BCF formula (2.67). The coefficient of any box integral in eq. (2.39) is obtained by multiplying the tree amplitudes represented here by gray blobs. These arise by literally cutting the propagators of the box and promoting the latter to on-shell states.

Example 1: solution of quadruple-cut constraints

In this example we solve the quadruple cut constraints (2.52)-(2.55) for a one-loop box with four massless external momenta. As illustrated in figure 2.10, there are two distinct solutions.

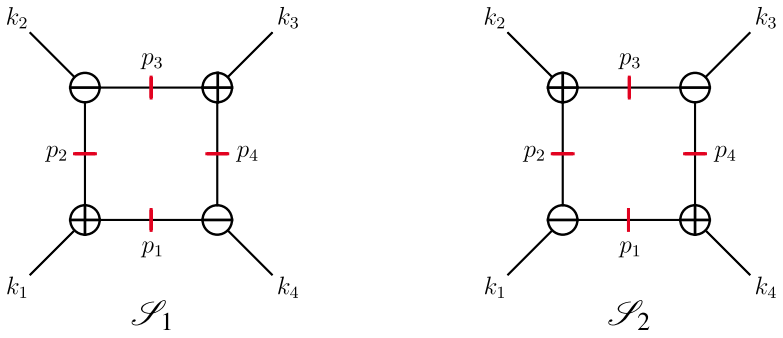

Figure 2.10. The two solutions to the quadruple-cut constraints (2.52)-(2.55) for a one-loop box integral with four massless external momenta.

For definiteness, consider solution $\mathscr{S}_1$. Consulting figure 2.8, the chiralities at the k_1- and k_4-vertices are seen to imply, respectively, that $\langle p_1| \propto \langle 1|$ and $|p_1] \propto |4]$ so that $p_1^\mu = \frac{1}{2}\langle p_1|\gamma^\mu|p_1]$ can be written as

$$p_1^\mu = t_1 \langle 1|\gamma^\mu|4]\,. \tag{2.68}$$

To determine the factor of proportionality we use momentum conservation at the k_1-vertex, $p_1 = p_2 + k_1$:

$$t_1 \langle 1|\gamma^\mu|4] = t_2 \langle 1|\gamma^\mu|2] + \frac{1}{2}\langle 1|\gamma^\mu|1] \tag{2.69}$$

from which we read off

$$t_1|4] = t_2|2] + \frac{1}{2}|1]\,. \tag{2.70}$$

Taking the bracket spinor product with $[2|$ yields $t_1[2\,4] = \frac{1}{2}[2\,1]$ so that

$$t_1 = \frac{[1\,2]}{2[4\,2]}\,. \tag{2.71}$$

The remaining quadruple-cut propagator momenta in figure 2.10 can be obtained completely analogously, and one finds

$$\mathscr{S}_1\text{:}\quad \begin{cases} p_1^\mu = \frac{[1\,2]}{2[4\,2]}\langle 1|\gamma^\mu|4] \\ p_2^\mu = -\frac{[1\,4]}{2[2\,4]}\langle 1|\gamma^\mu|2] \\ p_3^\mu = \frac{[3\,4]}{2[2\,4]}\langle 3|\gamma^\mu|2] \\ p_4^\mu = -\frac{[3\,2]}{2[4\,2]}\langle 3|\gamma^\mu|4] \end{cases} \qquad \mathscr{S}_2\text{:}\quad \begin{cases} p_1^\mu = \frac{\langle 1\,2\rangle}{2\langle 4\,2\rangle}\langle 4|\gamma^\mu|1] \\ p_2^\mu = -\frac{\langle 1\,4\rangle}{2\langle 2\,4\rangle}\langle 2|\gamma^\mu|1] \\ p_3^\mu = \frac{\langle 3\,4\rangle}{2\langle 2\,4\rangle}\langle 2|\gamma^\mu|3] \\ p_4^\mu = -\frac{\langle 3\,2\rangle}{2\langle 4\,2\rangle}\langle 4|\gamma^\mu|3]\,. \end{cases} \tag{2.72}$$

Example 2: calculation of box coefficients

As a simple example of how the BCF formula (2.67) is used in practice, we compute here the box coefficient of the one-loop four-gluon amplitude with external helicites $(1^-,2^-,3^+,4^+)$.

The quadruple cut isolates four corner amplitudes, illustrated in figure 2.11 for the two solutions $\mathscr{S}_1$ and $\mathscr{S}_2$ found in example 1 above. The assignments of internal helicities are dictated by the external helicities and consistency with the chiralities[14] at the vertices of the box. In this case, the assignment of helicities only allow gluons to propagate along the cut propagators.

On top of being gluonic, the corner amplitudes in figure 2.11 are either MHV or $\overline{\text{MHV}}$ and are therefore readily given by the Parke-Taylor formula (A.39). We use the convention that all momenta in the Parke-Taylor formula are outgoing, and the analytic continuation rule[15] that changing the sign of a momentum, $p_i \to -p_i$, is effected by changing the sign of the holomorphic spinor [29]: $\lambda_i^\alpha \to -\lambda_i^\alpha$ while $\widetilde{\lambda}_i^{\dot\alpha} \to \widetilde{\lambda}_i^{\dot\alpha}$.

[14] As can be seen from figure 2.8, a $\oplus$-vertex only allows for an $\overline{\text{MHV}}$-amplitude to be attached. Similarly, a $\ominus$-vertex only allows for an MHV-amplitude to be attached.

[15] The tracking of signs and the continuation rule are only necessary when the entire multiplet of states can circulate in the cut loop, to ensure that the contributions are added with the correct relative signs. Nonetheless, we include this technicality here for completeness.

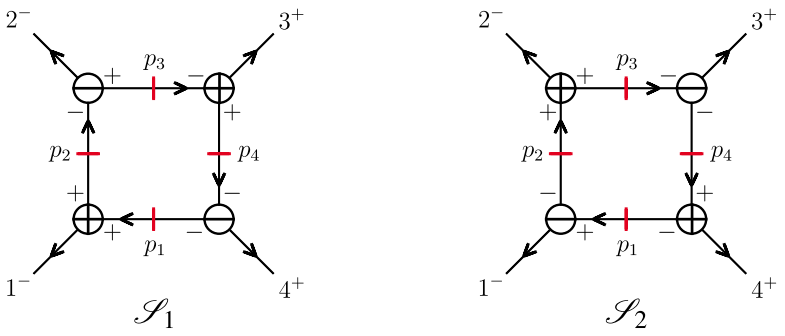

Figure 2.11. The quadruple-cut one-loop four-gluon amplitude with external helicities $(1^-,2^-,3^+,4^+)$, evaluated on solutions $\mathscr{S}_1$ and $\mathscr{S}_2$. The assigned internal and external helicities only allow gluons to propagate in the loop.

Putting the above remarks together, the quadruple-cut amplitude evaluated on the kinematical solution $\mathscr{S}_1$ yields

$$\begin{aligned}
\prod_{j=1}^{4} A_j^{\text{tree}}\Big|_{\mathscr{S}_1} &= \frac{i[-p_1,p_2]^3}{[p_2\,1][1,-p_1]}\,\frac{i\langle 2,-p_2\rangle^3}{\langle -p_2,p_3\rangle\langle p_3\,2\rangle}\,\frac{i[p_4\,3]^3}{[3,-p_3][-p_3,p_4]}\,\frac{i\langle -p_4,p_1\rangle^3}{\langle p_1\,4\rangle\langle 4,-p_4\rangle} \\
&= \frac{\left([p_1\,p_2]\langle 2\,p_2\rangle\right)^2\left([p_1\,p_2]\langle 2\,p_2\rangle\right)\left([p_4\,3]\langle p_4\,p_1\rangle\right)^2\left([p_4\,3]\langle p_4\,p_1\rangle\right)}{\left([p_2\,1]\langle p_2\,p_3\rangle\right)\langle 2\,p_3\rangle\left([1\,p_1]\langle p_1\,4\rangle\right)[p_3\,3]\left([p_3\,p_4]\langle 4\,p_4\rangle\right)} \\
&= \frac{\left(-[p_1\,1]\langle 2\,1\rangle\right)^2\left([p_1\,p_3]\langle 2\,p_3\rangle\right)\left([4\,3]\langle 4\,p_1\rangle\right)^2\left([p_3\,3]\langle p_3\,p_1\rangle\right)}{\left([p_1\,1]\langle p_1\,p_3\rangle\right)\langle 2\,p_3\rangle\left([1\,p_1]\langle p_1\,4\rangle\right)[p_3\,3]\left([p_3\,p_1]\langle 4\,p_1\rangle\right)} \\
&= \langle 1\,2\rangle^2[3\,4]^2 \\
&= is_{12}s_{14}A^{\text{tree}}_{--++}
\end{aligned} \tag{2.73}$$

where

$$A^{\text{tree}}_{--++} = \frac{i\langle 1\,2\rangle^4}{\langle 1\,2\rangle\langle 2\,3\rangle\langle 3\,4\rangle\langle 4\,1\rangle}\,. \tag{2.74}$$

Here, in the second equality of eq. (2.73), we made use of the abovementioned analytic continuation rule and judiciously rearranged the various spinor products. In the third equality we used momentum conservation at the vertices: for example, the equality $p_2 = p_1 - k_1$ implies $[p_1\,p_2]\langle 2\,p_2\rangle = -[p_1\,1]\langle 2\,1\rangle$.

The quadruple-cut amplitude evaluated on the second kinematical solution $\mathscr{S}_2$ turns out to yield the same result as in eq. (2.73). The BCF formula (2.67) then implies that the box coefficient of the $A^{(1)}(1^-,2^-,3^+,4^+)$ amplitude is

$$c_\square = \frac{1}{2}\sum_{a=1,2}\prod_{j=1}^{4} A_j^{\text{tree}}\Big|_{\mathscr{S}_a} = is_{12}s_{14}A^{\text{tree}}_{--++}\,. \tag{2.75}$$

This result is valid for any massless gauge theory, in particular for $\mathscr{N} = 4,2,1,0$ Yang-Mills theory.

Of course, calculating quadruple-cut amplitudes requires more work in practice, especially when the corner amplitudes are non-MHV, or the entire multiplet of states can propagate in the loop. We refer to ref. [17] for more examples.

2.3.2 Direct extraction of triangle coefficients

In the introduction of Section 2.3 we discussed an algorithm for determining the coefficient of any triangle integral: put its three propagators on-shell by applying to both sides of eq. (2.39) a triple cut. This leaves on the right hand side the triple-cut triangle integral along with triple-cut boxes containing one propagator in addition to the three being put on-shell. Using the prior knowledge of the box coefficients from the BCF formula (2.67) one can then disentangle the contributions of these contaminating boxes and determine the desired triangle coefficient.

In this section we will see how a judicious parametrization of the loop momentum allows us to visualize the complex integration contours discussed in the previous section. This in turn enables us to identify contours that single out the triangle integrals directly, avoiding any contamination from boxes.

A good parametrization of the loop momentum in this context is simply one in which the on-shell constraints are easy to solve. Let us recall example 1 in Section 2.3 where we considered the one-loop box integral with four massless external momenta. The quadruple-cut loop momentum ℓ was found to take the form $\langle k_1|\gamma^\mu|k_2]$ or $\langle k_2|\gamma^\mu|k_1]$, respectively for solutions $\mathscr{S}_1$ and $\mathscr{S}_2$; that is, up to addition of the external momenta k_1 and k_2, according to which propagator momentum is labeled ℓ. This suggests a natural ansatz for the loop momentum: express ℓ as a linear combination of the four latter vectors from the outset. At least, this is viable whenever two massless external momenta are available.

In fact, this observation carries over to the general case: given a pair of arbitrary vertex momenta (K_1, K_2), we can obtain a pair of massless momenta $(K_1^\flat, K_2^\flat)$ by applying the "flattening" procedure described in Appendix A. In terms of the flattened vectors, we can then parametrize the loop momentum as,

$$\ell^\mu = \alpha_1 K_1^{\flat\mu} + \alpha_2 K_2^{\flat\mu} + \alpha_3 \langle K_1^\flat|\gamma^\mu|K_2^\flat] + \alpha_4 \langle K_2^\flat|\gamma^\mu|K_1^\flat]\,. \tag{2.76}$$

With this parametrization in hand, let us now consider a general triangle integral, illustrated in figure 2.12.

Labeling the propagator momenta as

$$\begin{aligned} p_1 &\equiv \ell \\ p_2 &\equiv \ell - K_1 \\ p_3 &\equiv \ell - K_1 - K_2\,, \end{aligned} \tag{2.77}$$

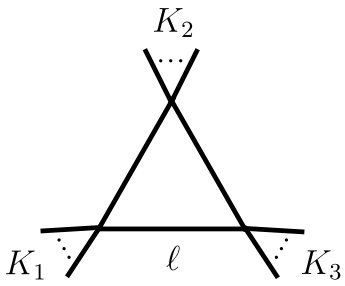

Figure 2.12. The general one-loop triangle integral. The $\cdots$ dots at each vertex represent the presence of an arbitrary number of massless legs. The vertex momenta K_i are sums of these momenta.

the triangle integral can be written in the compact form,

$$I_{\triangle}(K_1,K_2,K_3) = \int_{\mathbb{R}^D} \frac{d^D\ell}{(2\pi)^D} \prod_{i=1}^{3} \frac{1}{p_i^2(\ell)}\,. \tag{2.78}$$

Formally, the triple cut of this integral is defined as the replacement

$$\prod_{i=1}^{3} \frac{1}{p_i^2} \;\longrightarrow\; (-2\pi i)^3 \prod_{i=1}^{3} \delta^{\mathbb{C}}(p_i^2) \tag{2.79}$$

inside the integrand. In analogy with the discussion in the previous section, this amounts to pushing the real-slice integration range $\mathbb{R}^D$ into $\mathbb{C}^4$ in such a way as to encircle the solutions of the joint on-shell constraints $p_1^2 = p_2^2 = p_3^2 = 0$, while leaving the integrand unperturbed.

To find these complex integration contours, first observe that the parametrization (2.76) yields the following form of the squared propagator momenta

$$p_1^2 = \gamma\big(\alpha_1\alpha_2 - 4\alpha_3\alpha_4\big) \tag{2.80}$$

$$p_2^2 = \gamma\Big((\alpha_1 - 1)\Big(\alpha_2 - \tfrac{S_1}{\gamma}\Big) - 4\alpha_3\alpha_4\Big) \tag{2.81}$$

$$p_3^2 = \gamma\Big(\Big(\alpha_1 - \tfrac{S_2}{\gamma} - 1\Big)\Big(\alpha_2 - \tfrac{S_1}{\gamma} - 1\Big) - 4\alpha_3\alpha_4\Big)\,. \tag{2.82}$$

The general solution to the joint on-shell constraints $p_1^2 = p_2^2 = p_3^2 = 0$ then takes the form

$$\alpha_1 = \frac{\gamma(S_2+\gamma)}{\gamma^2 - S_1S_2}\,, \quad \alpha_2 = \frac{S_1S_2(S_1+\gamma)}{\gamma(S_1S_2-\gamma^2)}\,, \quad \alpha_3\alpha_4 = -\frac{S_1S_2(S_1+\gamma)(S_2+\gamma)}{4(\gamma^2-S_1S_2)^2}\,. \tag{2.83}$$

The structure of the last equation defines two distinct cases, according to whether S_1S_2 equals zero or not. Let us start by treating the first case, $S_1S_2 = 0$,

where the triple-cut constraints have two distinct classes of solutions,

$$\mathscr{S}_1\colon \quad (\alpha_1,\alpha_2,\alpha_3,\alpha_4) \;=\; \left(1+\frac{S_2}{\gamma},\, 0,\, z,\, 0\right) \tag{2.84}$$

$$\mathscr{S}_2\colon \quad (\alpha_1,\alpha_2,\alpha_3,\alpha_4) \;=\; \left(1+\frac{S_2}{\gamma},\, 0,\, 0,\, z\right) \tag{2.85}$$

with z denoting a free complex parameter.

Letting $C_{\alpha_i}(z_0)$ denote a small circle in the α_i-plane around z_0, the integration of $\prod_{i=1}^3 \frac{1}{p_i^2}$ over the two 4-tori

$$T_1 \;=\; C_{\alpha_1}\left(1+\tfrac{S_2}{\gamma}\right)\times C_{\alpha_2}(0)\times\Gamma_1\times C_{\alpha_4}(0) \tag{2.86}$$

$$T_2 \;=\; C_{\alpha_1}\left(1+\tfrac{S_2}{\gamma}\right)\times C_{\alpha_2}(0)\times C_{\alpha_3}(0)\times\Gamma_2 \tag{2.87}$$

will respectively localize $(\alpha_1,\alpha_2,\alpha_3,\alpha_4)\in\mathbb{C}^4$ to points in $\mathscr{S}_1$ or $\mathscr{S}_2$, thereby solving the triple-cut constraints. The factors Γ_1 and Γ_2 in eqs. (2.86)-(2.87) are a priori undetermined contours, reflecting the fact that the triple-cut constraints leave the respective parameters α_3 and α_4 completely free.

Accordingly, in the case where $S_1S_2=0$, we *define* the triple cut as the redefinition of contour

$$I_{\triangle}^{\text{triple-cut}} = \frac{1}{2}\sum_{a=1,2}\int_{T_a} d\alpha_1\wedge\cdots\wedge d\alpha_4 \left(\det_{\mu,i}\frac{\partial\ell^\mu}{\partial\alpha_i}\right)\prod_{i=1}^3\frac{1}{p_i^2(\alpha_1,\ldots,\alpha_4)} \tag{2.88}$$

where, like in the quadruple-cut case discussed in Section 2.3.1, we *assume* that one should simply average over the two tori in eqs. (2.86)-(2.87).

The Jacobian associated with the change of variables to the α_i-parameters evaluates to

$$\det_{\mu,i}\frac{\partial\ell^\mu}{\partial\alpha_i} = i\gamma^2\,, \tag{2.89}$$

as can be seen by writing the determinant as the square root of the Gram determinant of the four basis vectors in eq. (2.76), in analogy with the evaluation of the BCF determinant described in Section 2.3.1.

In order to compute the integral in eq. (2.88), let us start by carrying out the contour integrations over the three factors in eqs. (2.86) and (2.87) which are a priori known. The transformation formula (2.62) instructs us to evaluate the determinant

$$\det_{i,j}\frac{\partial p_i^2(\alpha_1,\ldots,\alpha_4)}{\partial\alpha_j}\bigg|_{\mathscr{S}_{1,2}} = 4\gamma(\gamma^2-S_1S_2)z \tag{2.90}$$

which follows directly from eqs. (2.80)-(2.82), without imposing $S_1S_2=0$.

Thus, in the case where $S_1 S_2 = 0$, the triple-cut triangle integral takes the form

$$I_{\triangle}^{\text{triple-cut}} = \frac{i\gamma}{8(\gamma^2 - S_1 S_2)} \sum_{a=1,2} \oint_{\Gamma_a} \frac{dz}{z} \tag{2.91}$$

where the contours Γ_a are a priori undetermined. The pole at $z = 0$, arising as a singularity of the Jacobian, is known as a *composite leading singularity*.

Now, to find useful choices of the contours Γ_a, recall that the triple cut of the right hand side of eq. (2.39) will involve the triple-cut triangle (2.88), as well as triple-cut boxes containing some additional propagator $\frac{1}{(\ell - P)^2}$. On the solution (2.84)-(2.85) to the triple-cut constraints, the inverse propagator evaluates to

$$\begin{aligned}
(\ell - P)^2\big|_{\mathscr{S}_i} &= (-2\ell \cdot P + P^2)\big|_{\mathscr{S}_i} && (2.92)\\
&= \big(-2(a_1^\mu z + a_0^\mu) P_\mu + P^2\big)\big|_{\mathscr{S}_i} && (2.93)\\
&= -2(a_1 \cdot P)(z - z_{\square,\,i})\,, && (2.94)
\end{aligned}$$

writing the loop momentum parametrization (2.76) slightly schematically.

Thus, the triple-cut box integrals take the form

$$\begin{aligned}
I_{\square}^{\text{triple-cut}} &= \frac{1}{2} \sum_{a=1,2} \int_{T_a} \frac{d\alpha_1 \wedge \cdots \wedge d\alpha_4 \left(\det_{\mu,i} \frac{\partial \ell^\mu}{\partial \alpha_i}\right)}{\prod_{i=1}^3 p_i^2(\alpha_1, \ldots, \alpha_4)} \times \frac{1}{(\ell - P)^2} && (2.95)\\
&= -\frac{i\gamma}{16(a_1 \cdot P)(\gamma^2 - S_1 S_2)} \sum_{a=1,2} \oint_{\Gamma_a} \frac{dz}{z(z - z_{\square,\,a})}\,. && (2.96)
\end{aligned}$$

To summarize what we have found so far, in the case where $S_1 S_2 = 0$, the result of applying the triple cut to both sides of eq. (2.39) is

$$\begin{aligned}
&\sum_{a=1,2} \oint_{\Gamma_a} \frac{dz}{z} \left(-\sum_i \frac{c_{\square,\,i}}{2(a_1 \cdot P_i)(z - z_{\square;\,i,a})} + c_{\triangle} \right)\\
&\qquad = \sum_{a=1,2} \sum_{\substack{\text{helicities,}\\ \text{species}}} \oint_{\Gamma_a} \frac{dz}{z} \prod_{j=1}^3 A_j^{\text{tree}}(z) \Big|_{\mathscr{S}_a} \qquad (2.97)
\end{aligned}$$

where the sum over i on the left hand side represents the sum over all triple-cut boxes.

The crucial observation now is that the triple-cut boxes have vanishing residues at $z = \infty$. Therefore, making the choice of contour $\Gamma_a = C_\varepsilon(\infty)$ in eq. (2.97) leaves us with the compact formula [30]

$$S_1 S_2 = 0: \quad c_{\triangle} = -\frac{1}{2} \sum_{a=1,2} \sum_{\substack{\text{helicities,}\\ \text{species}}} \oint_{C_\varepsilon(\infty)} \frac{dz}{z} \prod_{j=1}^3 A_j^{\text{tree}}(z) \Big|_{\mathscr{S}_a}\,. \tag{2.98}$$

Incidentally, as promised earlier, the 4-tori associated with the quadruple cut described formally in eq. (2.60) can now be written explicitly:

$$T_1^{\text{quad-cut}} = C_{\alpha_1}\Big(1+\tfrac{S_2}{\gamma}\Big)\times C_{\alpha_2}(0)\times C_{\alpha_3}(z_{\square,1})\times C_{\alpha_4}(0) \tag{2.99}$$

$$T_2^{\text{quad-cut}} = C_{\alpha_1}\Big(1+\tfrac{S_2}{\gamma}\Big)\times C_{\alpha_2}(0)\times C_{\alpha_3}(0)\times C_{\alpha_4}(z_{\square,2}) \tag{2.100}$$

where we here chose the contours Γ_a in eqs. (2.86)-(2.87) to encircle the poles where the additional box propagator $\frac{1}{(\ell-P)^2}$ becomes on-shell, cf. eqs. (2.92)-(2.94).

In the case where $S_1S_2 \neq 0$, the triple-cut constraints $p_1^2 = p_2^2 = p_3^2 = 0$ have only one class of solutions,

$$\mathscr{S}\colon\ (\alpha_1,\alpha_2,\alpha_3,\alpha_4) = \left(\frac{\gamma(S_2+\gamma)}{\gamma^2-S_1S_2},\ \frac{S_1S_2(S_1+\gamma)}{\gamma(S_1S_2-\gamma^2)},\ z,\ -\frac{S_1S_2(S_1+\gamma)(S_2+\gamma)}{4(\gamma^2-S_1S_2)^2\,z}\right) \tag{2.101}$$

which we have here chosen to parametrize by $z \equiv \alpha_3$. The derivation above extends readily to this case, except that there is now a single contour available over which one can integrate, rather than averaging over two distinct contour integrations. The appropriate change amounts to replacing $\frac{1}{2}\sum_{a=1,2}\oint_{\Gamma_a}(\cdots) \longrightarrow \oint_{\Gamma}(\cdots)$ in the above equations, wherever applicable. The triple-cut box integral here takes the form $\oint_\Gamma \frac{dz}{(z-z_{\square,1})(z-z_{\square,2})}$, but still has a vanishing residue at $z=\infty$. Thus, we can again take the contour Γ in the free parameter to encircle the infinity pole to conclude

$$S_1S_2 \neq 0\colon \quad c_{\triangle} = -\sum_{\substack{\text{helicities,}\\ \text{species}}} \oint_{C_\varepsilon(\infty)} \frac{dz}{z}\prod_{j=1}^{3} A_j^{\text{tree}}(z)\Big|_{\mathscr{S}}\,. \tag{2.102}$$

The formulas (2.98) and (2.102) take a remarkably simple form. In analogy with the BCF formula (2.67), the input needed to obtain the coefficient of any triangle integral in eq. (2.39) is the product of the tree amplitudes that arise by literally cutting the propagators of the triangle graph, as illustrated in figure 2.13.

Following a similar, but somewhat more involved, analysis one may obtain a formula for the coefficient of a generic bubble integral. We refer to eq. (5.28) in ref. [30] for its detailed form. Moreover, we refer to Section 2 of ref. [31] for a strategy for obtaining tadpole coefficients.

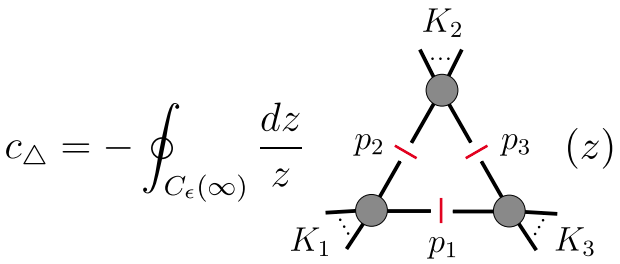

Figure 2.13. Schematic representation of the formulas (2.98) and (2.102). The input needed to produce the coefficient of any triangle integral in eq. (2.39) is the product of the tree amplitudes, represented here by gray blobs. These arise by literally cutting the propagators of the triangle and promoting the latter to on-shell states.

To summarize this section, generalized-unitarity calculations proceed by expressing the one-loop amplitude as a linear combination (2.39) of the basis integrals discussed in Section 2.2.1 with a priori unknown coefficients. These coefficients are then determined from tree-level data through explicit formulas, examples of which include the BCF formula (2.67) for the box coefficient, and Forde's prescription (2.98) and (2.102) for the triangle coefficients.

As we have seen, generalized-unitarity cuts amount to a redefinition of the integration contour: the original one-loop contour $\mathbb{R}^D$ is replaced by a linear combination of tori of real dimension 4, embedded in $\mathbb{C}^4$ and encircling the leading singularities of the one-loop integrand. However, up to this point we have not rigorously derived which particular linear combinations are valid, and which are not. In particular, in deriving both of the formulas (2.67) and (2.98) we made the (plausible) assumption that one should simply average over the two tori that were available in either case.

This naturally raises a related question: do the generalized cuts have an interpretation as an operation performed on *integrated expressions*? The Cutkosky rules state that the ordinary two-particle cuts (2.14) applied to a one-loop Feynman diagram compute the discontinuity of the diagram. It therefore seems reasonable to think that the quadruple cut (2.58) should have some interpretation as the discontinuity of a discontinuity. In reality, however, such an interpretation has a number of ambiguities associated with it and is difficult to make precise.

Generalized-unitarity cuts thus stand on a somewhat different footing than the ordinary two-particle cuts, as their only immediate interpretation is as a redefinition of the integration contour away from the real slice $\mathbb{R}^D$ into a linear combination of leading-singularity cycles. In Chapter 3 we will present a principle dictating how to select correct integration contours.

3. Maximal unitarity at two loops

In this chapter we take the first steps in developing a systematic extension of generalized unitarity to two loops. In analogy with the approach at one loop, the two-loop amplitude is first expanded in a basis of integrals, and our aim is to obtain formulas for the expansion coefficients in terms of tree-level amplitudes, analogous to those in eqs. (2.67), (2.98), (2.102). Throughout this chapter, we restrict our attention to four-gluon amplitudes and consider only the extraction of the coefficients of basis integrals with the maximal number of propagators.

For four massless external states, these integrals have the topology of a double box, illustrated in figure 3.1

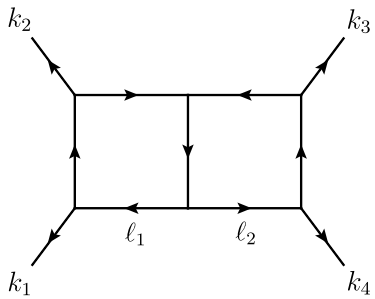

Figure 3.1. The double box integral $P^{**}_{2,2}[1]$.

and given by

$$P^{**}_{2,2}[f(\ell_1,\ell_2)] \;=\; \int \frac{d^D\ell_1}{(2\pi)^D}\,\frac{d^D\ell_2}{(2\pi)^D}\,\frac{f(\ell_1,\ell_2)}{\ell_1^2(\ell_1-k_1)^2(\ell_1-K_{12})^2(\ell_1+\ell_2)^2} \times \frac{1}{\ell_2^2(\ell_2-k_4)^2(\ell_2-K_{34})^2} \tag{3.1}$$

where $K_{i\cdots j} \equiv k_i + \cdots + k_j$, and the notation follows ref. [32]. Moreover, we refer to the function $f(\ell_1,\ell_2)$ as a *numerator insertion*, following the terminology in Section 2.2.1.

The basis composition of the four-point two-loop amplitude takes the form

$$A_4^{(2)} \;=\; c_{1,\sigma_1}(\varepsilon)\, P^{**}_{2,2;\,\sigma_1}[1] \;+\; c_{2,\sigma_1}(\varepsilon)\, P^{**}_{2,2;\,\sigma_1}[\ell_1 \cdot k_4] \;+\; \cdots \qquad (3.2)$$

where the $\cdots$ refer to contributions from other cyclic permutations of the double-box integrals, as well as from integrals with fewer propagators and rational terms. Although the integral coefficients c_1, c_2 etc. in general have non-trivial dependence on the dimensional regulator, we will restrict our attention to obtaining the leading $\mathcal{O}(\varepsilon^0)$ part.

Our approach to determine the two-loop integral coefficients is similar in spirit to the BCF approach reviewed in Section 2.3.1 for obtaining box coefficients. That is, we apply a *heptacut*[1] to both sides of the decomposition (3.2), setting all double-box propagators on-shell. As the two loop momenta have a total of eight degrees of freedom, setting seven propagators on-shell will leave one remaining degree of freedom. The effect of cutting all available propagators at two loops is therefore different from that at one loop where the quadruple cut used to extract the box coefficient freezes all components of the loop momentum.

As it turns out, however, it is possible to freeze the remaining degree of freedom z at two loops. This is achieved by integrating z over a small circle enclosing poles of the Jacobian that arises from linearizing the on-shell constraints. We will explain this in detail Section 3.1. In analogy with the discussion of generalized cuts at one loop in Section 2.3, the two-loop heptacut is appropriately defined as a redefinition of the range of integration in eq. (3.2), from $\mathbb{R}^D \times \mathbb{R}^D$ to a contour embedded in $\mathbb{C}^8$. This contour has real dimension 8 and encircles points where all seven propagators are on-shell and where, in addition, the Jacobian has poles. Each such point may be encircled by a T^8-torus, all of which are determined in Section 3.1, and the contour is some a priori undetermined linear combination of the T^8-tori obtained in this section. The two-loop contour is thus analogous to the quadruple-cut contour in Section 2.3.1, being a linear combination of the T^4-tori in eqs. (2.99)-(2.100).

In Section 3.2 we establish a selection principle determining which contours —that is, which linear combinations of the T^8-tori—produce correct results for the integral coefficients. We proceed in Section 3.3 to apply this principle to obtain formulas for the double-box coefficients in terms of contour integrations of products of tree-level amplitudes along valid contours. In Section 3.4 these formulas are applied to obtain the coefficients of various four-gluon amplitudes. Section 3.5 provides a comparison between the approach of Paper I and that of the leading-singularity method.

[1] To be accurate, as we are only concerned with finding the coefficients to $\mathcal{O}(\varepsilon^0)$, it suffices to consider only the four-dimensional components of the loop momentum as far as cuts are concerned.

We remark that the presentation in Sections 3.1-3.4 below is essentially that of Sections III-VI in Paper I, adding here a few comments and skipping a few technical derivations.

3.1 Maximal cuts at two loops

In this section we determine the T^8-tori associated with the double-box on-shell constraints

$$\begin{aligned} \ell_1^2 \,=\, 0\,, \qquad (\ell_1-k_1)^2 \,=\, 0\,, \qquad (\ell_1-K_{12})^2 \,=\, 0\,, \qquad \ell_2^2 = 0\,, \\ (\ell_2-k_4)^2 \,=\, 0\,, \qquad (\ell_2-K_{34})^2 \,=\, 0\,, \qquad (\ell_1+\ell_2)^2 \,=\, 0\,. \end{aligned} \tag{3.3}$$

The double box has seven propagators; if we cut all of them, that is put all of the momenta they are carrying to on-shell values, we will be left with one additional degree of freedom.

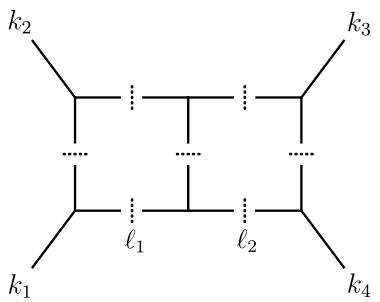

Figure 3.2. The heptacut double box.

At two loops, it is convenient to write the four-dimensional heptacut integral symbolically in terms of complex delta functions as follows

$$\begin{aligned} \int \frac{d^4\ell_1}{(2\pi)^4}\,\frac{d^4\ell_2}{(2\pi)^4}\,\delta^{\mathbb{C}}\big(\ell_1^2\big)\,\delta^{\mathbb{C}}\big((\ell_1-k_1)^2\big)\,\delta^{\mathbb{C}}\big((\ell_1-K_{12})^2\big)\,\delta^{\mathbb{C}}\big((\ell_1+\ell_2)^2\big) \\ \times\delta^{\mathbb{C}}\big(\ell_2^2\big)\,\delta^{\mathbb{C}}\big((\ell_2-k_4)^2\big)\,\delta^{\mathbb{C}}\big((\ell_2-K_{34})^2\big)\,. \end{aligned} \tag{3.4}$$

In analogy with the discussion in Section 2.3.1, this integral is properly defined as an integration of the integrand of eq. (3.1) (with $f(\ell_1,\ell_2)=1$) over some a priori unknown $\mathbb{C}^8$-embedded contour encircling the leading singularities of the integrand. The heptacut integral in eq. (3.4) is depicted in figure 3.2.

To solve the on-shell equations (3.3), we use the following parametrization of the loop momenta,

$$\begin{aligned}\ell_1^\mu &= \alpha_1 k_1^\mu + \alpha_2 k_2^\mu + \frac{s_{12}\alpha_3}{2\langle 1\,4\rangle[4\,2]}\langle 1^-|\,\gamma^\mu\,|2^-\rangle + \frac{s_{12}\alpha_4}{2\langle 2\,4\rangle[4\,1]}\langle 2^-|\,\gamma^\mu\,|1^-\rangle\,,\\ \ell_2^\mu &= \beta_1 k_3^\mu + \beta_2 k_4^\mu + \frac{s_{12}\beta_3}{2\langle 3\,1\rangle[1\,4]}\langle 3^-|\,\gamma^\mu\,|4^-\rangle + \frac{s_{12}\beta_4}{2\langle 4\,1\rangle[1\,3]}\langle 4^-|\,\gamma^\mu\,|3^-\rangle\,.\end{aligned} \tag{3.5}$$

Using this parametrization, the six corresponding heptacut equations involving only one loop momentum are

$$\begin{aligned}\ell_1^2 &= s_{12}\left(\alpha_1\alpha_2 + \tfrac{\alpha_3\alpha_4}{\chi(\chi+1)}\right) = 0\\ (\ell_1 - k_1)^2 &= s_{12}\left((\alpha_1-1)\alpha_2 + \tfrac{\alpha_3\alpha_4}{\chi(\chi+1)}\right) = 0\\ (\ell_1 - K_{12})^2 &= s_{12}\left((\alpha_1-1)(\alpha_2-1) + \tfrac{\alpha_3\alpha_4}{\chi(\chi+1)}\right) = 0\\ \ell_2^2 &= s_{12}\left(\beta_1\beta_2 + \tfrac{\beta_3\beta_4}{\chi(\chi+1)}\right) = 0\\ (\ell_2 - k_4)^2 &= s_{12}\left(\beta_1(\beta_2-1) + \tfrac{\beta_3\beta_4}{\chi(\chi+1)}\right) = 0\\ (\ell_2 - K_{34})^2 &= s_{12}\left((\beta_1-1)(\beta_2-1) + \tfrac{\beta_3\beta_4}{\chi(\chi+1)}\right) = 0\end{aligned} \tag{3.6}$$

where

$$\chi \equiv \frac{s_{14}}{s_{12}}\,. \tag{3.7}$$

We can simplify these equations, obtaining

$$\begin{aligned}\alpha_1 &= 1\,, \qquad \alpha_2 = 0\,, \qquad \alpha_3\alpha_4 = 0\,,\\ \beta_1 &= 0\,, \qquad \beta_2 = 1\,, \qquad \beta_3\beta_4 = 0\,.\end{aligned} \tag{3.8}$$

These equations have four distinct solutions. If we substitute these values into eq. (3.3), we find for the last equation

$$\begin{aligned}0 &= (\ell_1+\ell_2)^2 = 2\ell_1\cdot\ell_2\\ &= 2\left(k_1^\mu + \frac{s_{12}\alpha_3}{2\langle 1\,4\rangle[4\,2]}\langle 1^-|\,\gamma^\mu\,|2^-\rangle + \frac{s_{12}\alpha_4}{2\langle 2\,4\rangle[4\,1]}\langle 2^-|\,\gamma^\mu\,|1^-\rangle\right)\\ &\quad\times\left(k_{4\mu} + \frac{s_{12}\beta_3}{2\langle 3\,1\rangle[1\,4]}\langle 3^-|\,\gamma_\mu\,|4^-\rangle + \frac{s_{12}\beta_4}{2\langle 4\,1\rangle[1\,3]}\langle 4^-|\,\gamma_\mu\,|3^-\rangle\right)\,.\end{aligned} \tag{3.9}$$

For two of the four solutions to eqs. (3.8), this equation has two solutions, so that overall we find six solutions to the heptacut equations (3.6), (3.9). To each of the six solutions $\mathscr{S}_j$, we can associate a seven-torus in the parameters α_i and β_i that encircles the solution.

For the solution $\alpha_4 = 0 = \beta_4$, the last equation (3.9) simplifies to

$$0 = \left([4\,1] + \frac{s_{12}\alpha_3}{\langle 1\,4\rangle}\right)\left(\langle 1\,4\rangle - \frac{s_{12}\beta_3}{[1\,4]}\right), \tag{3.10}$$

which has two distinct solutions,

$$\begin{aligned} \mathscr{S}_1 : &\qquad \alpha_3 = -\chi\,, \quad \beta_3 \text{ arbitrary}\,; \\ \mathscr{S}_2 : &\qquad \beta_3 = -\chi\,, \quad \alpha_3 \text{ arbitrary}\,. \end{aligned} \tag{3.11}$$

In all solutions, we will relabel the remaining degree of freedom, calling it z.

Likewise, the solution $\alpha_3 = 0 = \beta_3$ also yields two solutions to eq. (3.9),

$$\begin{aligned} \mathscr{S}_3 : &\qquad \alpha_4 = -\chi\,, \quad \beta_4 = z\,; \\ \mathscr{S}_4 : &\qquad \beta_4 = -\chi\,, \quad \alpha_4 = z\,. \end{aligned} \tag{3.12}$$

For the remaining two solutions, the last equation (3.9) does not factorize, and we obtain only one solution; for $\alpha_3 = 0 = \beta_4$,

$$\mathscr{S}_5 : \qquad \alpha_4 = z, \quad \beta_3 = -(\chi+1)\frac{z+\chi}{z+\chi+1}\,; \tag{3.13}$$

and for $\alpha_4 = 0 = \beta_3$,

$$\mathscr{S}_6 : \qquad \alpha_3 = z, \quad \beta_4 = -(\chi+1)\frac{z+\chi}{z+\chi+1}\,. \tag{3.14}$$

In the last two solutions, we could equally well have chosen a different parametrization, where β_3 or β_4 respectively are set to z. This just amounts to a change of variables, of course, but does break the manifest symmetry between the two loops.

The existence of six kinematic solutions can also be understood from holomorphicity considerations of the cuts. When we cut all propagators, each of the six vertices in the double box has three massless momenta attached. We can write these momenta in terms of spinors, $k^\mu = \lambda^\alpha \sigma^\mu_{\alpha\dot\alpha}\tilde\lambda^{\dot\alpha}$. To restate our findings in figure 2.8, momentum conservation at each vertex [22] then implies that either,

1) the holomorphic spinors λ of the momenta are collinear (proportional), $\lambda_a \propto \lambda_b \propto \lambda_c$. We will depict such a vertex using a circled plus ($\oplus$). Such a vertex would allow only an $\overline{\text{MHV}}$ tree amplitude to be attached (of course the holomorphicity properties of the cut are independent of any tree amplitude).

2) the antiholomorphic spinors $\tilde\lambda$ of the momenta are collinear, $\tilde\lambda_a \propto \tilde\lambda_b \propto \tilde\lambda_c$. We will depict such a vertex using a circled minus ($\ominus$). Such a vertex would allow only an MHV tree amplitude to be attached.

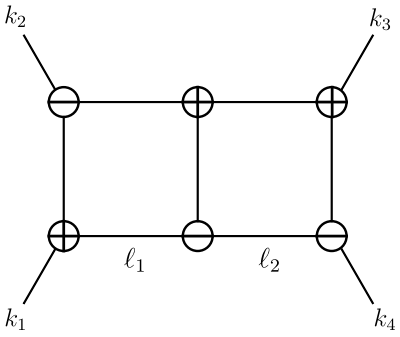

Solution $\mathscr{S}_1$, obtained by setting

$$\alpha_3 = -\chi\,, \qquad \beta_3 = z\,,$$
$$\alpha_4 = 0\,, \qquad \beta_4 = 0\,.$$

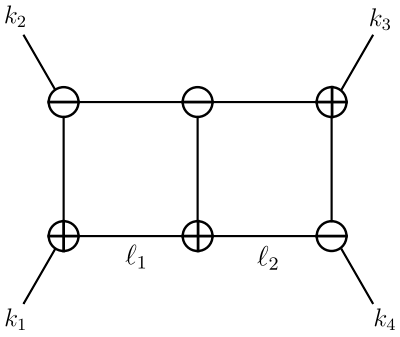

Solution $\mathscr{S}_2$, obtained by setting

$$\alpha_3 = z\,, \qquad \beta_3 = -\chi\,,$$
$$\alpha_4 = 0\,, \qquad \beta_4 = 0\,.$$

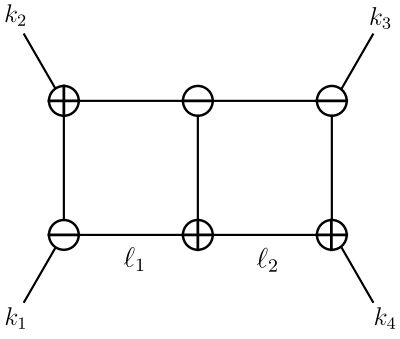

Solution $\mathscr{S}_3$, obtained by setting

$$\alpha_3 = 0\,, \qquad \beta_3 = 0\,,$$
$$\alpha_4 = -\chi\,, \qquad \beta_4 = z\,.$$

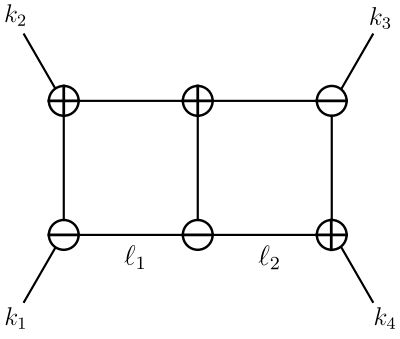

Solution $\mathscr{S}_4$, obtained by setting

$$\alpha_3 = 0\,, \qquad \beta_3 = 0\,,$$
$$\alpha_4 = z\,, \qquad \beta_4 = -\chi\,.$$

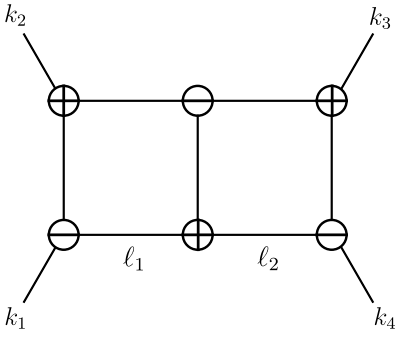

Solution $\mathscr{S}_5$, obtained by setting

$$\alpha_3 = 0\,, \qquad \beta_3 = -(\chi+1)\tfrac{z+\chi}{z+\chi+1}\,,$$
$$\alpha_4 = z\,, \qquad \beta_4 = 0\,.$$

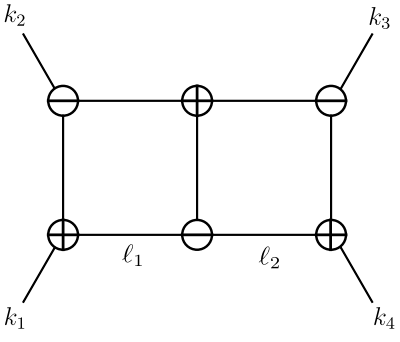

Solution $\mathscr{S}_6$, obtained by setting

$$\alpha_3 = z\,, \qquad \beta_3 = 0\,,$$
$$\alpha_4 = 0\,, \qquad \beta_4 = -(\chi+1)\tfrac{z+\chi}{z+\chi+1}\,.$$

Figure 3.3. The six classes of solutions to the heptacut equations (3.6) for the two-loop planar double box.

For general kinematics, neither the external holomorphic spinors λ_j nor the external antiholomorphic spinors $\tilde{\lambda}_j$ are collinear. A configuration with an uninterrupted chain of either $\oplus$ or $\ominus$ vertices connecting any two external legs is thus disallowed. There are exactly six ways of assigning these two labelings to vertices avoiding such chains, hence six solutions. The six solutions are shown diagrammatically in figure 3.3. From this figure we observe that parity $\oplus \longleftrightarrow \ominus$ exchanges the solutions $(\mathscr{S}_1 \longleftrightarrow \mathscr{S}_3)$, $(\mathscr{S}_2 \longleftrightarrow \mathscr{S}_4)$ and $(\mathscr{S}_5 \longleftrightarrow \mathscr{S}_6)$. The solutions within each pair are therefore referred to as parity-conjugate solutions.

In evaluating the contour integrals represented by the delta functions in eq. (3.4), we encounter two Jacobians: one from changing variables from the components of ℓ_j to the α_i and β_i; and one from actually performing the contour integrals in the latter variables. It is the latter Jacobian that is important for our purposes. The former Jacobian is equal to $J_\alpha J_\beta$, where

$$J_\alpha = \det_{\mu,i} \frac{\partial \ell_1^\mu}{\partial \alpha_i} = -\frac{i s_{12}^2}{4\chi(\chi+1)}, \qquad J_\beta = \det_{\mu,i} \frac{\partial \ell_2^\mu}{\partial \beta_i} = -\frac{i s_{12}^2}{4\chi(\chi+1)}. \quad (3.15)$$

To evaluate the latter Jacobian, we may note that three of the delta functions (or equivalently three of the contour integrals) involve only α variables, and three involve only β variables. We can thus split up the problem into three steps: computing the Jacobian associated with ℓ_1, that is with the α variables alone; computing the Jacobian associated with ℓ_2, that is with the β variables alone; and finally, computing the Jacobian associated with the middle propagator, involving both ℓ_1 and ℓ_2.

For each of the six solutions, we must compute the Jacobian independently. As an example, consider the second solution $\mathscr{S}_2$. The first Jacobian arises from considering the integral,

$$\int d\alpha_1 d\alpha_2 d\alpha_4\, \delta\Big[s_{12}\Big(\alpha_1\alpha_2 + \tfrac{\alpha_3\alpha_4}{\chi(\chi+1)}\Big)\Big]\, \delta\Big[s_{12}\Big((\alpha_1-1)\alpha_2 + \tfrac{\alpha_3\alpha_4}{\chi(\chi+1)}\Big)\Big] \times \delta\Big[s_{12}\Big((\alpha_1-1)(\alpha_2-1) + \tfrac{\alpha_3\alpha_4}{\chi(\chi+1)}\Big)\Big], \quad (3.16)$$

associated with the ℓ_1 loop. Define

$$\begin{pmatrix} g_1(\alpha_1,\alpha_2,\alpha_4) \\ g_2(\alpha_1,\alpha_2,\alpha_4) \\ g_3(\alpha_1,\alpha_2,\alpha_4) \end{pmatrix} = \begin{pmatrix} s_{12}\Big(\alpha_1\alpha_2 + \tfrac{\alpha_3\alpha_4}{\chi(\chi+1)}\Big) \\ s_{12}\Big((\alpha_1-1)\alpha_2 + \tfrac{\alpha_3\alpha_4}{\chi(\chi+1)}\Big) \\ s_{12}\Big((\alpha_1-1)(\alpha_2-1) + \tfrac{\alpha_3\alpha_4}{\chi(\chi+1)}\Big) \end{pmatrix}. \quad (3.17)$$

The first Jacobian is then,

$$J_1 = \det_{i,j} \frac{\partial g_i}{\partial \alpha_j} \;=\; s_{12}^3 \det \begin{pmatrix} \alpha_2 & \alpha_1 & \frac{\alpha_3}{\chi(\chi+1)} \\ \alpha_2 & \alpha_1 - 1 & \frac{\alpha_3}{\chi(\chi+1)} \\ \alpha_2 - 1 & \alpha_1 - 1 & \frac{\alpha_3}{\chi(\chi+1)} \end{pmatrix} \;=\; -\frac{s_{12}^3}{\chi(\chi+1)}\alpha_3 \tag{3.18}$$

The fact that the Jacobians appear in the denominator as determinants rather than as absolute values of determinants owes to the transformation formula (2.62) satisfied by the implicit complex contour integrations.

Similarly, the second Jacobian arises from considering the integral,

$$\int d\beta_1 d\beta_2 d\beta_4 \, \delta\Big[s_{12}\left(\beta_1\beta_2 + \tfrac{\beta_3\beta_4}{\chi(\chi+1)}\right)\Big] \, \delta\Big[s_{12}\left(\beta_1(\beta_2-1) + \tfrac{\beta_3\beta_4}{\chi(\chi+1)}\right)\Big] \times \delta\Big[s_{12}\left((\beta_1-1)(\beta_2-1) + \tfrac{\beta_3\beta_4}{\chi(\chi+1)}\right)\Big] \,, \tag{3.19}$$

associated with the ℓ_2 loop. Define

$$\begin{pmatrix} h_1(\beta_1,\beta_2,\beta_4) \\ h_2(\beta_1,\beta_2,\beta_4) \\ h_3(\beta_1,\beta_2,\beta_4) \end{pmatrix} \;=\; \begin{pmatrix} s_{12}\left(\beta_1\beta_2 + \frac{\beta_3\beta_4}{\chi(\chi+1)}\right) \\ s_{12}\left(\beta_1(\beta_2-1) + \frac{\beta_3\beta_4}{\chi(\chi+1)}\right) \\ s_{12}\left((\beta_1-1)(\beta_2-1) + \frac{\beta_3\beta_4}{\chi(\chi+1)}\right) \end{pmatrix} . \tag{3.20}$$

The second Jacobian is then,

$$J_2 = \det_{i,j} \frac{\partial h_i}{\partial \beta_j} \;=\; s_{12}^3 \det \begin{pmatrix} \beta_2 & \beta_1 & \frac{\beta_3}{\chi(\chi+1)} \\ \beta_2 - 1 & \beta_1 & \frac{\beta_3}{\chi(\chi+1)} \\ \beta_2 - 1 & \beta_1 - 1 & \frac{\beta_3}{\chi(\chi+1)} \end{pmatrix} \;=\; \frac{s_{12}^3}{\chi(\chi+1)}\beta_3 \,. \tag{3.21}$$

The remaining integration we must consider is over α_3 and β_3,

$$\frac{1}{2}\int d\alpha_3 d\beta_3 \frac{J_\alpha J_\beta}{J_1 J_2} \, \delta\left[\frac{s_{12}}{2\chi}(\alpha_3+\chi)(\beta_3+\chi)\right] = \frac{1}{32 s_{12}^2}\int \frac{d\alpha_3 d\beta_3}{\alpha_3\beta_3} \, \delta\left[\frac{s_{12}}{2\chi}(\alpha_3+\chi)(\beta_3+\chi)\right] , \tag{3.22}$$

which leaves a remaining contour integration over z (*i.e.* α_3), along with the overall inverse Jacobian,

$$J^{-1}(z) = -\frac{1}{16 s_{12}^3 z(z+\chi)} \,. \tag{3.23}$$

The computation for the other five solutions is similar; it turns out that we obtain the same overall Jacobian for all solutions. The contour for the z integration remains to be chosen; for this solution, there are two possible non-trivial

contours, one encircling $z=0$, and the other, encircling $z=-\chi$. (We set aside a possible non-trivial contour encircling $z=\infty$, as its contribution when integrating an arbitrary multiplying function $f(z)$ sums to zero when combined with the contributions of these two contours.)

The poles at $z=0$ and $z=-\chi$ are known as *composite leading singularities*; encircling these poles corresponds, in the language of ref. [33], to cutting an effective eighth propagator. In addition, for solutions $\mathscr{S}_{5,6}$, the denominator of $\beta_{3,4}$ (eqs. (3.13) and (3.14)) can give rise to additional poles at $z=-\chi-1$ in tensor integrals. (As noted in Section 2.2.1, in a slight abuse of language, we refer to integrals with no free indices, but numerator powers of the loop momenta contracted into external vectors, as "tensor integrals".)

Collecting the information above, we have the following T^8-tori we can utilize in seeking equations for integral coefficients,

$$\begin{aligned}
T_{1,1} &= \tau\times C_{\alpha_3}(-\chi)\times C_{\alpha_4}(0)\times C_{\beta_3=z}(0)\times C_{\beta_4}(0)\\
T_{1,2} &= \tau\times C_{\alpha_3}(-\chi)\times C_{\alpha_4}(0)\times C_{\beta_3=z}(-\chi)\times C_{\beta_4}(0)\\
T_{2,1} &= \tau\times C_{\alpha_3=z}(0)\times C_{\alpha_4}(0)\times C_{\beta_3}(-\chi)\times C_{\beta_4}(0)\\
T_{2,2} &= \tau\times C_{\alpha_3=z}(-\chi)\times C_{\alpha_4}(0)\times C_{\beta_3}(-\chi)\times C_{\beta_4}(0)\\
T_{3,1} &= \tau\times C_{\alpha_3}(0)\times C_{\alpha_4}(-\chi)\times C_{\beta_3}(0)\times C_{\beta_4=z}(0)\\
T_{3,2} &= \tau\times C_{\alpha_3}(0)\times C_{\alpha_4}(-\chi)\times C_{\beta_3}(0)\times C_{\beta_4=z}(-\chi)\\
T_{4,1} &= \tau\times C_{\alpha_3}(0)\times C_{\alpha_4=z}(0)\times C_{\beta_3}(0)\times C_{\beta_4}(-\chi)\\
T_{4,2} &= \tau\times C_{\alpha_3}(0)\times C_{\alpha_4=z}(-\chi)\times C_{\beta_3}(0)\times C_{\beta_4}(-\chi)\\
T_{5,1} &= \tau\times C_{\alpha_3}(0)\times C_{\alpha_4=z}(0)\times C_{\beta_3}\left(-\tfrac{(1+\chi)(z+\chi)}{z+\chi+1}\right)\times C_{\beta_4}(0)\\
T_{5,2} &= \tau\times C_{\alpha_3}(0)\times C_{\alpha_4=z}(-\chi)\times C_{\beta_3}\left(-\tfrac{(1+\chi)(z+\chi)}{z+\chi+1}\right)\times C_{\beta_4}(0)\\
T_{5,3} &= \tau\times C_{\alpha_3}(0)\times C_{\alpha_4=z}(-\chi-1)\times C_{\beta_3}\left(-\tfrac{(1+\chi)(z+\chi)}{z+\chi+1}\right)\times C_{\beta_4}(0)\\
T_{6,1} &= \tau\times C_{\alpha_3=z}(0)\times C_{\alpha_4}(0)\times C_{\beta_3}(0)\times C_{\beta_4}\left(-\tfrac{(1+\chi)(z+\chi)}{z+\chi+1}\right)\\
T_{6,2} &= \tau\times C_{\alpha_3=z}(-\chi)\times C_{\alpha_4}(0)\times C_{\beta_3}(0)\times C_{\beta_4}\left(-\tfrac{(1+\chi)(z+\chi)}{z+\chi+1}\right)\\
T_{6,3} &= \tau\times C_{\alpha_3=z}(-\chi-1)\times C_{\alpha_4}(0)\times C_{\beta_3}(0)\times C_{\beta_4}\left(-\tfrac{(1+\chi)(z+\chi)}{z+\chi+1}\right)
\end{aligned} \tag{3.24}$$

where each subscript denotes the variable in whose plane the circle lies, and where

$$\tau = C_{\alpha_1}(1)\times C_{\alpha_2}(0)\times C_{\beta_1}(0)\times C_{\beta_2}(1)\,, \tag{3.25}$$

corresponding to the on-shell values in eq. (3.8). We will refer to these eight-tori as *leading-singularity cycles*.

Naively, we could deform the original contour of integration for the double box (3.1), along the product of real axes for all components of ℓ_1 and ℓ_2, to any linear combination of contours in eq. (3.24) that we wish. However, an

arbitrary deformation will not preserve the vanishing of total derivatives such as

$$\int \frac{d^D\ell}{(2\pi)^D} \frac{\varepsilon(\ell,k_1,k_2,k_4)}{\ell^2(\ell-k_1)^2(\ell-k_1-k_2)^2(\ell+k_4)^2}\,. \tag{3.26}$$

In order to ensure that such objects vanish as they must, we impose constraints on the contours. We derive these in the next section.

3.2 Constraint equations for contours

Integral reductions are implicitly part of the simplifications applied to the sum over Feynman diagrams defining an amplitude in order to obtain the basis decomposition (3.2). The basis at two loops will contain integrals with up to eight propagators in the planar[2] case [32], though a specific complete and independent choice of integrals for a general amplitude has not yet been written down.

As we saw in Section 2.2.1, integral reductions at one loop involve only rewriting dot products of the loop momentum in terms of linear combinations of propagators and external invariants, along with the use of Lorentz invariance and parity to eliminate some integrals. For the box integral, in particular, the only non-trivial constraint arises from the use of parity, which requires that

$$\int \frac{d^D\ell}{(2\pi)^D} \frac{\varepsilon(\ell,k_1,k_2,k_4)}{\ell^2(\ell-k_1)^2(\ell-k_1-k_2)^2(\ell+k_4)^2} = 0\,. \tag{3.27}$$

This constraint must be respected by the unitarity procedure; otherwise, applying a cut to the original integral and to the integral after reduction would yield different, and hence inconsistent, answers. Thus, we arrive at the following principle dictating how maximal-cut contours must be chosen in order to ultimately produce correct results for the integral coefficients:

Selection principle for contours. *Contours must be chosen so as to annilate any loop integrand which has a vanishing integration on* $(\mathbb{R}^D)^{\otimes L}$ *where L denotes the loop order.*

At one loop, this constraint simply expresses invariance of the contour under parity conjugation of the on-shell solutions. Indeed, in the case of the quadruple cut, recall from the discussion below eq. (2.60) that there are two 4-tori encircling the leading singularities of the integrand. In Section 2.3.1 it was not clear which linear combinations $\omega_1 T^4_\varepsilon(L) + \omega_2 T^4_\varepsilon(L^\bullet)$ define valid integration contours, and we simply *assumed* that the choice $\omega_1 = \omega_2 = \frac{1}{2}$, defining the quadruple cut in eq. (2.61) specifies a valid contour.

[2]The same restriction to eight propagators or fewer presumably applies in the non-planar case as well, using arguments along the same lines as given in ref. [32].

From the above selection principle one can immediately infer $\omega_1 = \omega_2$. Namely, changing the contour $\mathbb{R}^D \longrightarrow \omega_1 T_\varepsilon^4(L) + \omega_2 T_\varepsilon^4(L^\bullet)$ in eq. (3.27), one finds the constraint equation $\omega_1 - \omega_2 = 0$, as shown in Section II of Paper I. (Setting the winding numbers equal to the value $\frac{1}{2}$ is simply a normalization, guaranteeing that the quadruple cut of the box integral itself is essentially one, cf. the left hand side of eq. (2.66).)

Similar constraints arise at two loops. In particular, we must require that the vanishing of the following Levi-Civita insertions

$$\begin{aligned} &P^{**}_{2,2}[\varepsilon(\ell_1,k_2,k_3,k_4)]\,, \quad P^{**}_{2,2}[\varepsilon(\ell_2,k_2,k_3,k_4)]\,, \quad P^{**}_{2,2}[\varepsilon(\ell_1,\ell_2,k_1,k_2)]\,, \\ &P^{**}_{2,2}[\varepsilon(\ell_1,\ell_2,k_1,k_3)]\,, \quad P^{**}_{2,2}[\varepsilon(\ell_1,\ell_2,k_2,k_3)]\,, \end{aligned} \tag{3.28}$$

continues to hold for integration over our chosen linear combination of contours. This is the complete set of Levi-Civita symbols that arises during integral reduction, after using momentum conservation.

At two loops, additional reductions are required in order to arrive at a linearly-independent set of basis integrals. These are usually obtained through integration-by-parts (IBP) relations; that is, they correspond to adding a total derivative to the original integrand. Each such total derivative, or equivalently each non-trivial reduction identity, gives rise to a constraint requiring that the unitarity procedure give vanishing coefficients for the additional terms; or equivalently, that the unitarity procedure respect the reduction equations. This is not automatically true contour-by-contour, and hence gives rise to non-trivial constraints on the choice of contours, and the weighting of different solutions.

In two-loop four-point amplitudes, we can express all dot products of loop momenta with external vectors in terms of eight dot products: $\ell_j \cdot k_1$, $\ell_j \cdot k_2$, $\ell_j \cdot k_4$, and $\ell_j \cdot v$, where $v^\mu = \varepsilon(\mu, k_1, k_2, k_4)$. Just as at one loop, odd powers of v will give rise to vanishing integrals, as expressed in the Levi-Civita constraints discussed above. Even powers can again be re-expressed in terms of the other dot products (up to terms involving the (-2ε)-dimensional components of the loop momentum). All integrals can then be rewritten in terms of the six dot products of the loop momenta with the external momenta.

Of these six dot products, three of them — $\ell_1 \cdot k_1$, $\ell_1 \cdot k_2$, $\ell_2 \cdot k_4$ — can be rewritten as linear combinations of the propagator denominators and external invariants. One additional dot product of ℓ_2 — say $\ell_2 \cdot k_2$ — can be rewritten in terms of the remaining two ($\ell_1 \cdot k_4$ and $\ell_2 \cdot k_1$), propagator denominators, and external invariants. The remaining two dot products are called irreducible. At a first stage, then, before using IBP identities, we can reduce an arbitrary double-box integral appearing in a gauge-theory amplitude to a linear combination of the 22 different integrals that can arise with powers of the two irreducible numerators.

We have the following naively-irreducible integrals,

$$P^{**}_{2,2}[(\ell_1\cdot k_4)^m\,(\ell_2\cdot k_1)^n]\,,\qquad \begin{cases} 0\le m,n\le 4\\ 0\le m+n\le 6\end{cases} \tag{3.29}$$

In the massless case, it turns out that there are 20 IBP relations between these integrals, which allow further reductions. These reductions allow us to pick certain pairs, for example,

$$P^{**}_{2,2}[1]\ \text{ and }\ P^{**}_{2,2}[\ell_1\cdot k_4]\,, \tag{3.30}$$

as master integrals for the set in eq. (3.29), and thus also as basis integrals for an amplitude.

The remaining integrals dictated by the Feynman rules for gauge theory are given in terms of these two by integration-by-parts identities. For example,

$$\begin{aligned}
P^{**}_{2,2}[\ell_2\cdot k_1] &= P^{**}_{2,2}[\ell_1\cdot k_4]\\
P^{**}_{2,2}[(\ell_1\cdot k_4)(\ell_2\cdot k_1)] &= \frac{1}{8}\chi s_{12}^2 P^{**}_{2,2}[1]-\frac{3}{4}s_{12}P^{**}_{2,2}[\ell_1\cdot k_4]+\cdots\\
P^{**}_{2,2}[(\ell_2\cdot k_1)^2] &= -\frac{\varepsilon\chi s_{12}^2}{4(1-2\varepsilon)}P^{**}_{2,2}[1]+\frac{(\chi+3\varepsilon)s_{12}}{2(1-2\varepsilon)}P^{**}_{2,2}[\ell_1\cdot k_4]+\cdots\\
P^{**}_{2,2}[(\ell_1\cdot k_4)^2] &= -\frac{\varepsilon\chi s_{12}^2}{4(1-2\varepsilon)}P^{**}_{2,2}[1]+\frac{(\chi+3\varepsilon)s_{12}}{2(1-2\varepsilon)}P^{**}_{2,2}[\ell_1\cdot k_4]+\cdots\\
P^{**}_{2,2}[(\ell_1\cdot k_4)(\ell_2\cdot k_1)^2] &= -\frac{(1-3\varepsilon)\chi s_{12}^3}{16(1-2\varepsilon)}P^{**}_{2,2}[1]+\frac{(3-9\varepsilon-2\varepsilon\chi)s_{12}^2}{8(1-2\varepsilon)}P^{**}_{2,2}[\ell_1\cdot k_4]+\cdots\\
P^{**}_{2,2}[(\ell_1\cdot k_4)^2(\ell_2\cdot k_1)] &= -\frac{(1-3\varepsilon)\chi s_{12}^3}{16(1-2\varepsilon)}P^{**}_{2,2}[1]+\frac{(3-9\varepsilon-2\varepsilon\chi)s_{12}^2}{8(1-2\varepsilon)}P^{**}_{2,2}[\ell_1\cdot k_4]+\cdots\\
P^{**}_{2,2}[(\ell_2\cdot k_1)^3] &= \frac{\varepsilon\chi(1-2\chi-3\varepsilon)s_{12}^3}{16(1-\varepsilon)(1-2\varepsilon)}P^{**}_{2,2}[1]\\
&\quad+\frac{\big(2\chi^2-3\varepsilon(1-2\chi)+\varepsilon^2(9+2\chi)\big)s_{12}^2}{8(1-\varepsilon)(1-2\varepsilon)}P^{**}_{2,2}[\ell_1\cdot k_4]+\cdots\\
P^{**}_{2,2}[(\ell_1\cdot k_4)^3] &= \frac{\varepsilon\chi(1-2\chi-3\varepsilon)s_{12}^3}{16(1-\varepsilon)(1-2\varepsilon)}P^{**}_{2,2}[1]\\
&\quad+\frac{\big(2\chi^2-3\varepsilon(1-2\chi)+\varepsilon^2(9+2\chi)\big)s_{12}^2}{8(1-\varepsilon)(1-2\varepsilon)}P^{**}_{2,2}[\ell_1\cdot k_4]+\cdots
\end{aligned} \tag{3.31}$$

where the ellipses denote additional integrals with fewer propagators. We must require that these equations (and the other 12 we do not display explicitly) are preserved by the choice of contours. The contour integrals which implement the augmented heptacut will yield vanishing results for the integrals with fewer propagators, so they do not enter the constraint equations. As we are considering only four-dimensional cuts, the augmented heptacuts are effectively four-dimensional.

In order to find the explicit form of the constraint equations, denote the weight of contour $T_{j,r}$ by $a_{r,j}$,

$$\begin{aligned} a_{1,j} &\longrightarrow \text{ encircling } z=0 \text{ for solution } \mathscr{S}_j \\ a_{2,j} &\longrightarrow \text{ encircling } z=-\chi \text{ for solution } \mathscr{S}_j \\ a_{3,j} &\longrightarrow \text{ encircling } z=-\chi-1 \text{ for solution } \mathscr{S}_j\,. \end{aligned} \tag{3.32}$$

For a numerator insertion of $f(\ell_1,\ell_2)$ in the numerator of the double box, the augmented heptacut is then,

$$\begin{aligned} &\sum_{j=1}^{4}\sum_{r=1}^{2} a_{r,j}\oint_{T_{j,r}} d^4\alpha_i d^4\beta_i\, f(\ell_1,\ell_2)\times \text{Propagators}(\ell_1,\ell_2)\Big|_{\text{param}} \\ &+\sum_{j=5}^{6}\sum_{r=1}^{3} a_{r,j}\oint_{T_{j,r}} d^4\alpha_i d^4\beta_i\, f(\ell_1,\ell_2)\times \text{Propagators}(\ell_1,\ell_2)\Big|_{\text{param}} \end{aligned} \tag{3.33}$$

where the notation $|_{\text{param}}$ indicates that we use the parametrization of ℓ_1 and ℓ_2 given in eq. (3.5). The signs in front of each coefficient $a_{r,j}$ in the result will depend on the orientation chosen for the corresponding contour; but this sign will drop out of final formulas for integral coefficients so long as this orientation is chosen consistently throughout the calculation.

We can write down a compact expression for the augmented heptacut of the general tensor integral,

$$\begin{aligned} P^{**}_{2,2}[(\ell_1\cdot k_4)^m(\ell_2\cdot k_1)^n] \;=\; -\frac{1}{128}\Bigg[&\delta_{m,0}\left(\frac{s_{12}}{2}\right)^{n-3}\oint_{\Gamma_1}\frac{dz}{z}(z+\chi)^{n-1} \\ &+\delta_{n,0}\left(\frac{s_{12}}{2}\right)^{m-3}\oint_{\Gamma_2}\frac{dz}{z}(z+\chi)^{m-1} \\ &+\delta_{m,0}\left(\frac{s_{12}}{2}\right)^{n-3}\oint_{\Gamma_3}\frac{dz}{z}(z+\chi)^{n-1} \\ &+\delta_{n,0}\left(\frac{s_{12}}{2}\right)^{m-3}\oint_{\Gamma_4}\frac{dz}{z}(z+\chi)^{m-1} \\ &+\left(\frac{s_{12}}{2}\right)^{m+n-3}\oint_{\Gamma_5}\frac{dz}{z}(z+\chi)^{m-1}\left(-\frac{z}{z+\chi+1}\right)^n \\ &+\left(\frac{s_{12}}{2}\right)^{m+n-3}\oint_{\Gamma_6}\frac{dz}{z}(z+\chi)^{m-1}\left(-\frac{z}{z+\chi+1}\right)^n\Bigg] \end{aligned} \tag{3.34}$$

where Γ_j denotes the z component of $\sum_r a_{r,j}T_{j,r}$, and where in our notation, the contour integral implicitly includes a factor of $1/(2\pi i)$, as noted in Section **??**.

We can evaluate this expression using the contours as weighted in eq. (3.33); we find,

$$P^{**}_{2,2}[1] \;=\; -\frac{1}{16\chi s_{12}^3}\sum_{j=1}^{6}(a_{1,j}-a_{2,j}) \tag{3.35}$$

$$P^{**}_{2,2}[(\ell_1\cdot k_4)^m] \;=\; -\frac{1}{32 s_{12}^2}\left(\frac{\chi s_{12}}{2}\right)^{m-1}\sum_{j\neq 1,3} a_{1,j} \tag{3.36}$$

$$\begin{aligned} P^{**}_{2,2}[(\ell_2\cdot k_1)^n] \;=\; & -\frac{1}{32 s_{12}^2}\left(\frac{\chi s_{12}}{2}\right)^{n-1} \\ & \times(-a_{2,6}+a_{3,6}-a_{2,5}+a_{3,5}+a_{1,1}+a_{1,3}) \end{aligned} \tag{3.37}$$

$$\begin{aligned} P^{**}_{2,2}[(\ell_1\cdot k_4)^m(\ell_2\cdot k_1)^n] \;=\; & \frac{1}{64 s_{12}}\left(-\frac{s_{12}}{2}\right)^{m+n-2}\Big[\theta\big(\min(m,n)-\tfrac{5}{2}\big)(\chi+1)(\chi+2) \\ & +\theta\big(\min(m,n)-\tfrac{3}{2}\big)(m+n-3)(\chi+1)+\theta\big(\min(m,n)-\tfrac{1}{2}\big)\Big](a_{3,6}+a_{3,5}) \end{aligned} \tag{3.38}$$

where $m,n\geq 1$ and the last result is valid only for $0\leq m+n\leq 6$ and $0\leq m,n\leq 4$ (corresponding to the numerator insertions allowed in gauge theory in $D=4-2\varepsilon$ dimensions).

With these expressions, we now turn to the constraint equations. Let us begin with the equations arising from the insertion of Levi-Civita tensors (3.28). As an example, let us consider $\varepsilon(\ell_1,k_2,k_3,k_4)$,

$$\begin{aligned} 0 \;=\; & P^{**}_{2,2}[\varepsilon(\ell_1,k_2,k_3,k_4)] \\ =\; & -\frac{1}{16 s_{12}^3}\left(\oint_{\Gamma_1}\frac{dz}{z}\frac{\varepsilon\left(k_1^\mu-\frac{s_{12}}{2}\frac{\langle 1^-|\gamma^\mu|2^-\rangle}{\langle 1^-|4|2^-\rangle}\chi,k_2,k_3,k_4\right)}{z+\chi}\right. \\ & +\oint_{\Gamma_2}\frac{dz}{z}\frac{\varepsilon\left(k_1^\mu+\frac{s_{12}}{2}\frac{\langle 1^-|\gamma^\mu|2^-\rangle}{\langle 1^-|4|2^-\rangle}z,k_2,k_3,k_4\right)}{z+\chi}+\oint_{\Gamma_3}\frac{dz}{z}\frac{\varepsilon\left(k_1^\mu-\frac{s_{12}}{2}\frac{\langle 2^-|\gamma^\mu|1^-\rangle}{\langle 2^-|4|1^-\rangle}\chi,k_2,k_3,k_4\right)}{z+\chi} \\ & +\oint_{\Gamma_4}\frac{dz}{z}\frac{\varepsilon\left(k_1^\mu+\frac{s_{12}}{2}\frac{\langle 2^-|\gamma^\mu|1^-\rangle}{\langle 2^-|4|1^-\rangle}z,k_2,k_3,k_4\right)}{z+\chi}+\oint_{\Gamma_5}\frac{dz}{z}\frac{\varepsilon\left(k_1^\mu+\frac{s_{12}}{2}\frac{\langle 2^-|\gamma^\mu|1^-\rangle}{\langle 2^-|4|1^-\rangle}z,k_2,k_3,k_4\right)}{z+\chi} \\ & \left.+\oint_{\Gamma_6}\frac{dz}{z}\frac{\varepsilon\left(k_1^\mu+\frac{s_{12}}{2}\frac{\langle 1^-|\gamma^\mu|2^-\rangle}{\langle 1^-|4|2^-\rangle}z,k_2,k_3,k_4\right)}{z+\chi}\right). \end{aligned} \tag{3.39}$$

Evaluating this expression on the augmented heptacut (3.33) we obtain

$$\begin{aligned} 0 \;=\; & \frac{1}{32 s_{12}^2}\left[(a_{2,2}+a_{2,6}-a_{1,1}+a_{2,1})\,\varepsilon\!\left(\frac{\langle 1^-|\,\gamma^\mu\,|2^-\rangle}{\langle 1^-|\,4\,|2^-\rangle}, k_2, k_3, k_4\right)\right. \\ & \left. +\,(a_{2,5}+a_{2,4}-a_{1,3}+a_{2,3})\,\varepsilon\!\left(\frac{\langle 2^-|\,\gamma^\mu\,|1^-\rangle}{\langle 2^-|\,4\,|1^-\rangle}, k_2, k_3, k_4\right)\right] \qquad (3.40) \\ =\; & \frac{1}{32 s_{12}^2}\big(a_{2,2}+a_{2,6}-a_{2,5}-a_{2,4}-a_{1,1}+a_{2,1}+a_{1,3}-a_{2,3}\big) \\ & \times\varepsilon\!\left(\frac{\langle 1^-|\,\gamma^\mu\,|2^-\rangle}{\langle 1^-|\,4\,|2^-\rangle}, k_2, k_3, k_4\right), \end{aligned}$$

where the last line follows from the fact that the two Levi-Civita symbols appearing on the first line are equal but opposite in value.

The constraints arising from the insertions of respectively $\varepsilon(\ell_2, k_2, k_3, k_4)$ and $\varepsilon(\ell_1, \ell_2, k_i, k_j)$ with $(i,j) \in \{(1,2),(1,3),(2,3)\}$ are obtained similarly. In total, we have the following constraint equations from the five Levi-Civita insertions,

$$\begin{aligned} a_{2,2}+a_{2,6}-a_{2,5}-a_{2,4}-a_{1,1}+a_{2,1}+a_{1,3}-a_{2,3} &= 0 \\ a_{1,2}-a_{2,2}-a_{1,6}+a_{3,6}+a_{1,5}-a_{3,5}-a_{1,4}+a_{2,4}-a_{2,1}+a_{2,3} &= 0 \\ a_{2,6}-a_{3,6}-a_{2,5}+a_{3,5}-a_{1,1}+a_{1,3} &= 0 \qquad (3.41) \\ a_{2,6}-a_{2,5}-a_{1,1}+a_{1,3} &= 0 \\ a_{1,2}-a_{1,6}+a_{2,6}+a_{1,5}-a_{2,5}-a_{1,4}-a_{1,1}+a_{1,3} &= 0, \end{aligned}$$

or equivalently

$$\begin{aligned} a_{1,2}-a_{1,6}+a_{1,5}-a_{1,4} &= 0 \\ a_{2,2}-a_{2,4}+a_{2,1}-a_{2,3} &= 0 \\ a_{2,6}-a_{2,5}-a_{1,1}+a_{1,3} &= 0 \qquad (3.42) \\ a_{3,6}-a_{3,5} &= 0. \end{aligned}$$

This set has one equation less: not all the equations from the Levi-Civita symbols are independent. We see that these equations are solved by insisting that the contours for parity-conjugate pairs of solutions ($\mathscr{S}_1 \longleftrightarrow \mathscr{S}_3$, $\mathscr{S}_2 \longleftrightarrow \mathscr{S}_4$ and $\mathscr{S}_5 \longleftrightarrow \mathscr{S}_6$) carry equal weights. This nicely generalizes the one-loop constraint on contours, discussed below eq. (3.27).

We next impose the constraints following from the IBP reductions. Evaluating both sides of equations (3.31) along with the remaining 12 reduction equations not displayed above, and setting $\varepsilon = 0$, we find two additional constraint equations,

$$\begin{aligned} a_{1,2}+a_{1,6}+a_{1,5}+a_{1,4} &= -a_{2,6}+a_{3,6}-a_{2,5}+a_{3,5}+a_{1,1}+a_{1,3}, \\ a_{3,6}+a_{3,5} &= -\frac{1}{2}\sum_{j=1}^{6}(a_{1,j}-a_{2,j})+\frac{3}{2}\sum_{j\neq 1,3} a_{1,j}. \qquad (3.43) \end{aligned}$$

In principle, one might expect 18 additional equations from the remaining reduction identities; but these all turn out to be automatically satisfied on the solutions of this pair of equations.

Beyond ensuring that all the reduction identities are valid, we ultimately want to determine the coefficients of the two basis integrals (3.30). Because the system of equations leaves many undetermined weights $a_{r,j}$, we have the freedom to choose values which also kill one or the other of the basis integrals. That is, we can choose contours for which one or the other of the basis integrals has vanishing augmented heptacut. To project out the second basis integral, $P^{**}_{2,2}[\ell_1 \cdot k_4]$, we should also require that eq. (3.36) with $m = 1$ vanish,

$$\sum_{j\neq 1,3} a_{1,j} = 0\,. \tag{3.44}$$

To project out the first basis integral, $P^{**}_{2,2}[1]$, we should require that eq. (3.35) vanish,

$$\sum_{j=1}^{6} (a_{1,j} - a_{2,j}) = 0\,. \tag{3.45}$$

The following values

$$\begin{aligned}
a_{1,1} &= -2u+v, \quad a_{2,1} = u\,,\\
a_{1,2} &= -2u+v, \quad a_{2,2} = u\,,\\
a_{1,3} &= -2u+v, \quad a_{2,3} = u\,,\\
a_{1,4} &= -2u+v, \quad a_{2,4} = u\,,\\
a_{1,5} &= 2u-v, \quad a_{2,5} = v, \quad a_{3,5} = 2u\,,\\
a_{1,6} &= 2u-v, \quad a_{2,6} = v, \quad a_{3,6} = 2u\,,
\end{aligned} \tag{3.46}$$

(where u, v are real parameters) solve all the constraint equations (3.42), (3.43), although we emphasize that it is not the most general solution. In addition, these values also set the heptacut of the basis integral $P^{**}_{2,2}[\ell_1 \cdot k_4]$ to zero, thereby allowing us to extract the coefficient of the first basis integral, $P^{**}_{2,2}[1]$. We will call a specific choice of contours weighted by these values P_1, leaving the dependence on u and v implicit. A particularly simple solution is given by $u = \frac{1}{2}$ and $v = 1$. This choice is illustrated schematically in figure 3.4(a).

Similarly, the following values,

$$\begin{aligned}
a_{1,1} &= -2u+v, \quad a_{2,1} = u\,,\\
a_{1,2} &= -2u+v, \quad a_{2,2} = u\,,\\
a_{1,3} &= -2u+v, \quad a_{2,3} = u\,,\\
a_{1,4} &= -2u+v, \quad a_{2,4} = u\,,\\
a_{1,5} &= 6u-v, \quad a_{2,5} = v, \quad a_{3,5} = 6u\,,\\
a_{1,6} &= 6u-v, \quad a_{2,6} = v, \quad a_{3,6} = 6u\,,
\end{aligned} \tag{3.47}$$

(where again u, v are real parameters) solve all the constraint equations (3.42), (3.43), sets to zero the heptacut of the basis integral $P^{**}_{2,2}[1]$, and thereby extracts the coefficient of $P^{**}_{2,2}[\ell_1 \cdot k_4]$. We will call a specific choice of contours

weighted by these values P_2, again leaving the dependence on u and v implicit. The choice $u = \frac{1}{2}$ and $v = 1$ again gives a particularly simple solution. It is illustrated schematically in figure 3.4(b).

In general, contours which satisfy all constraint equations (3.42, 3.43) and moreover set the heptacut of all but one master integral to zero will directly extract the coefficient of this one master integral. Accordingly, we refer to such contours as *master contours*.

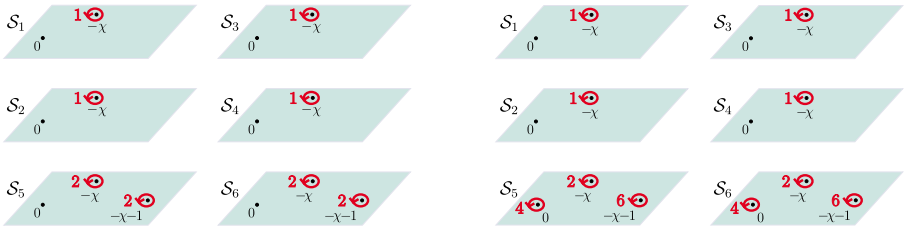

Figure 3.4. Schematic representation of contours for the coefficients of the two basis double boxes: (a) the scalar double box, $P^{**}_{2,2}[1]$ (b) the double box with an irreducible numerator insertion, $P^{**}_{2,2}[\ell_1 \cdot k_4]$. The contours encircle the leading singularities distributed across the six kinematical solutions; the integers next to the contours indicate the winding number. Both representations are for the choice $u = \frac{1}{2}$ and $v = 1$ in eqs. (3.46) and (3.47).

Before turning to the extraction procedure, we may observe that the four-dimensional heptacuts do not suffice to extract information about the coefficients beyond $\mathcal{O}(\varepsilon^0)$. The problem is that we can find non-vanishing linear combinations of tensor integrals whose heptacut integrand vanishes identically for all six solutions. As a result, not only do integrals over all contours $T_{j,a}$ vanish, but even integrals constructed by multiplying the integrand by an arbitrary function of the remaining degree of freedom z would vanish. We call such linear combinations *magic*. Examples of magic combinations include,

$$M_1 = P^{**}_{2,2}[2,2] + \frac{s_{12}}{2} P^{**}_{2,2}[2,1] + \frac{s_{12}}{2} P^{**}_{2,2}[1,2] - \chi \left(\frac{s_{12}}{2}\right)^2 P^{**}_{2,2}[1,1], \quad (3.48)$$

$$M_2 = P^{**}_{2,2}[3,2] + \frac{s_{12}}{2} P^{**}_{2,2}[3,1] + \frac{s_{12}}{2} P^{**}_{2,2}[2,2] - \chi \left(\frac{s_{12}}{2}\right)^2 P^{**}_{2,2}[2,1], \quad (3.49)$$

where the abbreviated notation $P^{**}_{2,2}[m,n]$ is defined by,

$$P^{**}_{2,2}[m,n] \equiv P^{**}_{2,2}[(\ell_1 \cdot k_4)^m (\ell_2 \cdot k_1)^n]. \quad (3.50)$$

After use of IBP reduction equations, the magic combinations do not vanish, but the coefficients of both master integrals are of $\mathcal{O}(\varepsilon)$.

3.3 Master formulas for integral coefficients

With solutions to the constraint equations that also isolate specific basis integrals in hand, we can write down a procedure for computing the coefficients of the integrals in the master equation (3.2). To do so, we apply the augmented heptacuts to the left-hand side of the master equation. The basic heptacut will break apart the two-loop amplitude into a product of six on-shell tree amplitudes, one for each vertex in the double box. We will be left with the integral over the z contour. On the right-hand side, we have the two basis integrals (3.30) chosen earlier. Here, apply the augmented heptacut, and perform all integrations. This gives us the relation,

$$\begin{aligned}\frac{1}{128}\left(\frac{2}{s_{12}}\right)^3 \sum_{i=1}^{6} \oint_{\Gamma_i} \frac{dz}{z(z+\chi)}(-i)\prod_{j=1}^{6} A_j^{\text{tree}}(z) \\ = \frac{c_1}{16\chi s_{12}^3}\sum_{j=1}^{6}(a_{1,j}-a_{2,j}) + \frac{c_2}{32 s_{12}^2}\sum_{j\neq 1,3} a_{1,j}\,. \end{aligned} \tag{3.51}$$

In this equation, the product of amplitudes arises from a factor of a tree-level amplitude at each vertex of the double box with all seven propagators cut.

As explained in the previous section, through a judicious choice of contours, we can make the coefficient of c_2 in this equation vanish, or alternatively the coefficient of c_1 vanish. This would then allow us to solve for c_1 and c_2, respectively. We gave such choices in eqs. (3.46) and (3.47). Using them, we can write an expression for c_1,

$$c_1 \;=\; \frac{i\chi}{8u}\oint_{P_1}\frac{dz}{z(z+\chi)}\prod_{j=1}^{6} A_j^{\text{tree}}(z)\,, \tag{3.52}$$

and for c_2,

$$c_2 \;=\; -\frac{i}{4 s_{12} u}\oint_{P_2}\frac{dz}{z(z+\chi)}\prod_{j=1}^{6} A_j^{\text{tree}}(z)\,. \tag{3.53}$$

The right-hand sides of these equations must be summed over possible helicity and particle-species assignments. The explicit integration is understood to be over the z component of P_1 and P_2 respectively, with the integrations over the other α_i and β_i implicit in the solutions $\mathscr{S}_j$, and with the dependence of P_j on the parameters u and v left implicit. The formulas (3.52) and (3.53) represent the central result of this chapter. They are valid for any gauge theory, and indeed for any amplitude satisfying the power-counting rules of gauge theory. These formulas are not manifestly independent of the choice of contour, but the constraint equations ensure that they are. We will see explicit examples in the next section. Of course, the independence of the final result of the choice of contour does not mean that the results at intermediate steps are indepen-

dent; certain choices of contour may in fact simplify analytic or numerical calculations. We have already seen hints of this in the choices of P_1 and P_2, where some values of u and v will require evaluation of fewer contours, and hence possibly fewer numerical evaluations if the formulas (3.52) and (3.53) are used in a numerical setting.

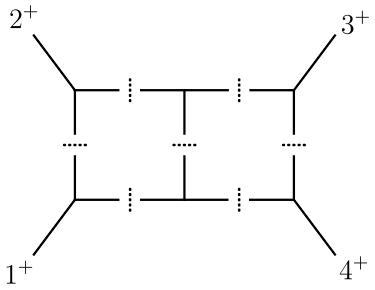

Figure 3.5. Graphical representation of $\prod_{j=1}^{6} A_j^{\text{tree}}(z)\Big|_{D=4}$ for the all-plus QCD amplitude.

At one loop, one can choose a basis so that integral coefficients are independent of the dimensional regulator ε, and four-dimensional cuts suffice to compute all of them. (Computing the rational terms requires use of D-dimensional cuts.) At two loops, the coefficients of integral reductions, and hence generally of integrals in eq. 3.2, will depend explicitly on ε. In particular, c_1 and c_2 above will depend explicitly on ε. In general, this dependence cannot be extracted from four-dimensional heptacuts alone, because of the vanishing of magic combinations discussed in Section 3.2. We can also see the need for cuts beyond four dimensions, or considerably relaxing some of the heptacut conditions, by considering the two-loop all-plus amplitude, $A_4^{\text{2-loop}}(++++)$, computed in ref. [34]. In this case, the product of tree amplitudes in eqs. (3.52) and (3.53) will necessarily vanish in four dimensions, because there is no assignment of internal helicities in figure 3.5 that will leave all three-point amplitudes non-vanishing. The same observation still holds if we relax some of the cut conditions, examining hexacuts or pentacuts.

3.4 Examples

In this section, we apply the formalism developed in previous sections to several examples of two-loop four-point amplitudes. We use the master formulas (3.52) and (3.53) to compute the coefficients to $\mathcal{O}(\varepsilon^0)$ of the two double box basis integrals, $P^{**}_{2,2}[1]$ and $P^{**}_{2,2}[\ell_1 \cdot k_4]$. We consider three different contributions to four-gluon amplitudes in supersymmetric theories with $\mathcal{N} = 4, 2, 1$ supersymmetries: the s- and t-channel contributions to $A_4^{\text{2-loop}}(1^-, 2^-, 3^+, 4^+)$,

and the s-channel contributions to $A_4^{\text{2-loop}}(1^-,2^+,3^-,4^+)$. (The t-channel contributions to the latter amplitudes can be obtained by relabeling the arguments of the s-channel contribution.)

We will express the results as multiples of the tree-level four-gluon amplitudes,

$$A^{\text{tree}}_{--++} = \frac{i\langle 1\,2\rangle^4}{\langle 1\,2\rangle\langle 2\,3\rangle\langle 3\,4\rangle\langle 4\,1\rangle}\,, \tag{3.54}$$

and

$$A^{\text{tree}}_{-+-+} = \frac{i\langle 1\,3\rangle^4}{\langle 1\,2\rangle\langle 2\,3\rangle\langle 3\,4\rangle\langle 4\,1\rangle}\,. \tag{3.55}$$

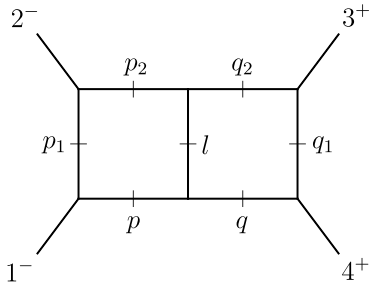

Figure 3.6. The labeling of internal momenta used in Section 3.4, here shown for the s-channel contribution to $A_4^{\text{2-loop}}(1^-,2^-,3^+,4^+)$.

In this section, it will be convenient to have a label for each cut propagator in the double box. Accordingly, we adopt a different labeling from previous sections, displayed in figure 3.6.

3.4.1 The s-channel contribution to $A_4^{\text{2-loop}}(1^-,2^-,3^+,4^+)$

For this contribution, shown above in figure 3.6, the helicities of the external states allow only gluons to propagate in either loop. For this reason, we will get the same result independent of the number of supersymmetries. We find that for all six solutions to the on-shell equations,

$$\prod_{j=1}^{6} A_j^{\text{tree}} \;=\; -is_{12}^2 s_{23} A^{\text{tree}}_{--++}\,. \tag{3.56}$$

We can then use eq. (3.52) to obtain

$$\begin{aligned} c_1 \;&=\; -is_{12}^2 s_{23} A^{\text{tree}}_{--++}\left(\frac{(v-2u)i}{4u} - \frac{iv}{4u} - \frac{i}{2}\right) \\ &=\; -s_{12}^2 s_{23} A^{\text{tree}}_{--++}\,; \end{aligned} \tag{3.57}$$

and eq. (3.53) to obtain

$$\begin{aligned} c_2 &= -is_{12}^2 s_{23} A^{\text{tree}}_{--++} \left(-\frac{(v-2u)i}{s_{12}u\chi} - \frac{(6u-v)i}{2s_{12}u\chi} + \frac{i}{s_{12}\chi} + \frac{iv}{2s_{12}u\chi} \right) \\ &= 0\,. \end{aligned} \tag{3.58}$$

We see that the dependence on the parameters u and v has disappeared, as expected. In the $\mathcal{N}=4$ theory, these turn out to be the exact coefficients; in theories with fewer supersymmetries, there are additional terms of $\mathcal{O}(\varepsilon)$ in these coefficients.

3.4.2 The t-channel contribution to $A_4^{\text{2-loop}}(1^-,2^-,3^+,4^+)$

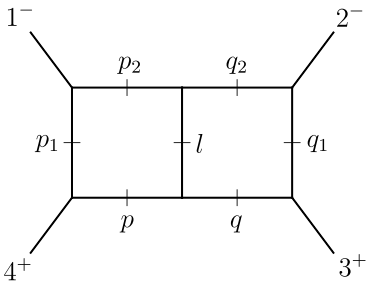

Figure 3.7. The heptacut for the t-channel contribution to $A_4^{\text{2-loop}}(1^-,2^-,3^+,4^+)$.

We turn next to the computation of the coefficients in the t-channel contribution to the same amplitude considered in the previous section. The heptacut for this contribution is shown in figure 3.7. In applying the formulas for the coefficients, we have cyclicly permuted the external momentum arguments, $(1,2,3,4) \longrightarrow (4,1,2,3)$, so that we must replace $\chi \longrightarrow \chi^{-1}$. Otherwise, they are of course unchanged.

In this contribution, computing the required products of tree amplitudes is more involved, and the computation also requires sums over supermultiplets of states propagating in the loops. As an example, we work through the computation of the product in solution $\mathcal{S}_2$. We have two possible helicity assignments for the internal lines, shown in figure 3.8. For gluon internal lines, we multiply the amplitudes at the six vertices to obtain,

$$\prod_{j=1}^{6} A_j^{\text{tree, gluon}} = -\frac{1}{\Delta} \times \begin{cases} A^4 & \text{for configuration A}\,, \\ B^4 & \text{for configuration B}\,, \end{cases} \tag{3.59}$$

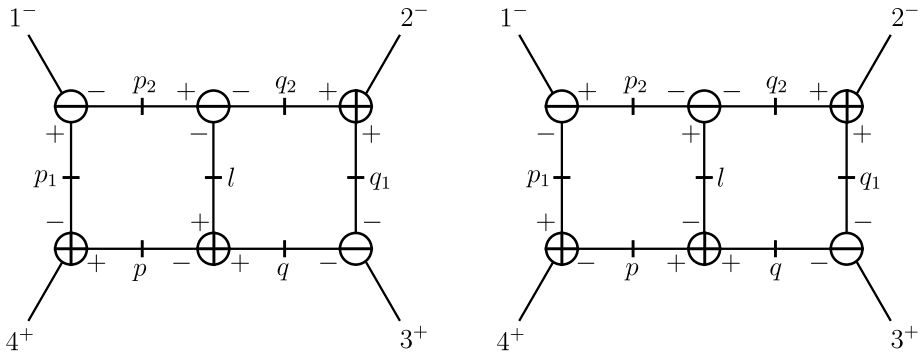

Figure 3.8. The two distinct assignments of internal helicities in solution $\mathscr{S}_2$ for the t-channel double-box contributions to $A_4^{2\text{-loop}}(1^-,2^-,3^+,4^+)$: (a) configuration A and (b) configuration B.

where

$$\begin{aligned} A^4 &= \big([p\,4]\,\langle 1\,p_2\rangle\,\langle q_2\,l\rangle\,[l\,q]\,\langle q\,q_1\rangle\,[q_1\,q_2]\big)^4 \\ B^4 &= \big([4\,p_1]\,\langle p_1\,1\rangle\,\langle p_2\,q_2\rangle\,[q\,p]\,\langle q\,q_1\rangle\,[q_1\,q_2]\big)^4 \\ \Delta &= [p\,4]\,[4\,p_1]\,[p_1\,p]\,\langle p_1\,1\rangle\,\langle 1\,p_2\rangle\,\langle p_2\,p_1\rangle\,\langle p_2\,q_2\rangle\,\langle q_2\,l\rangle\,\langle l\,p_2\rangle\,[l\,q] \\ &\quad \times [q\,p]\,[p\,l]\,\langle q\,q_1\rangle\,\langle q_1\,3\rangle\,\langle 3\,q\rangle\,[q_1\,q_2]\,[q_2\,2]\,[2\,q_1] \end{aligned} \tag{3.60}$$

and the minus sign in eq. (3.59) comes from the factor of i in each $A_j^{\text{tree, gluon}}$.

The helicity assignments of the internal lines allow only gluons to propagate in the right (q) loop, whereas the entire supersymmetric multiplet of states can propagate in the left (p) loop. For $\mathscr{N}=4$ super Yang-Mills, the sum over states yields,

$$\sum_{\substack{\mathscr{N}=4\\ \text{multiplet}}} \prod_{j=1}^{6} A_j^{\text{tree}}\Big|_{\mathscr{S}_2} = -\frac{(A+B)^4}{\Delta}\,. \tag{3.61}$$

On the other hand, from refs. [35] and [33] we know that in the $\mathscr{N}=4$ theory,

$$\sum_{\substack{\mathscr{N}=4\\ \text{multiplet}}} \prod_{j=1}^{6} A_j^{\text{tree}}\Big|_{\mathscr{S}_2} = -is_{12}s_{23}^2 A_{--++}^{\text{tree}}\,. \tag{3.62}$$

As a calculational shortcut, we use the equality of the expressions in eqs. (3.61) and (3.62) to fix the relative sign of A and B in eq. (3.60). (Of course, the relative signs can also be determined *a priori*, without reference to results in the literature, by carefully tracking the direction — incoming or outgoing — of the momenta at a given vertex and using the analytic continuation rule that changing the sign of a momentum, $p_i \to -p_i$, is effected by changing the sign

of the holomorphic spinor [29]: $\lambda_i^\alpha \to -\lambda_i^\alpha$ while $\widetilde{\lambda}_i^{\dot\alpha} \to \widetilde{\lambda}_i^{\dot\alpha}$.) One finds

$$\begin{aligned} A &= [p\,4]\,\langle 1\,p_2\rangle\,\langle q_2\,l\rangle\,[l\,q]\,\langle q\,q_1\rangle\,[q_1\,q_2] \\ B &= -[4\,p_1]\,\langle p_1\,1\rangle\,\langle p_2\,q_2\rangle\,[q\,p]\,\langle q\,q_1\rangle\,[q_1\,q_2]\,. \end{aligned} \tag{3.63}$$

Ref. [36] teaches us that the sum over the $\mathcal{N} = 4,2,1,0$ multiplet of states is related to the $\mathcal{N} = 4$ state sum via

$$\sum_{\substack{\text{SUSY}\\ \text{multiplet}}} \prod_{j=1}^{6} A_j^{\text{tree}} = \frac{(A+B)^{\mathcal{N}}(A^{4-\mathcal{N}}+B^{4-\mathcal{N}})}{(A+B)^4}\left(1-\tfrac{1}{2}\delta_{\mathcal{N},4}\right) \sum_{\substack{\mathcal{N}=4\\ \text{multiplet}}} \prod_{j=1}^{6} A_j^{\text{tree}} \tag{3.64}$$

so that the sum over the supersymmetric multiplet of states can be calculated from the gluonic contributions alone (indeed, recall that A and B in eq. (3.60) were obtained from the product of purely gluonic amplitudes corresponding to configurations A and B, respectively).

We can simplify the expression for the ratio between the supersymmetric state sums in eq. (3.64) by factoring out as many common factors of A and B as possible (exploiting momentum conservation fully). Setting $A = \alpha F$ and $B = \beta F$, for $\mathcal{N} = 4,2,1$ the ratio appearing in eq. (3.64) simplifies to

$$R = \frac{(\alpha+\beta)^{\mathcal{N}}(\alpha^{4-\mathcal{N}}+\beta^{4-\mathcal{N}})}{(\alpha+\beta)^4}\left(1-\tfrac{1}{2}\delta_{\mathcal{N},4}\right) \tag{3.65}$$

$$= \frac{\left(\alpha^{4-\mathcal{N}}+\beta^{4-\mathcal{N}}\right)\left(1-\tfrac{1}{2}\delta_{\mathcal{N},4}\right)}{(\alpha+\beta)^{4-\mathcal{N}}} \tag{3.66}$$

$$= 1-(4-\mathcal{N})\left(\frac{\alpha}{\alpha+\beta}\right)+(4-\mathcal{N})\left(\frac{\alpha}{\alpha+\beta}\right)^2. \tag{3.67}$$

where the last equality holds only for $\mathcal{N} = 4,2,1$; it can be obtained by expanding the numerator $\left(\alpha^{4-\mathcal{N}}+\beta^{4-\mathcal{N}}\right)\left(1-\tfrac{1}{2}\delta_{\mathcal{N},4}\right)$ in eq. (3.66) in β around $-\alpha$.

In the case at hand, we can use momentum conservation ($l = p_2 + q_2$ and $p_1 = p - k_4$) to rewrite A and B as follows,

$$\begin{aligned} A &= [p\,4]\,\langle 1\,p_2\rangle\,\langle q_2\,p_2\rangle\,[p_2\,q]\,\langle q\,q_1\rangle\,[q_1\,q_2] \\ B &= -[4\,p]\,\langle p\,1\rangle\,\langle p_2\,q_2\rangle\,[q\,p]\,\langle q\,q_1\rangle\,[q_1\,q_2] \end{aligned} \tag{3.68}$$

and identify

$$\begin{aligned} \alpha &= \langle 1\,p_2\rangle\,[p_2\,q] \\ \beta &= -[q\,p]\,\langle p\,1\rangle \\ F &= [p\,4]\,\langle q_2\,p_2\rangle\,\langle q\,q_1\rangle\,[q_1\,q_2]\,. \end{aligned} \tag{3.69}$$

Momentum conservation implies that $\alpha+\beta = -\langle 1\,4\rangle\,[4\,q]$, and thus,

$$\frac{\alpha}{\alpha+\beta} = -\frac{\langle 1\,p_1\rangle\,[p_1\,q]}{\langle 1\,4\rangle\,[4\,q]} = -\frac{\langle 1\,p_1\rangle\,[p_1\,3]}{\langle 1\,4\rangle\,[4\,3]}\,, \tag{3.70}$$

where the second equality uses the proportionality of antiholomorphic spinors, $\tilde{\lambda}_q \propto \tilde{\lambda}_3$. (This proportionality holds only for some of the other six solutions $\mathscr{S}_i$ in addition to $\mathscr{S}_2$.) The ratio thus simplifies to,

$$R = 1 + (4-\mathscr{N}) \left(\frac{\langle 1\, p_1 \rangle [p_1\, 3]}{\langle 1\, 4 \rangle [4\, 3]} \right) + (4-\mathscr{N}) \left(\frac{\langle 1\, p_1 \rangle [p_1\, 3]}{\langle 1\, 4 \rangle [4\, 3]} \right)^2 . \tag{3.71}$$

We can solve for the explicit values of the cut momenta using the parametrization (3.5) with the external momenta cyclicly permuted (for the t-channel configuration), and using the on-shell values defining $\mathscr{S}_2$ given in eqs. (3.8) and (3.11). We find,

$$p_1^\mu \equiv p^\mu - k_4^\mu = \frac{s_{14} z}{2 \langle 4\, 3 \rangle [3\, 1]} \langle 4^- | \gamma^\mu | 1^- \rangle , \tag{3.72}$$

so that,

$$\begin{aligned} \langle 1\, p_1 \rangle [p_1\, 3] &= \langle 1^- | \gamma^\mu | 3^- \rangle p_{1\mu} = \frac{s_{14} z}{2 \langle 4\, 3 \rangle [3\, 1]} \langle 1^- | \gamma^\mu | 3^- \rangle \langle 4^- | \gamma_\mu | 1^- \rangle \\ &= \frac{\langle 4\, 1 \rangle}{\langle 4\, 3 \rangle} s_{14} z , \end{aligned} \tag{3.73}$$

and thus,

$$\frac{\langle 1\, p_1 \rangle [p_1\, 3]}{\langle 1\, 4 \rangle [4\, 3]} = \chi z . \tag{3.74}$$

This gives us our final form for the ratio,

$$R = 1 + (4-\mathscr{N}) \chi z + (4-\mathscr{N}) \chi^2 z^2 , \tag{3.75}$$

and for the product of tree amplitudes,

$$\sum_{\substack{\text{SUSY} \\ \text{multiplet}}} \prod_{j=1}^{6} A_j^{\text{tree}} \Big|_{\mathscr{S}_2} = -i s_{12} s_{23}^2 A_{--++}^{\text{tree}} \Big(1 + (4-\mathscr{N}) \chi z + (4-\mathscr{N}) \chi^2 z^2 \Big) . \tag{3.76}$$

In this solution to the heptacut equations, the supersymmetric multiplet runs only in one of the loops. In other solutions (in particular, $\mathscr{S}_6$), the multiplet can run in both loops. The treatment of this case is similar but more elaborate. It turns out [36] that the sum over the multiplet can again be evaluated purely from the gluonic contributions. The main difference is that in this case there are three gluonic contributions A^4, B^4, C^4 (compared to the two in eq. (3.60)). One can again fix the relative sign of B and C by insisting that the $\mathscr{N} = 4$ supersymmetric result $-\frac{(A+B+C)^4}{\Delta}$ be equal to eq. (3.62), and from the obvious analog of eq. (3.64) one then finds the results for the supermultiplet sums for $\mathscr{N} = 4, 2, 1, 0$. These expressions can again be simplified as above.

Summing over all six solutions, and plugging the result into our master formulas (3.52) and (3.53), taken with $u = \frac{1}{2}$ and $v = 1$, we find

$$\begin{aligned} c_1 &= -s_{12}s_{23}^2 A^{\text{tree}}_{--++}\left(1+\frac{1}{4}(1-\delta_{\mathscr{N},4})(4-\mathscr{N})!\,\chi(\chi+1)^{\delta_{\mathscr{N},1}}\right) \\ c_2 &= \frac{3}{2}s_{23}^2 A^{\text{tree}}_{--++}(1-\delta_{\mathscr{N},4})(4-\mathscr{N})!\,\chi(\chi+1)^{\delta_{\mathscr{N},1}}\,, \end{aligned} \tag{3.77}$$

valid for $\mathscr{N} = 4, 2, 1$.

3.4.3 The s-channel contribution to $A_4^{\text{2-loop}}(1^-, 2^+, 3^-, 4^+)$

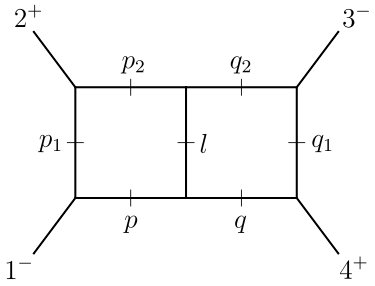

Figure 3.9. The heptacut for the s-channel contribution to $A_4^{\text{2-loop}}(1^-, 2^+, 3^-, 4^+)$.

The heptacut for the s-channel contribution to $A_4^{\text{2-loop}}(1^-, 2^+, 3^-, 4^+)$ is shown in figure 3.9. We will evaluate this contribution in two different ways, illustrating both the result's independence of the precise choice of contour, and also illustrating the potential advantages of a judicious choice of contour in a given calculation.

Rather than using our master formulas (3.52) and (3.53), let us evaluate the augmented heptacut integral for a general contour, before imposing the constraint equations. Adding up the contributions from all six solutions, we find

$$\begin{aligned} &\sum_{i=1}^{6} \oint_{\Gamma_i} \frac{dz}{z(z+\chi)} \prod_{j=1}^{6} A_j^{\text{tree}}(z) \\ &= -is_{12}^2 s_{23} A^{\text{tree}}_{-+-+}\left[\sum_{j=1}^{6} \frac{a_{1,j}-a_{2,j}}{\chi} - (4-\mathscr{N})\frac{a_{1,6}-a_{3,6}-a_{2,5}}{(\chi+1)^2}\right. \\ &\quad \left. + \left(\left(1-\tfrac{1}{2}\delta_{\mathscr{N},4}\right)\frac{\chi^{4-\mathscr{N}}+1}{(\chi+1)^{4-\mathscr{N}}} - 1\right)\left(\frac{a_{1,3}-a_{2,3}}{\chi} + \frac{a_{1,4}-a_{2,4}}{\chi}\right)\right]. \end{aligned} \tag{3.78}$$

In this expression, we need to impose the constraint equations in order to restrict the evaluation to a valid contour; and then we would seek to project onto

each basis integral in turn. Now, suppose we can find a pair of solutions to the constraint equations which projects onto the first or second basis integral, respectively, *and* in addition, satisfies $a_{1,3} - a_{2,3} + a_{1,4} - a_{2,4} = 0$. Using such a contour would set the second line of eq. (3.78) equal to zero and therefore produce a particularly simple algebraic expression for c_1 and c_2 directly, without need for additional simplification. Choosing $u = \frac{1}{3}$ and $v = 1$ in P_1 and P_2 gives such a contour.

This gives us the results

$$\begin{aligned} c_1 &= -s_{12}^2 s_{23} A^{\text{tree}}_{-+-+} \left(1 - \frac{3}{4}(4-\mathcal{N})\frac{\chi}{(\chi+1)^2}\right) \\ c_2 &= -\frac{3}{2} s_{12} s_{23} A^{\text{tree}}_{-+-+} \frac{4-\mathcal{N}}{(\chi+1)^2}\,, \end{aligned} \tag{3.79}$$

valid for $\mathcal{N} = 4, 2, 1$. The t-channel contribution can be obtained by exchanging $s_{12} \longleftrightarrow s_{23}$ and $\chi \longrightarrow \chi^{-1}$.

If we compare the expressions obtained above for the coefficients c_i to those obtained using the choice suggested in Section 3.3, $u = \frac{1}{2}$ and $v = 1$, we find that the expressions are equal by virtue of the identity

$$\frac{1}{\chi}\left(\left(1 - \tfrac{1}{2}\delta_{\mathcal{N},4}\right)\frac{\chi^{4-\mathcal{N}}+1}{(\chi+1)^{4-\mathcal{N}}} - 1\right) = -\frac{4-\mathcal{N}}{(\chi+1)^2}\,, \tag{3.80}$$

valid for $\mathcal{N} = 4, 2, 1$. This identity can of course easily be proven without reference to the current discussion, but the point we wish to emphasize is that the flexibility in choosing contours suggests certain algebraic simplifications which are not immediately obvious.

The double box coefficients given in eqs. (3.57, 3.58, 3.77, 3.79) agree with the $\mathcal{O}(\varepsilon^0)$ terms of the corresponding coefficients, supplied to us by Lance Dixon [37], in the amplitudes computed by Bern, De Freitas, and Dixon [38].

We emphasize that though we have only given explicit results for supersymmetric theories, the method can also be applied to find the double-box coefficients of QCD amplitudes. The only required change in the calculation is that the tree-level data fed into the master formulas in eqs. (3.52)-(3.53) should be computed for QCD instead.

A mystery, left to be resolved in the next chapter, is the surplus of six free winding numbers $a_{i,j}$ characterizing the maximal-cut contours. Namely, recall from eq. (3.32) that there are 14 such winding numbers. The contour constraint equations (3.42)-(3.43) impose 6 constraints, supplied by the 2 additional constraints from requiring that one master double box be set to one, and the other to zero on the cut. In total, one appears to be left with $14 - 6 - 2 = 6$ free parameters in the two-loop master contours, in contrast to the situation in one-loop generalised unitarity where the master contours contain no free parameters.

3.5 Comparison with the leading-singularity method

The use of composite leading singularities to freeze loop integrations to points in $\mathbb{C}^8$ is common to the approach in Paper I and that of the leading-singularity method, and it is worth explaining the difference between these two approaches.

The leading-singularity method has notably only been explored for $\mathcal{N} = 4$ supersymmetric Yang-Mills (SYM) theory. It employs purely *integrand-level* reductions to the Feynman-diagram expansion defining the amplitude. For example, at one loop, the $\mathcal{N} = 4$ SYM amplitudes have vanishing triangle and bubble contributions in eq. (2.39) due to diagram-by-diagram cancelations between the different types of particles circulating in the loop. Also at higher loops, $\mathcal{N} = 4$ supersymmetry will give rise to many similar cancelations, resulting in a relatively limited set of integrals. Now, as the integrands on either side of the reduction equation are equal, one may choose *any* linear combination of leading-singularity contours to determine integral coefficients. For generic gauge theories, the restriction to using only integrand-level reductions has the disadvantage of leaving a relatively large number of (linearly dependent) integrals—for QCD of the same order of magnitude as the Feynman diagram expansion itself.

In contrast, in the approach reviewed in this chapter, we make use of additional reductions coming from IBP identities. This has the virtue of producing an extremely compact result for the amplitude. For example, for four massless external states, the Feynman rules for gauge theory produce 22 double-box integrals with various powers of the loop momenta in the integrand numerator. Through IBP relations, these are reduced to two linearly independent double boxes. Similarly, for five massless states, the 76 pentagon-boxes produced by the Feynman rules are reduced via IBP's (and two Gram determinant constraints) to a single pentagon-box integral. Thus, the use of IBP reductions leads to somewhat remarkable simplifications, yielding in some sense a minimal representation of the amplitude. However, as the reduction equation for the two-loop amplitude no longer holds at the level of the integrand, to avoid contamination from spurious terms, one is now obliged to choose linear combinations of leading-singularity contours that respect the IBP (and possibly Gram determinant) constraints.

To rephrase these considerations more concretely, let us go back to the basis composition of the four-point amplitude,

$$A_4^{(2)} \;=\; c_{1,\sigma_1} P^{**}_{2,2;\,\sigma_1}[1] \;+\; c_{2,\sigma_1} P^{**}_{2,2;\,\sigma_1}[\ell_1 \cdot k_4] \;+\; \cdots \tag{3.81}$$

which, as we recall, in the parametrization (3.5) of the loop momenta has the heptacut

$$\sum_{i=1}^{6} \oint_{\Gamma_i} \frac{dz}{z(z+\chi)} \Big(c_{1,\sigma_1} + c_{2,\sigma_1} (\ell_1 \cdot k_4) \Big|_{\mathscr{S}_i}(z) \Big) = \sum_{i=1}^{6} \oint_{\Gamma_i} \frac{dz}{z(z+\chi)} \prod_{j=1}^{6} A_j^{\text{tree}}(z) \Big|_{\mathscr{S}_i} . \tag{3.82}$$

With the integral coefficients in eqs. (3.57), (3.58), (3.77), (3.79) one can examine whether the equality in eq. (3.82) also holds at the *integrand* level. In other words, for any fixed solution $\mathscr{S}_i$ to the heptacut under consideration, does the candidate equality

$$\forall z \in \mathbb{C}\text{:} \quad c_{1,\sigma_1} \,+\, c_{2,\sigma_1} (\ell_1 \cdot k_4) \Big|_{\mathscr{S}_i}(z) \;\stackrel{?}{=}\; \prod_{j=1}^{6} A_j^{\text{tree}}(z) \Big|_{\mathscr{S}_i} \tag{3.83}$$

hold true? For $\mathscr{N} = 4$ super Yang-Mills theory, the answer is trivially yes: both sides are equal to a constant (namely $-s_{12}^2 s_{23} A^{\text{tree}}$ for the s-channel cut, and $-s_{12} s_{23}^2 A^{\text{tree}}$ for the t-channel cut). This is a reflection of the fact that $\mathscr{N} = 4$ supersymmetry is sufficiently powerful to cancel all double-box integrals in the Feynman-diagram expansion but the scalar ones. In hindsight, this observation shows that, for $\mathscr{N} = 4$ SYM, any choice of contours Γ_i in eq. (3.82) will produce correct results for the coefficients c_1, c_2. These observations immediately extend to the five-gluon MHV amplitude [20] where the analog of eq. (3.83) now involves non-trivial functions of z.

In contrast, for $\mathscr{N} = 2,1$ super Yang-Mills theory, the candidate equality (3.83) cannot hold, as one can easily see by considering the limit as the loop momenta become large. Indeed, in both of these gauge theories, for any heptacut one may consider there always exists a kinematical solution for which

$$\prod_{j=1}^{6} A_j^{\text{tree}}(z) \;\sim\; z^2 \qquad \text{as} \qquad z \to \infty \tag{3.84}$$

whereas for all the kinematical solutions,

$$c_{1,\sigma_1} \,+\, c_{2,\sigma_1} (\ell_1 \cdot k_4)(z) \;\sim\; z \text{ or } z^0 \qquad \text{as} \qquad z \to \infty\,. \tag{3.85}$$

The reason why eq. (3.83) fails to hold for these gauge theories is that there is not enough supersymmetry to cancel double boxes with quadratic numerator insertions, as reflected in eq. (3.84). To produce a minimal representation of amplitudes in $\mathscr{N} < 4$ Yang-Mills theory, we use IBP relations to reduce the set of double-box integrals to the basis elements $\{P^{**}_{2,2;\,\sigma_1}[1],\ P^{**}_{2,2;\,\sigma_1}[\ell_1 \cdot k_4]\}$. As a result, the integrands on either side of the basis decomposition in eq. (3.81) are only equal up to terms which integrate to zero on $\mathbb{R}^D \times \mathbb{R}^D$, and the contours Γ_i in eq. (3.82) must be chosen so as to annihilate such terms.

4. Uniqueness of two-loop master contours

The selection principle in Chapter 3 for determining the complex integration contours that underlie generalized cuts, though fulfilling its practical purpose, leaves a question of a more fundamental nature. Namely, the box and triangle contours in Section 2.3 are unambiguously defined, so what is the origin of the six free parameters in the analogous two-loop master contours? Are there additional constraints on the contours which have not yet been taken into account, or is there some other explanation?

The path followed in this chapter toward a resolution of this mystery will take us through a number of unexpected discoveries. The first is an appealing physical interpretation of the heptacut Jacobian poles, intimately linked with the resolution. The second is a complete classification of the solutions to the heptacut of the general double-box integral. As we shall see, these solutions are naturally associated with Riemann surfaces whose topology is determined by the number of states at the vertices of the double-box graph and whose precise geometry, once illuminated, dispels the mystery.

We remark that the presentation in Sections 4.1-4.4 is essentially that of Sections 3, 5 and Appendix A in Paper III, adding here a few comments, observations and illustrations. In Section 4.5 we provide a brief introduction to the so-called symbol of transcendental functions.

4.1 Maximal cut of the general double box

The integrals considered throughout this chapter have the topology of a double box, illustrated in figure 4.1. Ignoring pentagon-boxes, these are the integrals in the basis decomposition of the two-loop amplitude

$$A^{(2)} = \sum_i c_i(\varepsilon)\,\text{Integral}_i + \text{Rational} \tag{4.1}$$

that contain the maximal number of propagators.[1]

[1] We choose to ignore pentagon-boxes in this thesis as we expect the explicit octacuts they contain to allow a straightforward extraction of their coefficients, analogous to the quadruple cut at one loop.

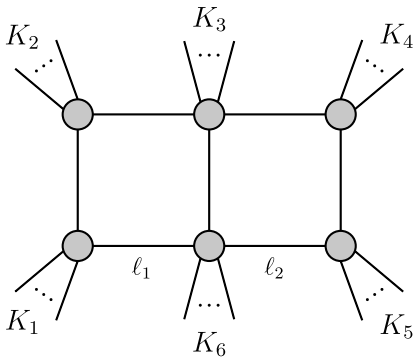

Figure 4.1. The general double-box integral. The $\cdots$ dots at each vertex represent the presence of an arbitrary number of massless legs. Each of the vertices, shown as gray blobs, is given a label $i = 1,\ldots,6$ which equals the index of the associated external momentum K_i.

Employing a different notation than that of Chapter 3, more suited to the purposes of the present chapter, the general double-box integral is defined by

$$I_{(N_1,N_2,N_3,N_4,N_5,N_6)}[\Phi] \equiv \int \frac{d^D\ell_1}{(2\pi)^D}\frac{d^D\ell_2}{(2\pi)^D}\left(\frac{\Phi(\ell_1,\ell_2)}{\ell_1^2\,(\ell_1-K_1)^2\,(\ell_1-K_1-K_2)^2}\right.$$
$$\left.\times\frac{1}{(\ell_1+\ell_2+K_6)^2\,\ell_2^2\,(\ell_2-K_5)^2\,(\ell_2-K_4-K_5)^2}\right) \tag{4.2}$$

where N_i denotes the number of external legs at vertex i in figure 4.1.

For future purposes in this chapter we sketch here a few details of the calculation of the heptacut of the general double-box integral in eq. (4.2) which otherwise mostly proceeds in analogy with the calculation described in Section 3.1. The heptacut is defined by the joint on-shell constraints

$$\ell_1^2 = 0 \tag{4.3}$$
$$(\ell_1-K_1)^2 = 0 \tag{4.4}$$
$$(\ell_1-K_1-K_2)^2 = 0 \tag{4.5}$$
$$\ell_2^2 = 0 \tag{4.6}$$
$$(\ell_2-K_5)^2 = 0 \tag{4.7}$$
$$(\ell_2-K_4-K_5)^2 = 0 \tag{4.8}$$
$$(\ell_1+\ell_2+K_6)^2 = 0\,. \tag{4.9}$$

In this chapter, we will use the following convenient parametrization of the loop momenta

$$\ell_1^\mu = \alpha_1 K_1^{\flat\mu} + \alpha_2 K_2^{\flat\mu} + \alpha_3 \langle K_1^\flat | \gamma^\mu | K_2^\flat] + \alpha_4 \langle K_2^\flat | \gamma^\mu | K_1^\flat] \tag{4.10}$$

$$\ell_2^\mu = \beta_1 K_4^{\flat\mu} + \beta_2 K_5^{\flat\mu} + \beta_3 \langle K_4^\flat | \gamma^\mu | K_5^\flat] + \beta_4 \langle K_5^\flat | \gamma^\mu | K_4^\flat] . \tag{4.11}$$

which unlike that of eq. (3.5) does not involve a rescaling of the parameters.

Re-expressed in terms of the loop momentum parametrization (4.10)-(4.11), the on-shell constraints (4.3)-(4.8) (corresponding to cutting the six outer propagators in figure 4.1) take the form

$$\begin{aligned} &\alpha_1 = \tfrac{\gamma_1(S_2+\gamma_1)}{\gamma_1^2 - S_1 S_2} , \qquad \alpha_2 = \tfrac{S_1 S_2 (S_1+\gamma_1)}{\gamma_1 (S_1 S_2 - \gamma_1^2)} , \qquad \alpha_3 \alpha_4 = -\tfrac{S_1 S_2 (S_1+\gamma_1)(S_2+\gamma_1)}{4(\gamma_1^2 - S_1 S_2)^2} \\ &\beta_1 = \tfrac{S_4 S_5 (S_5+\gamma_2)}{\gamma_2 (S_4 S_5 - \gamma_2^2)} , \qquad \beta_2 = \tfrac{\gamma_2 (S_4+\gamma_2)}{\gamma_2^2 - S_4 S_5} , \qquad \beta_3 \beta_4 = -\tfrac{S_4 S_5 (S_4+\gamma_2)(S_5+\gamma_2)}{4(\gamma_2^2 - S_4 S_5)^2} . \end{aligned} \tag{4.12}$$

We observe that in this parametrization, the variables $\alpha_1, \alpha_2, \beta_1, \beta_2$ are directly fixed, while the remaining variables obey simple constraints of the form $\alpha_3 \alpha_4$ = constant.

Replacing all propagators in eq. (4.2) by complex delta functions (setting Φ=1) and integrating out the six that correspond to the outer propagators in figure 4.1, a contribution to the heptacut double-box integral is

$$J_1 = C \oint \frac{d\alpha_3 d\beta_3}{\alpha_3 \beta_3} \, \delta^{\mathbb{C}}\big((\ell_1 + \ell_2 + K_6)^2\big) \quad \text{where} \quad C \equiv \frac{\gamma_1 \gamma_2}{(\gamma_1^2 - S_1 S_2)(\gamma_2^2 - S_4 S_5)} . \tag{4.13}$$

We note that the variables α_3 or β_3 are not always good integration variables: on certain solutions to eq. (4.12) they may happen to be constant, cf. figure 3.3. In such cases, they should be traded for α_4 or β_4 through $\frac{d\alpha_3}{\alpha_3} \to -\frac{d\alpha_4}{\alpha_4}$, and/or $\frac{d\beta_3}{\beta_3} \to -\frac{d\beta_4}{\beta_4}$. Notice the relative signs which were ignored in Chapter 3. These arise from the fact that, in solving for the complex delta functions, one should use determinants rather than absolute values of determinants, as discussed below eq. (2.62).

Integrating out the remaining complex delta function in eq. (4.13) then produces the following contribution to the maximal cut of the general double box,

$$J\big|_{z \equiv \alpha_3} = C \oint_\Gamma \frac{dz}{z} \Big(B_0(z)^2 - 4 B_1(z) B_{-1}(z) \Big)^{-1/2} \tag{4.14}$$

where $z \equiv \alpha_3$ and

$$B_1 = \langle K_4^\flat | \gamma_\mu | K_5^\flat] \Big(\alpha_1 K_1^{\flat\mu} + \alpha_2 K_2^{\flat\mu} + z \langle K_1^\flat | \gamma^\mu | K_2^\flat] + \alpha_4(z) \langle K_2^\flat | \gamma^\mu | K_1^\flat] + K_6^\mu \Big) \quad (4.15)$$

$$B_0 = \Big(\beta_1 K_{4\mu}^\flat + \beta_2 K_{5\mu}^\flat + K_{6\mu} \Big) \times \Big(\alpha_1 K_1^{\flat\mu} + \alpha_2 K_2^{\flat\mu} + z \langle K_1^\flat | \gamma^\mu | K_2^\flat] + \alpha_4(z) \langle K_2^\flat | \gamma^\mu | K_1^\flat] + K_6^\mu \Big) - \tfrac{1}{2} K_6^2 \quad (4.16)$$

$$B_{-1} = - \frac{S_4 S_5 (S_4 + \gamma_2)(S_5 + \gamma_2) \langle K_5^\flat | \gamma_\mu | K_4^\flat]}{4(\gamma_2^2 - S_4 S_5)^2} \times \Big(\alpha_1 K_1^{\flat\mu} + \alpha_2 K_2^{\flat\mu} + z \langle K_1^\flat | \gamma^\mu | K_2^\flat] + \alpha_4(z) \langle K_2^\flat | \gamma^\mu | K_1^\flat] + K_6^\mu \Big) . \quad (4.17)$$

Here $\alpha_1, \alpha_2, \alpha_4(z), \beta_1, \beta_2$ are given by eq. (4.12), whereas z is unconstrained, reflecting the degree of freedom left over after imposing the seven cut constraints. Despite appearances, we will see that in all cases with less than 10 massless particles, the argument of the square root in eq. (4.14) is in fact a perfect square.

Similar formulas arise when solving instead for $z = \alpha_4, \beta_3$ or β_4 and are given explicitly in eqs. (3.28)-(3.39) in Paper II. We emphasize that the maximal cut of the general double box is a sum over such contributions, as exemplified in eq. (3.34).

4.2 Kinematical solutions and Jacobian poles

In this section we consider the classes of solutions to the joint heptacut constraints (4.3)-(4.9). As the loop momenta have a total of eight degrees of freedom $(\alpha_1, \ldots, \alpha_4, \beta_1, \ldots, \beta_4)$, the result of imposing seven on-shell constraints will be to fix all but one of these parameters. The various choices of freezing the loop parameters to particular values that solve these constraints span a number of distinct kinematical solutions, whose unconstrained variable $z \in \mathbb{C}$ parametrizes a Riemann surface (for example, a Riemann sphere). As we shall see, the Riemann surfaces associated with the kinematical solutions are not disjoint, but rather they have pointwise intersections located at the poles of the Jacobian discussed in the previous section.

The number of kinematical solutions to the heptacut constraints is determined by the distribution of external momenta at the vertices of the double-box graph, and an important role in the classification is played by the vertices that join three massless lines. In order to state the classification, we introduce

some notation which will be used throughout this chapter,[2]

$$\begin{aligned} N_i &\equiv \text{\# of external legs at vertex } i \qquad \text{for} \quad i = 1,\ldots,6 \\ n_i &\equiv \text{total \# of legs at vertex } i \qquad \text{for} \quad i = 1,\ldots,6 \\ \mu_j &\equiv \begin{cases} (1-\delta_{n_1,3})(1-\delta_{n_2,3}) & \text{for} \quad j=1 \\ (1-\delta_{n_3,3})(1-\delta_{n_6,3}) & \text{for} \quad j=2 \\ (1-\delta_{n_4,3})(1-\delta_{n_5,3}) & \text{for} \quad j=3\,. \end{cases} \end{aligned} \tag{4.18}$$

The variable μ_j keeps track of whether each of the three vertical lines in the double-box graph in figure 4.1 is part of some three-point vertex or not, and respectively equals zero or one. For mnemonic convenience, we will denote the values of μ_j by letters as follows

$$\begin{aligned} \mu_j = \mathrm{m} \quad &\Longleftrightarrow \quad \mu_j = 0 \\ \mu_j = \mathrm{M} \quad &\Longleftrightarrow \quad \mu_j = 1\,. \end{aligned} \tag{4.19}$$

To give an example of how three-point vertices play a role in determining the number of kinematical solutions, let us consider the third equation in eq. (4.12),

$$\alpha_3 \alpha_4 \propto S_1 S_2\,. \tag{4.20}$$

We observe that if the right hand side is nonzero, one gets an invertible relation between α_3 and α_4, leaving either of them as an equivalent free parameter. If, on the other hand, the right hand side is zero, this equation has two distinct solutions, $\alpha_3 = 0$ or $\alpha_4 = 0$. The latter situation occurs whenever the leftmost vertical line of the double-box graph is part of some three-point vertex (in the above notation denoted by m), and the splitting of one into two solutions of eq. (4.12) is a reflection of the existence of two types of massless on-shell three-point vertices in $3+1$ dimensions, already observed in figure 2.8. Indeed, assuming for the moment that $S_1 = 0$, it follows from eq. (4.10) that $\alpha_3 = 0$ implies

$$|\ell_1] \propto |\ell_1 - K_1] \propto |K_1] \tag{4.21}$$

whereas $\alpha_4 = 0$ implies

$$\langle \ell_1| \propto \langle \ell_1 - K_1| \propto \langle K_1|\,, \tag{4.22}$$

consistent with eq. (2.57).

Below we discuss the number of kinematical solutions to the heptacut constraints (4.3)-(4.9) and the intersections of their associated Riemann surfaces for each of a total of four cases. These four cases are defined by having all, exactly two, exactly one and none of the vertical lines in the double-box graph be part of some three-point vertex.

[2] We deliberately repeat the definition of N_i here, to make its distinction from n_i clear.

4.2.1 Case 1: $(\mu_1, \mu_2, \mu_3) = (\mathrm{m}, \mathrm{m}, \mathrm{m})$

Let us first consider the integral topologies where each vertical line of the double-box graph is part of at least one three-point vertex. This category includes, for instance, all topologies with four or five massless external states, but also an infinite sequence of topologies at higher points.

At this point, recall our findings for the case of four external massless momenta in Chapter 3: there are six classes of kinematical solutions to the heptacut constraints (4.3)-(4.9). The solutions are uniquely characterized by the distribution of chiralities ($\oplus$ or $\ominus$) at the three-point vertices. Disallowed distributions are those with uninterrupted chains of same-chirality vertices along the vertical or horizontal lines; all other configurations are allowed for generic external kinematics.

Classification of kinematical solutions

As it turns out, the classification of kinematical solutions in the case of four massless external states extends uniformly to cover all case 1 topologies. We can establish this in two steps.

Let us start by noting that for an allowed solution, three-point vertices lying on a common vertical line must have opposite chirality. For the leftmost and rightmost lines, this is already visible from the discussion around eqs. (4.21) and (4.22). For example, having two $\oplus$ vertices on the leftmost vertical line cannot be achieved for generic external momenta because it would require

$$\langle K_1| \propto \langle \ell_1 - K_1| \propto \langle K_2| \tag{4.23}$$

and thus $K_1 \cdot K_2 = 0$. Similarly, for generic external momenta, forcing two $\oplus$ vertices to appear in the central vertical line can be shown to require the four-momentum in the central propagator to vanish, leaving no free parameter.

This already places an upper bound of $2^3 = 8$ on the number of kinematical solutions. Not all of these configurations are allowed, however. For instance, three $\oplus$ vertices lying on a horizontal line would force all angle bracket spinors on that line to be proportional to each other, in analogy with eq. (4.23).

More generally, consider the distribution of chiralities at the vertices of the 7-particle topology shown in figure 4.2.

This distribution of chiralities does not obviously impose any constraints on the external kinematics. Closer inspection, however, reveals that this assignment contains a one-loop sub-box on the right loop (of the two-mass-easy type), with opposite chiralities at its two massless corners. But as is known from studies of one-loop boxes, for generic external momenta, opposite corners of a two-mass-easy box must have identical chiralities [17]. Thus, the configuration in figure 4.2 in fact does impose constraints on the external momenta and is therefore disallowed. We have verified, by exhaustion, that all chirality assignments not forbidden in such ways lead to healthy kinematical solutions.

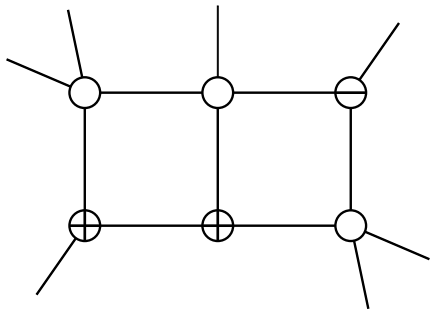

Figure 4.2. A generic integral belonging to case 1: all three vertical lines are part of some three-point vertex. The shown chirality assignment is forbidden, as explained in the main text.

To summarize this discussion, we have derived three simple rules which establish that there are exactly six kinematical solutions for all topologies within case 1:

- Rule 1. Two same-chirality vertices cannot appear in a vertical line.
- Rule 2. Three same-chirality vertices cannot appear in an horizontal line.
- Rule 3. In rule 2, opposite-chirality vertices at opposite corners of a one-loop sub-box should be counted like same-chirality adjacent vertices (cf. the right loop in figure 4.2).

Interpretation of Jacobian poles

As it turns out, the six kinematical solutions to the heptacut constraints (4.3)-(4.9) are not completely disjoint: as illustrated in figure 4.3, for any given kinematical solution $\mathscr{S}_i$, depicted there as a Riemann sphere, there are two special points where it coincides with a different kinematical solution. We now proceed to locate these special points and show that the six Riemann spheres link into a chain.

To clarify the exposition, we will consider a particular representative of case 1 and write out explicitly the kinematical solutions and the Jacobian determinants. For example, let us choose the integral topology whose vertex momenta (as defined in figure 4.1) are

$$\begin{aligned} K_1 &= k_1 + k_2\,, & K_2 &= k_3\,, & K_3 &= 0\,, \\ K_4 &= k_4\,, & K_5 &= k_5\,, & K_6 &= 0\,, \end{aligned} \tag{4.24}$$

with the k_i being lightlike vectors. In terms of the spinor ratios

$$\begin{aligned} P_1 &= -\frac{\langle K_1^\flat\, k_5\rangle}{2\langle k_3\, k_5\rangle}\,, & P_2 &= -\frac{\langle K_1^\flat\, k_4\rangle}{2\langle k_3\, k_4\rangle}\,, & Q_1 &= -\frac{[k_5\, K_1^\flat]}{2[k_4\, K_1^\flat]}\,, \\ P_1^\bullet &= -\frac{[K_1^\flat\, k_5]}{2[k_3\, k_5]}\,, & P_2^\bullet &= -\frac{[K_1^\flat\, k_4]}{2[k_3\, k_4]}\,, & Q_1^\bullet &= -\frac{\langle k_5\, K_1^\flat\rangle}{2\langle k_4\, K_1^\flat\rangle}\,, \end{aligned} \tag{4.25}$$

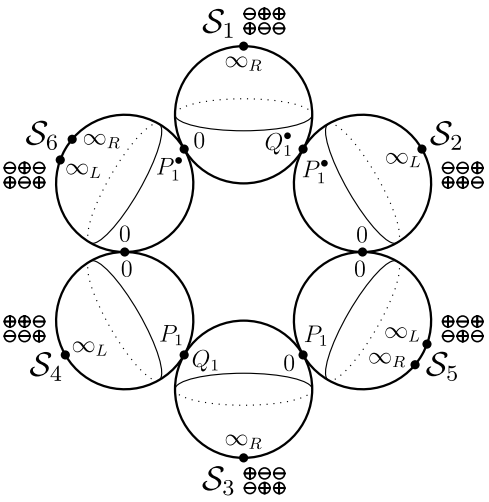

Figure 4.3. The six different classes of kinematical solutions to the heptacut constraints (4.3)-(4.9), illustrated here as Riemann spheres (intended to represent the complex degree of freedom z left unfrozen by the heptacut constraints), in case 1. The kinematical solutions are characterized by the distribution of chiralities at the vertices of the double-box graph (see figure 4.1), shown next to each sphere. Each Riemann sphere coincides with the two adjacent spheres in the chain at a single point, illustrated as a black dot. These points are precisely the poles of the heptacut Jacobian. The Riemann spheres contain additional singularities, denoted by ∞_L and ∞_R, associated with respectively the left or right loop momentum becoming infinite (respectively occuring as $z=\infty$ or $z=P_2^{(\bullet)}$ in eqs. (4.25)-(4.27)). Parity-conjugate kinematical solutions appear antipodally in the chain.

the six kinematical solutions $\mathscr{S}_1,\ldots,\mathscr{S}_6$ are obtained by fixing the parameters of the loop momenta to the values

$$\mathscr{S}_1,\ldots,\mathscr{S}_6\colon\quad \begin{cases} \alpha_1=1\,, & \beta_1=0 \\ \alpha_2=0\,, & \beta_2=1 \end{cases} \tag{4.26}$$

$$\mathscr{S}_1\colon\ \begin{cases} \alpha_3=P_1^\bullet\,, & \beta_3=z \\ \alpha_4=0\,, & \beta_4=0 \end{cases};\qquad \mathscr{S}_2\colon\ \begin{cases} \alpha_3=z\,, & \beta_3=Q_1^\bullet \\ \alpha_4=0\,, & \beta_4=0 \end{cases}$$

$$\mathscr{S}_3\colon\ \begin{cases} \alpha_3=0\,, & \beta_3=0 \\ \alpha_4=P_1\,, & \beta_4=z \end{cases};\qquad \mathscr{S}_4\colon\ \begin{cases} \alpha_3=0\,, & \beta_3=0 \\ \alpha_4=z\,, & \beta_4=Q_1 \end{cases}$$

$$\mathscr{S}_5\colon\ \begin{cases} \alpha_3=0\,, & \beta_3=-\frac{\langle k_5\,k_3\rangle(z-P_1)}{2\langle k_4\,k_3\rangle(z-P_2)} \\ \alpha_4=z\,, & \beta_4=0 \end{cases};\qquad \mathscr{S}_6\colon\ \begin{cases} \alpha_3=z\,, & \beta_3=0 \\ \alpha_4=0\,, & \beta_4=-\frac{[k_5\,k_3](z-P_1^\bullet)}{2[k_4\,k_3](z-P_2^\bullet)} \end{cases} \tag{4.27}$$

with $z \in \mathbb{C}$ a free parameter. The associated heptacut Jacobians are

$$J_i(z) = \frac{1}{s_{45}\big((s_{13}+s_{23})(s_{15}+s_{25})-s_{12}s_{35}\big)} \times \begin{cases} \pm\big(z(1-z/P_1^\bullet)\big)^{-1} & \text{for } i=2,6 \\ \pm\big(z(1-z/P_1)\big)^{-1} & \text{for } i=4,5 \\ -\big(z(1-z/Q_1^\bullet)\big)^{-1} & \text{for } i=1 \\ -\big(z(1-z/Q_1)\big)^{-1} & \text{for } i=3\,. \end{cases} \tag{4.28}$$

In the first two lines of eq. (4.28), the plus or minus signs refer respectively to the first or second indicated kinematical solution. Now, consider first the intersection between $\mathscr{S}_4$ and $\mathscr{S}_6$. In $\mathscr{S}_4$ we have $\alpha_3 = 0$ but α_4 free, while in $\mathscr{S}_6$ we have $\alpha_4 = 0$ and α_3 free; the intersection is simply a point, located within $\mathscr{S}_4$ at $\alpha_4 = 0$ and within $\mathscr{S}_6$ at $\alpha_3 = 0$. At this point, β_3 equals zero while β_4 takes on a finite value explicitly given in eqs. (4.25) and (4.27).

To understand better why $\mathscr{S}_4$ and $\mathscr{S}_6$ coincide at a point, let us examine what is happening to the loop momentum ℓ_1 at $z = 0$ in $\mathscr{S}_4$. By assumption, either vertex 1 or 2 in figure 4.1 is a three-point vertex; let us consider here the former case. It is straightforward to see that in the parametrization (4.10) the on-shell constraints (4.3)-(4.5) and (4.9) are solved within $\mathscr{S}_6$ by setting $(\alpha_1, \alpha_2, \alpha_3, \alpha_4) = (\frac{S_2+\gamma_1}{\gamma_1}, 0, z, 0)$. At $z = 0$ we then observe that

$$\ell_1^\mu \;=\; \frac{S_2+\gamma_1}{\gamma_1} K_1^\mu \;\propto\; K_1^\mu\,, \tag{4.29}$$

i.e., the loop momentum is collinear with that of a massless external particle.

This collinearity can be immediately understood from figure 4.3: at the intersection of $\mathscr{S}_4$ and $\mathscr{S}_6$, the lower-left vertex must simultaneously be of the $\ominus$ and $\oplus$ type, and therefore the momenta connected by this vertex are mutually collinear. Moreover, when both of the momenta K_1 and K_2 are massless, the simultaneous collinearity conditions at the two left-most vertices imply that the momentum of the particle exchanged between these vertices must vanish. Indeed, we see that in this case, eq. (4.29) implies that $\ell_1 - K_1 = 0$. Physically, this corresponds to a soft divergence region, giving rise to an infrared divergence in the original two-loop integral. In a gauge theory, the exchanged soft particle producing such a singularity will necessarily be a soft gluon, as can be argued from the behavior of the three-point vertices.

Similarly, the intersection between $\mathscr{S}_2$ and $\mathscr{S}_5$ occurs at a point where $\alpha_3 = \alpha_4 = 0$. By symmetry, there are similar intersections at points where $\beta_3 = \beta_4 = 0$, merging $\mathscr{S}_1$ with $\mathscr{S}_6$, and $\mathscr{S}_3$ with $\mathscr{S}_5$. Finally, the intersections between $\mathscr{S}_1$ and $\mathscr{S}_2$, and between $\mathscr{S}_3$ and $\mathscr{S}_4$, occur at points where the momenta in the central three-point vertices become collinear.

Let us conclude this discussion by the observation that the poles of the Jacobian determinants in eq. (4.28) coincide with the intersection points of the six

Riemann spheres shown in figure 4.3. We have checked that this phenomenon extends to all integral topologies in case 1.

Residue relations across solutions

At the location of any Jacobian pole, each loop momentum ℓ_i as evaluated from either of the two intersecting spheres assumes identical values; for example,

$$\ell_i(0)\big|_{\mathscr{S}_4} \;=\; \ell_i(0)\big|_{\mathscr{S}_6} \qquad \text{for} \quad i=1,2\,. \tag{4.30}$$

As a result of this, given an arbitrary function $f(\ell_1(z),\ell_2(z))$ that does not share these poles, one has the identities

$$\operatorname*{Res}_{z=Q_1^\bullet} J(z)\,f(\ell_1(z),\ell_2(z))\big|_{\mathscr{S}_1} \;=\; -\operatorname*{Res}_{z=P_1^\bullet} J(z)\,f(\ell_1(z),\ell_2(z))\big|_{\mathscr{S}_2} \tag{4.31}$$

$$\operatorname*{Res}_{z=0} J(z)\,f(\ell_1(z),\ell_2(z))\big|_{\mathscr{S}_2} \;=\; -\operatorname*{Res}_{z=0} J(z)\,f(\ell_1(z),\ell_2(z))\big|_{\mathscr{S}_5} \tag{4.32}$$

$$\operatorname*{Res}_{z=P_1} J(z)\,f(\ell_1(z),\ell_2(z))\big|_{\mathscr{S}_5} \;=\; -\operatorname*{Res}_{z=0} J(z)\,f(\ell_1(z),\ell_2(z))\big|_{\mathscr{S}_3} \tag{4.33}$$

$$\operatorname*{Res}_{z=Q_1} J(z)\,f(\ell_1(z),\ell_2(z))\big|_{\mathscr{S}_3} \;=\; -\operatorname*{Res}_{z=P_1} J(z)\,f(\ell_1(z),\ell_2(z))\big|_{\mathscr{S}_4} \tag{4.34}$$

$$\operatorname*{Res}_{z=0} J(z)\,f(\ell_1(z),\ell_2(z))\big|_{\mathscr{S}_4} \;=\; -\operatorname*{Res}_{z=0} J(z)\,f(\ell_1(z),\ell_2(z))\big|_{\mathscr{S}_6} \tag{4.35}$$

$$\operatorname*{Res}_{z=P_1^\bullet} J(z)\,f(\ell_1(z),\ell_2(z))\big|_{\mathscr{S}_6} \;=\; -\operatorname*{Res}_{z=0} J(z)\,f(\ell_1(z),\ell_2(z))\big|_{\mathscr{S}_1}\,. \tag{4.36}$$

We note that the uniform pattern of signs owes to the conventions explained below eq. (4.13). As explained in Section 4.4, these identities can be applied in computations of heptacut two-loop amplitudes $J(z)\prod_{j=1}^6 A_j^{\text{tree}}(z)\Big|_{\mathscr{S}_i}$ to explain the vanishing of certain residues, as well as the seemingly accidental equality between pairs of other residues.

To summarize Section 4.2.1, we have found that in case 1 there are six classes of kinematical solutions to the heptacut constraints (4.3)-(4.9), each of which is labeled by a free complex variable $z\in\mathbb{C}$, parametrizing a Riemann sphere. The six Riemann spheres thus associated with the kinematical solutions intersect pairwise in six points, linking into a chain as illustrated in figure 4.3. Within each sphere, the Jacobian factor that arose from linearizing the cut constraints gives rise to a measure which has two poles, located at the intersection with the neighboring spheres in the chain. These poles were called hidden or composite leading singularities in refs. [19, 20, 33]. Pleasingly, we find that they are directly related to the physical collinear and infrared singularities of the theory.[3]

[3] One may inquire about the Jacobian poles coming from three-point vertices in the center of the double-box graph. While these certainly do correspond to a dangerous infrared-singular region of integration, in this case there is not necessarily a divergence. For instance, the fully massive four-point double box, belonging to case 3 below, is infrared finite.

4.2.2 Case 2: (μ_1, μ_2, μ_3) = (M, m, m), (m, M, m) or (m, m, M)

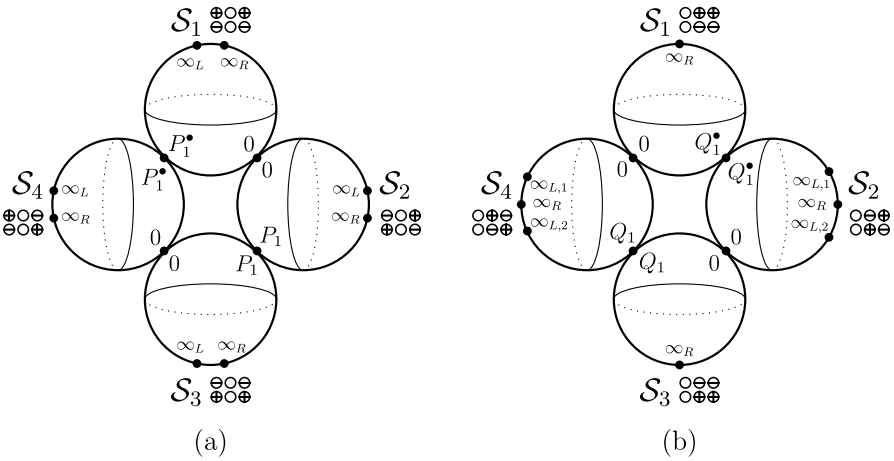

Figure 4.4. The four different classes of kinematical solutions to the heptacut constraints in case 2: exactly two vertical lines of the double-box graph are part of some three-point vertex. Figure (a) illustrates the (m, M, m) subcase, whereas figure (b) illustrates the (M,m,m) subcase. The only difference between these two subcases is the number of points contained in each sphere at which one of the loop momenta becomes infinite. We observe that in both subcases the number of independent residues one can take is 8.

This is the case where exactly two vertical lines of the double-box graph are part of some three-point vertex. The analysis leading to rules 1-3 in Section 4.2.1 remains valid and shows that there are exactly four kinematical solutions for any topology belonging to this case. These solutions are uniquely characterized by those assignments of vertex chiralities where no two $\oplus$ or $\ominus$ occur in the same vertical line. Based on our insights from the previous subsection, it is natural to expect that the four Riemann spheres associated with the kinematical solutions again have pointwise intersections and are linked into a chain. This picture turns out to be correct, and we will now elaborate on some of its details.

For the double-box topologies of the type (m, M, m), one finds that the intersection points coincide with the poles of the Jacobian in eq. (4.14), in complete analogy with case 1. Moreover, each of these intersection points is associated with the simultaneous collinearity of the momenta in some three-point vertex of the double-box graph, again in exact analogy with case 1. The kinematical solutions of subcase (m, M, m) are illustrated in figure 4.4(a).

Seemingly, a new technical issue arises for the topologies of type (M, m, m):[4] the square root in eq. (4.14) suggests that the Jacobian contains branch

[4]By assumption, at least one of the vertex momenta K_3 or K_6 (defined in figure 4.1) vanishes. Without loss of generality, we take K_6 to vanish here.

cuts. Despite appearances, the radicand is in fact a perfect square, as can easily be seen by writing the central-propagator condition $0 = (\ell_1 + \ell_2)^2 = \langle \ell_1 \, \ell_2 \rangle [\ell_1 \, \ell_2]$ in the factorized form

$$\begin{aligned}(\ell_1+\ell_2)^2 &= \frac{1}{\alpha_1^2\beta_2^2}\Big(\big(\alpha_1\langle K_1^\flat| + \alpha_4\langle K_2^\flat|\big)\big(\beta_2|K_5^\flat\rangle + \beta_3|K_4^\flat\rangle\big)\Big) \\ &\qquad \times \Big(\big(\alpha_1[K_1^\flat| + \alpha_3[K_2^\flat|\big)\big(\beta_2|K_5^\flat] + \beta_4|K_4^\flat]\big)\Big) \\ &= 0\,. \end{aligned} \tag{4.37}$$

Plugging eq. (4.37) into eq. (4.13) and performing the last integration yields an explicitly rational formula for the Jacobian, containing poles rather than branch cuts.

The (M, m, m) subcase thus presents no new features compared to the (m, M, m) subcase, except in one regard, illustrated in figure 4.4(b): the number of points in each Riemann sphere at which one of the loop momenta becomes infinite. This can be understood as follows. For solutions $\mathscr{S}_2$ and $\mathscr{S}_4$, the fact that $S_1 S_2 \neq 0$ implies that $\alpha_3 \sim z$ and $\alpha_4 \sim \frac{1}{z}$, allowing for two distinct points on each of these spheres at which the left loop momentum ℓ_1 becomes infinite, denoted respectively as $\infty_{L,1}$ and $\infty_{L,2}$ in figure 4.4(b). On the other hand, in solutions $\mathscr{S}_1$ and $\mathscr{S}_3$ the loop momentum ℓ_1 assumes a constant value independent of z.[5] In particular, neither of these spheres contain any point at which ℓ_1 becomes infinite.

The above reasoning readily extends to case 1 and explains the positioning of the infinity poles in figure 4.3.

From figures 4.3 and 4.4 we observe that in both case 1 and 2, the number of independent residues one can take is 8. Here, the qualifier "independent" refers to the fact that on any given Riemann sphere, the residues necessarily add to zero, allowing any one residue to be expressed in terms of the remaining ones on the sphere. Thus, counting the number of poles shown in figures 4.3 and 4.4, and subtracting the number of Riemann spheres to compensate for the redundancy, we find 8 independent residues in all cases considered so far.

[5] To be somewhat more detailed, the chirality distributions in solutions $\mathscr{S}_1$ and $\mathscr{S}_3$ allow us to construct an "effective" one-loop box, obtained by collapsing the horizontal propagators between same-chirality labels on the right loop. As it turns out, the solution to the quadruple-cut constraints of this one-loop box is exactly equal to the left loop momentum ℓ_1 in the original heptacut double box. But as the quadruple cut freezes all components of the one-loop box momentum, this implies that the ℓ_1 obtained from $\mathscr{S}_1$ and $\mathscr{S}_3$ cannot have any dependence on z.

4.2.3 Case 3: (μ_1, μ_2, μ_3) = (M, M, m), (M, m, M) or (m, M, M)

In double-box topologies where exactly one vertical line of the graph is part of some three-point vertex, the rules of Section 4.2.1 imply that there are two kinematical solutions.

In the (M, M, m) case, one of the two Riemann spheres can be parametrized by $z \equiv \alpha_3$ (and its parity conjugate by $z \equiv \alpha_4$), and so the equations (4.14)-(4.17) readily apply. Because $B_{-1} = 0$, the Jacobian (4.14) is manifestly a rational function and has only poles in z. Exactly as in the previous cases, these poles are located at the intersections of the Riemann spheres; in particular, the Jacobian has exactly two poles on each sphere.

In the (M, m, M) case, assuming again (without loss of generality) that $K_6 = 0$, we can proceed as in the (M, m, m) case above, following eq. (4.37). The same expression remains valid here and makes manifest the fact that the Jacobians are rational functions (of the variables $\alpha_3, \alpha_4, \beta_3$ or β_4). Again, the poles of the Jacobians coincide with the intersections of the Riemann spheres corresponding to the kinematical solutions.

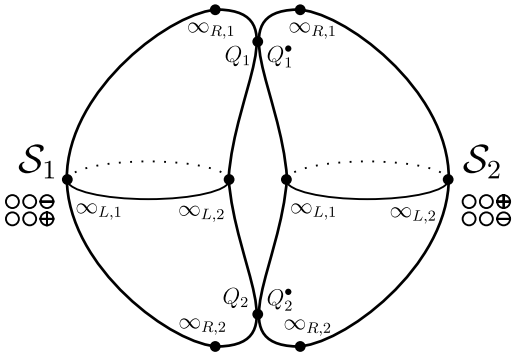

Figure 4.5. The two different classes of kinematical solutions to the heptacut constraints in subcase (M, M, m) of case 3. The subcases (M, m, M) and (m, M, M) are similar. Again the number of independent residues one can take is 8.

The two kinematical solutions associated with the subcase (M, M, m) are illustrated in figure 4.5 which also shows that the number of independent residues one can take is again 8, as in the previous cases. The other subcases (M, m, M) and (m, M, M) are similar.

4.2.4 Case 4: $(\mu_1, \mu_2, \mu_3) = (\mathrm{M}, \mathrm{M}, \mathrm{M})$

This is the case in which the double-box graph contains no three-point vertices. For the scattering of massless particles, the first time this occurs is for 10 particles, as depicted in figure 4.6.

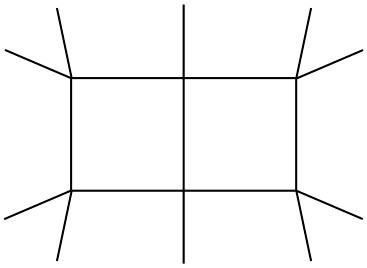

Figure 4.6. The integral $I_{(2,2,1,2,2,1)}$, the simplest example of an integral with more than three particles at all vertices, and whose heptacut Jacobian $J(z)$ accordingly has branch cuts that cannot be removed by any reparametrization $z \to \varphi(z)$. As argued in the main text, this is presumably related to the appearance of functions in the analytic expression for $I_{(2,2,1,2,2,1)}$ which cannot be expressed in terms of generalized polylogarithms.

To analyze this case, we return to the Jacobian determinant in eq. (4.14) which takes the form

$$J = \oint_{\Gamma_i} \frac{dz}{\sqrt{Q(z)}} \tag{4.38}$$

where $Q(z) = z^2(B_0(z)^2 - 4B_1(z)B_{-1}(z))$ is a quartic polynomial. Numerically, we find that for generic 10-particle kinematics, the four roots r_i of this polynomial are distinct. This means that, contrary to the previous cases, the Jacobian contains genuine branch cuts (meaning that they cannot be removed by any redefinition of z). The integration variable z in eq. (4.38) therefore parametrizes a two-sheeted cover of the Riemann sphere. This is topologically equivalent to an elliptic curve (i.e., a genus one Riemann surface), as illustrated in figure 4.7. In particular, there is a single class of kinematical solutions to the heptacut constraints (4.3)-(4.9) in this case.

For an elliptic curve there are two natural cycles over which the z integration in eq. (4.38) can be performed, generalizing the notion of a residue – namely, its topological cycles Γ_1 and Γ_2, respectively shown in red and blue in figure 4.7. In terms of the z variable, these are cycles which enclose a pair of branch points. Integrations over such cycles produce so-called complete elliptic integrals of the first kind $K(t)$ where the argument t is some cross-ratio of the four roots of the radicand $Q(z)$. As they arise when performing the loop integration on a compact T^8 contour, the integration cycles Γ_1 and Γ_2 define leading singularity cycles of the double-box integral.

As illustrated in figure 4.7, the number of poles at which one of the loop momenta becomes infinite is 8. This can easily be explained as follows. The fact that $S_1 S_2 \neq 0$ implies that $\alpha_3 \sim z$ and $\alpha_4 \sim \frac{1}{z}$, allowing for two distinct points on each sheet of the elliptic curve at which the left loop momentum ℓ_1 becomes infinite; these points are denoted as $\infty_{L,i}$ in the figure. Moreover, since each of the sheets can equivalently be parametrized in terms of β_3 or β_4, the fact that $S_4 S_5 \neq 0$ implies that $\beta_3 \sim z$ and $\beta_4 \sim \frac{1}{z}$, allowing for two distinct points on each sheet at which the right loop momentum ℓ_2 becomes infinite; these points are denoted as $\infty_{R,i}$. Thus, there are in total 8 poles on the elliptic curve.

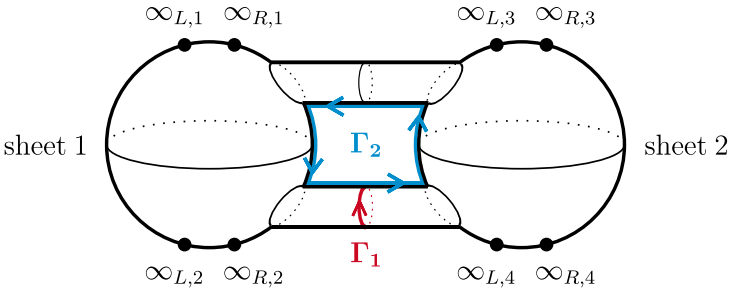

Figure 4.7. The single class of kinematical solutions to the heptacut constraints in case 4 where the double-box graph contains no three-point vertices. Here, the Jacobian develops branch cuts, and the heptacut loop-momentum parameter z thus parametrizes a two-sheeted cover of the Riemann sphere. The two sheets are shown glued together along their branch cuts, illustrating how this Riemann surface is topologically equivalent to an elliptic curve. The topological cycles Γ_1 and Γ_2, respectively shown in red and blue, enclose two distinct pairs of branch points and provide natural contours of integration for the heptacut double box in eq. (4.38). We observe that there are eight poles at which one of the loop momenta becomes infinite. In this case one finds a total of nine independent leading-singularity cycles, as explained in the main text.

The residues of these 8 poles are not all independent, however. For instance, their sum is zero as it is corresponds to a contractible cycle, as can be seen from figure 4.7. If all the infinity poles are only simple poles, which is the case if all numerator insertions in the double-box integral are at most linear in each of the loop momenta ℓ_1, ℓ_2, there would exist a second, less obvious relation[6]. However, the large-momentum behavior of theories such as pure Yang-Mills or QCD are not such as to produce only simple poles, and so this relation does not apply. Including the two topological cycles Γ_i in our

[6]This relation is easier to describe when the elliptic curve is viewed as the complex plane modulo the doubly-periodic identification $z \simeq z+1$, $z \simeq z+\tau$. While the first relation mentioned in the main text arises from integrating a form $\omega(z)$ along the boundary of a fundamental domain, the second relation arises from integrating $\omega(z)z$. In the absence of double poles, the latter relation relates the sum of the residues weighted by z to integrals over Γ_1 and Γ_2. We refer the reader to ref. [39] for more details; in particular, to Chapter III, Proposition 2.1.

counting, we thus find a total of 9 independent leading-singularity cycles in case 4, in contradistinction with the previous cases 1-3.

Finally, let us summarize our discussion of the number of solutions to the maximal cut of the double-box graph in figure 4.1. We have observed that as the number of three-point vertices in the double-box graph grows, the number of associated Riemann surfaces increases from one surface (of genus one) to two spheres linked by pointwise intersections, and further on to four, and finally six spheres thus linked.

The branching of kinematical solutions can be understood intuitively from the observation that the equation $x_1 x_2 = m$ with $m \neq 0$ has a single connected component as its solution when x_1 and x_2 are allowed to be complex; but two essentially-disconnected components when $m = 0$. Applied to, e.g., the equation $\alpha_3 \alpha_4 \propto S_1 S_2$ in eq. (4.12), this insight leads us to expect a splitting of one Riemann sphere into two as $S_1 S_2 \to 0$.[7] This is indeed what happens, as exemplified by the splitting of the sphere $\mathscr{S}_1$ in figure 4.5 into the spheres $\mathscr{S}_3$ and $\mathscr{S}_4$ in figure 4.4(a) whose left-most pair of double-box vertices then acquires chiralities. Taking the limit $\mu_2 \to \mathrm{m}$ of figure 4.4(a), the middle pair of vertices will acquire chiralities, splitting the spheres $\mathscr{S}_2$ and $\mathscr{S}_4$ into the respective pairs $(\mathscr{S}_1, \mathscr{S}_2)$ and $(\mathscr{S}_3, \mathscr{S}_4)$ in figure 4.3. In contrast, the solutions $(\mathscr{S}_1, \mathscr{S}_3)$ in figure 4.4(a) admit only one chirality assignment to the middle vertices, as dictated by the rules in Section 4.2.1, and are transformed into the solutions $(\mathscr{S}_5, \mathscr{S}_6)$ in figure 4.3. As the resulting six solutions shown in figure 4.3 have chiralities assigned to all pairs of vertices, the splitting of Riemann spheres terminates at this stage. A summary of the chiral branchings described here is given in figure 4.8.

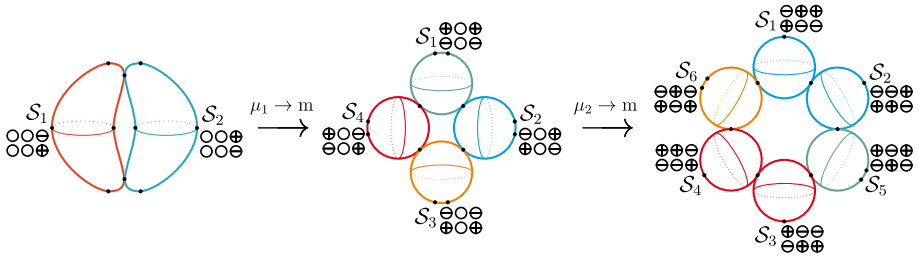

Figure 4.8. The chiral branchings described in the main text above. Daughter spheres are drawn with the same (or similar) color as the mother spheres. The two Riemann spheres on the left should be thought of as arising from a $\mu_3 \to \mathrm{m}$ limit of the elliptic curve in figure 4.7.

Let us also remark that by giving generic small masses to the internal lines of the double-box integral with four lightlike external momenta, we expect

[7] We thank D. Kosower for this observation.

that the six spheres that arose in the massless case are turned into a smooth elliptic curve.

Finally, it should be mentioned that the algebraic problem of solving the on-shell constraints (4.3)-(4.9) can be recast as a geometric problem in momentum twistor space where it amounts to finding two lines which appropriately intersect a set of lines encoding the external momenta. Besides geometric elegance, this formulation has the conceptual advantage of being inherently coordinate free. We refer to ref. [40] for the one-loop case, and to Section 4 of Paper III for the two-loop case.

Maximal cuts versus integrated expressions

Widely propagated folklore holds that there should be a close connection between the maximal cut of a given integral and the analytic form of its integrated expression. The appearance of an elliptic curve in case 4 provides closer evidence of such a connection, as we will now argue. As shown in ref. [41], eq. (8.1), the integral in figure 4.6 can be represented as a one-scale integral as follows

$$I_{(2,2,1,2,2,1)} = \int_u^\infty \frac{du'}{\sqrt{\tilde{Q}(u')}} \times (\mathrm{Li}_3(\cdots) + \cdots) \tag{4.39}$$

where $\tilde{Q}(u')$ defines the same elliptic curve as $Q(z)$ in eq. (4.38). It may be shown that the sunrise integral with massive propagators admits a very similar integral representation, with the integrand of eq. (4.39) containing $\log(\cdots)$ instead of $\mathrm{Li}_3(\cdots)$ [42]. This integral was studied analytically in great detail in refs. [43, 44] and references therein, and was found not to be expressible in terms of polylogarithms. Given the similarity with eq. (4.39), we thus find it extremely unlikely that $I_{(2,2,1,2,2,1)}$ is expressible in terms of (multiple) polylogarithms. Thus the topology of the Riemann surface parametrizing the heptacut solutions appears to be reflected in the integrated expression.

Moreover, as argued in Appendix B of Paper III, such more general functions must necessarily be present in the scattering amplitudes of $\mathcal{N} = 4$ super Yang-Mills theory. In this appendix it is shown that a particular two-loop N^{3}MHV amplitude for the scattering of 10 massless scalars is given by the single integral $I_{(2,2,1,2,2,1)}$, thus ruling out any possible cancelations. This suggests that the realm of $\mathcal{N} = 4$ SYM extends beyond that of polylogarithms.

Another observation one can make along these lines is that two-loop integrands with associated T^8-contours, such as double boxes and double triangles, contain transcendentality-4 functions in the finite (i.e., $\mathcal{O}(\varepsilon^0)$) part of their integrated expressions. In contrast, the finite part of the bubble-box contains only transcendentality-3 functions, consistent with the bubble-box integrand having no associated T^8-contours.[8]

[8] We refer to eqs. (22)-(25) of ref. [45] for the analytical result for the scalar double box, and to eq. (13) of ref. [46] for the analytical result for the double box with the $(\ell_1 + k_4)^2$ numerator

4.3 Uniqueness of two-loop master contours

Let us now recapitulate the situation from Chapter 3 where we used heptacuts to determine the double-box coefficients of the massless four-point amplitude. As illustrated in figure 3.4, the contours associated with the heptacut may encircle 14 different leading singularities, in the notation of Chapter 3 denoted as[9]

$$\begin{aligned} a_{1,i} &\longrightarrow \text{encircling } z=0 \text{ for solution } \mathscr{S}_i \\ a_{2,i} &\longrightarrow \text{encircling } z=-\chi \text{ for solution } \mathscr{S}_i \\ a_{3,j} &\longrightarrow \text{encircling } z=-\chi-1 \text{ for solution } \mathscr{S}_j \end{aligned} \tag{4.40}$$

where $i=1,\ldots,6$, $j=5,6$ and $\chi \equiv \frac{s_{14}}{s_{12}}$. Here, the 12 winding numbers $a_{1,i}$ and $a_{2,i}$ are associated with Jacobian poles whereas the 2 winding numbers $a_{3,5}$ and $a_{3,6}$ are associated with the poles ∞_R in $\mathscr{S}_5$ and $\mathscr{S}_6$ in figure 4.3. The consistency conditions on the maximal-cut contours that they must annihilate any integrand that integrates to zero on $\mathbb{R}^D \times \mathbb{R}^D$ were shown to translate into the following linear constraints on the winding numbers,

$$\begin{aligned} a_{1,2}+a_{1,5}-a_{1,4}-a_{1,6} &= 0 \\ a_{2,1}+a_{2,2}-a_{2,3}-a_{2,4} &= 0 \\ a_{2,6}-a_{1,1}-a_{2,5}+a_{1,3} &= 0 \\ a_{3,5}-a_{3,6} &= 0 \\ a_{1,2}+a_{1,5}+a_{1,4}+a_{1,6} &= -a_{2,6}+a_{1,1}-a_{2,5}+a_{1,3}+a_{3,5}+a_{3,6} \\ a_{3,5}+a_{3,6} &= -\tfrac{1}{2}\textstyle\sum_{j=1}^{6}(a_{1,j}-a_{2,j})+\tfrac{3}{2}\sum_{j\neq 1,3}a_{1,j} \end{aligned} \tag{4.41}$$

where the first four followed from the vanishing integrations of integrands involving Levi-Civita contractions of loop momenta and the last two followed from integration-by-parts identities between tensor double-box integrals. Imposing these constraints on the winding numbers leaves $14-6=8$ free parameters in the contours.

Moreover, in the case of four massless external momenta, there turn out to be exactly two linearly independent master integrals of the double-box topology. The particular masters used in Chapter 3 have the maximal cuts

$$\chi s_{12}^3 I^{\text{cut}}_{1,1,0,1,1,0}[1] = \sum_{i=1}^{6}(a_{1,i}-a_{2,i}) \tag{4.42}$$

$$2s_{12}^2 I^{\text{cut}}_{1,1,0,1,1,0}[\ell_1\cdot k_4] = \sum_{i\neq 1,3} a_{1,i} \tag{4.43}$$

insertion. Moreover, the double triangle was calculated in ref. [47], and the result given in eqs. (23)-(24) (see figures 1, 2 and eq. (1) for an explanation of the notation). Finally, the bubble-box was calculated in ref. [48], and the result is given in eqs. (3.13)-(3.15).

[9] Recall that in Chapter 3 we employed a rescaled version of the loop momentum parametrization (4.10)-(4.11) used here. As a result of the rescaling, all nonzero Jacobian poles are located at $z=-\chi$.

where we remind the reader of the numerator insertion notation explained in eq. (4.2). As we saw, it is possible to find contours $(a_{1,i}, a_{2,i}, a_{3,j})$ satisfying the constraint equations (4.41) with the additional property of setting the right hand sides of eqs. (4.42) and (4.43) respectively equal to one and zero (or vice versa). This is exemplified in eqs. (3.46)-(3.47), though we emphasize that these are not the most general solutions. Such contours thus isolate the contribution of a single master integral in the basis decomposition (3.2) and are therefore referred to as master contours. With the 8 free parameters in the contours that remained in the previous paragraph, we thus find a total of $8-2=6$ free parameters in the two-loop master contours.

This stands in contrast to the situation at one loop, reviewed in Section 2.3 where we found uniquely defined contours associated with the boxes and triangles; formulas for the extraction of bubbles and tadpoles, similarly, do not contain any ambiguity. From this point of view, the appearance of 6 unconstrained variables in the analogous two-loop master contours thus comes as something of a surprise.

By considering figure 4.3, this phenomenon can now easily be explained: all of the Jacobian poles belong to two Riemann spheres and so are counted twice in the above counting (4.40). Due to this, a contour which encircles the $z=0$ pole in $\mathscr{S}_2$ and in $\mathscr{S}_5$ with identical winding numbers in the two spheres, and no other poles, is equivalent to a zero-cycle. The addition of such zero-cycles defines an equivalence relation on the vector space spanned by the leading-singularity contours: any two contours related by the addition of such zero-cycles are equivalent.

This manifests itself as the invariance of the contour constraint equations (4.41) under the translations[10]

$$
\begin{aligned}
(a_{2,1}, a_{2,2}) &\longrightarrow (a_{2,1}, a_{2,2}) + (\xi_1, -\xi_1) && (4.44)\\
(a_{1,2}, a_{1,5}) &\longrightarrow (a_{1,2}, a_{1,5}) + (\xi_2, -\xi_2) && (4.45)\\
(a_{2,5}, a_{1,3}) &\longrightarrow (a_{2,5}, a_{1,3}) + (\xi_3, \xi_3) && (4.46)\\
(a_{2,3}, a_{2,4}) &\longrightarrow (a_{2,3}, a_{2,4}) + (\xi_4, -\xi_4) && (4.47)\\
(a_{1,4}, a_{1,6}) &\longrightarrow (a_{1,4}, a_{1,6}) + (\xi_5, -\xi_5) && (4.48)\\
(a_{2,6}, a_{1,1}) &\longrightarrow (a_{2,6}, a_{1,1}) + (\xi_6, \xi_6)\,, && (4.49)
\end{aligned}
$$

corresponding to the addition of a zero-cycle encircling each Jacobian pole with the winding numbers $(\xi_i, \pm\xi_i) \in \mathbb{Z}\times\mathbb{Z}$ on the two Riemann spheres containing the pole. These equivalence relations allow us to add to an arbitrary

[10] Please note that in this section, in order to make the connection with Chapter 3 as clear as possible, we adopt the conventions of this reference on the orientations of contours encircling poles in the various Riemann spheres and on the signs of the Jacobians. These conventions differ from those used in Chapter 3, in particular, with respect to the minus signs described below eq. (4.13). The pattern of relative signs between the zero-cycle winding numbers $(\xi_i, \pm\xi_i)$ in eqs. (4.44)-(4.49) owes to the omission of these minus signs in Chapter 3.

contour, characterized by the winding numbers $(a_{1,i}, a_{2,i}, a_{3,j})$, the zero-cycle with $(\xi_i) = (-a_{2,1}, -a_{1,2}, -a_{2,5}, -a_{2,3}, -a_{1,4}, -a_{2,6})$ to obtain an equivalent contour characterized by 8 independent parameters. This shows that the leading singularity contours are characterized by 8 rather than 14 winding numbers.

4.3.1 Invariant labeling of contours

To get around the redundancy built into the notation (4.40), we will from now on adopt the following notation for the independent winding numbers

$$\Omega = (\omega_{1\cap 2},\ \omega_{2\cap 5},\ \omega_{5\cap 3},\ \omega_{3\cap 4},\ \omega_{4\cap 6},\ \omega_{6\cap 1},\ \omega_{5,\infty_R},\ \omega_{6,\infty_R})\,. \tag{4.50}$$

Here $\omega_{i\cap j}$ denotes the winding around the intersection point of $\mathscr{S}_i$ and $\mathscr{S}_j$ of a small circle supported in either of these spheres, with positive orientation in $\mathscr{S}_i$ or with negative orientation in $\mathscr{S}_j$. Analogously, ω_{j,∞_R} denotes the winding around the point ∞_R in $\mathscr{S}_j$ where the right loop momentum ℓ_2 becomes infinite (see figure 4.3). Of course, we could trade some of the variables in eq. (4.50) for winding numbers around the other infinity poles in figure 4.3, but we find the above choice to be the most convenient. Also note that (4.50) has the added advantage over the notation (4.40) of not making reference to a particular parametrization of the Riemann spheres $\mathscr{S}_i$, hence the title of this subsection.

The 8 winding numbers ω_i in eq. (4.50) are equal to the following linear combinations of the $a_{i,j}$

$$\begin{aligned}\Omega\ = \big(&a_{2,1}+a_{2,2},\ \ -a_{1,2}-a_{1,5},\ \ a_{2,5}-a_{1,3},\ \ a_{2,3}+a_{2,4},\\ &-a_{1,4}-a_{1,6},\ \ a_{2,6}-a_{1,1},\ \ a_{3,5},\ \ a_{3,6}\big)\,.\end{aligned} \tag{4.51}$$

In analogy with the notation (4.50) for the winding numbers around the leading singularities, let us introduce the following notation for the residues. The residue at the intersection point of the spheres $\mathscr{S}_i$ and $\mathscr{S}_j$, computed from the viewpoint of sphere $\mathscr{S}_i$, will be labeled $\mathrm{Res}_{i\cap j}$. Alternatively, we could consider the same residue, but computed from the viewpoint of $\mathscr{S}_j$. As noted around eqs. (4.31)-(4.36), the result would be equal and opposite. Thus, we can re-express these identities in a very compact form by declaring $\mathrm{Res}_{i\cap j}$ to be antisymmetric,

$$\mathrm{Res}_{i\cap j}\Phi(z) = -\mathrm{Res}_{j\cap i}\Phi(z)\,. \tag{4.52}$$

Here Φ denotes an arbitrary function of the loop momenta. The other residues will be labeled $\mathrm{Res}_{i,\infty_L}$ and $\mathrm{Res}_{i,\infty_R}$, according to either the left or right loop momentum of the double-box graph approaching infinity. The identities (4.31)-(4.36) are dual to the contour equivalence relations (4.44)-(4.49); an application of them is given in Section 4.4.

Re-expressing the contour constraint equations (4.41) in terms of the winding numbers (4.50)-(4.51), they are found to take the form

$$\begin{aligned}
\omega_{2\cap 5} - \omega_{4\cap 6} &= 0 \\
\omega_{1\cap 2} - \omega_{3\cap 4} &= 0 \\
\omega_{6\cap 1} - \omega_{5\cap 3} &= 0 \\
\omega_{5,\infty_R} - \omega_{6,\infty_R} &= 0 \\
\omega_{2\cap 5} + \omega_{4\cap 6} &= \omega_{5\cap 3} + \omega_{6\cap 1} - \omega_{5,\infty_R} - \omega_{6,\infty_R} \\
\omega_{5,\infty_R} + \omega_{6,\infty_R} &= \tfrac{1}{2}(\omega_{1\cap 2} + \omega_{3\cap 4} + \omega_{5\cap 3} + \omega_{6\cap 1}) - \omega_{2\cap 5} - \omega_{4\cap 6}
\end{aligned} \tag{4.53}$$

while the heptacut master double boxes used in Chapter 3 evaluate to

$$\chi s_{12}^3 I^{\text{cut}}_{1,1,0,1,1,0}[1] = \omega_{1\cap 2} + \omega_{2\cap 5} + \omega_{5\cap 3} + \omega_{3\cap 4} + \omega_{4\cap 6} + \omega_{6\cap 1} \tag{4.54}$$

$$2s_{12}^2 I^{\text{cut}}_{1,1,0,1,1,0}[\ell_1 \cdot k_4] = \omega_{2\cap 5} + \omega_{4\cap 6}\,. \tag{4.55}$$

We observe that upon imposing the 6 constraint equations (4.53) on the 8 winding numbers $\omega_{i\cap j}$ given in eq. (4.50), we are left with 2 unconstrained parameters. This number of free parameters exactly equals the number of master double-box integrals at four points. In other words, we observe that in terms of the ω-variables, there is a unique master contour associated with each of the master double-box integrals in eqs. (4.54)-(4.55). These contours are respectively characterized by the winding numbers

$$\Omega_1 = \frac{1}{4}(1,0,1,1,0,1,1,1) \quad \text{and} \quad \Omega_2 = -\frac{1}{4}(1,-2,1,1,-2,1,3,3)\,. \tag{4.56}$$

More generally, as shown in Paper IV, any four-point double-box configuration belonging to case 1 (referred to in Paper IV as class (c)), has 8 independent leading-singularity winding numbers subject to 6 constraints. The number of remaining free parameters is thus $8-6=2$, equal to the number of linearly independent master double boxes in this case. Moreover, any four-point double-box configuration belonging to case 2 (referred to in Paper IV as class (b)), has 8 independent leading-singularity winding numbers subject to 5 constraints. The number of remaining free parameters is thus $8-5=3$, equal to the number of linearly independent master double boxes in this case. In both these cases, the free parameters can be set to appropriate values, yielding uniquely defined master contours associated with each double-box master integral. We refer to eq. (6.3) of Paper IV for the master contours in case 2; and to eq. (6.5) for the master contours in case 1.

The observed uniqueness of master contours at two loops is in perfect analogy with the situation in one-loop generalized unitarity [17, 30] and constitutes the main result of this chapter.

It is worth remarking that the Levi-Civita constraints in the top four equations in eq. (4.53) (expressing parity invariance of the master contours), can

be rephrased geometrically as follows. Since parity-conjugate solutions appear antipodally in the chains of Riemann spheres in figures 4.3, 4.4, 4.5, parity $\oplus \longleftrightarrow \ominus$ has the effect of rotating these chains by 180°. Parity invariance is thus simply the statement that the master contours are invariant under such rotations.

4.4 Residues of maximally cut amplitudes

As we have seen in Chapter 3, the residues of the heptacut two-loop amplitude $J(z)\prod_{j=1}^{6} A_j^{\text{tree}}(z)\Big|_{\mathscr{S}_i}$ at the Jacobian poles form the input out of which the double-box coefficients of the amplitude are computed. An amusing application of the identities (4.31)-(4.36) arises in the context of evaluating these residues, relating them across different kinematical solutions. As a result, these identities explain the vanishing of certain residues, as well as the seemingly accidental equality between pairs of other residues. This in turn allows one to cut the work of evaluating these residues in half.

As an example, let us consider the heptacut illustrated in figure 4.9 of the two-loop amplitude $A^{(2)}(1^-,2^-,3^+,4^+,5^+)$. The helicities assigned to the internal and external states allow only gluons to propagate in the loops; this in turn implies [36] that the results for the heptacut amplitude within $\mathscr{N} = 4,2,1,0$ Yang-Mills theory are identical.

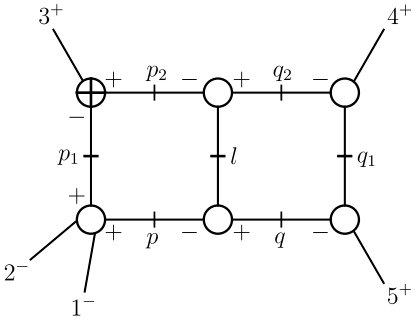

Figure 4.9. A heptacut of the two-loop amplitude $A^{(2)}(1^-,2^-,3^+,4^+,5^+)$. The heptacut two-loop amplitude $J(z)\prod_{j=1}^{6} A_j^{\text{tree}}(z)\Big|_{\mathscr{S}_i}$ only receives nonvanishing contributions from kinematical solutions consistent with the assigned internal helicities.

The heptacut $J(z)\prod_{j=1}^{6} A_j^{\text{tree}}(z)\Big|_{\mathscr{S}_i}$ shown in figure 4.9 of this amplitude only receives nonvanishing contributions from kinematical solutions consistent with the internal helicites shown there – in particular kinematical solutions whose

$(3, p_1, p_2)$-vertex is $\overline{\text{MHV}}$. By inspection of figure 4.3 we thus see that

$$\prod_{j=1}^{6} A_j^{\text{tree}}(z)\Big|_{\mathscr{S}_i} = 0 \qquad \text{for} \quad i = 1,2,6\,. \tag{4.57}$$

For the heptacut amplitude evaluated at the remaining three kinematical solutions, direct calculation reveals the residues at the Jacobian poles to be

$$\frac{1}{iA^{\text{tree}}_{--+++}} \operatorname*{Res}_{z=(0,Q_1)} J(z) \prod_{j=1}^{6} A_j^{\text{tree}}(z)\Big|_{\mathscr{S}_3} = (1,-1) \tag{4.58}$$

$$\frac{1}{iA^{\text{tree}}_{--+++}} \operatorname*{Res}_{z=(0,P_1)} J(z) \prod_{j=1}^{6} A_j^{\text{tree}}(z)\Big|_{\mathscr{S}_4} = (0,1) \tag{4.59}$$

$$\frac{1}{iA^{\text{tree}}_{--+++}} \operatorname*{Res}_{z=(0,P_1)} J(z) \prod_{j=1}^{6} A_j^{\text{tree}}(z)\Big|_{\mathscr{S}_5} = (0,-1)\,. \tag{4.60}$$

One observes that the residues at $z = 0$ in solutions $\mathscr{S}_4$ and $\mathscr{S}_5$ are vanishing. This can now be easily explained by eqs. (4.35) and (4.32) as a consequence of the vanishing (4.57) of the heptacut amplitude on solutions $\mathscr{S}_6$ and $\mathscr{S}_2$, respectively. Moreover, eq. (4.34) relates the residues at the nonzero Jacobian poles in $\mathscr{S}_3$ and $\mathscr{S}_4$; similarly, eq. (4.33) relates residues in $\mathscr{S}_3$ and $\mathscr{S}_5$. In conclusion, the identities (4.31)-(4.36) allow us to cut the work of evaluating the residues of the heptacut two-loop amplitude at the Jacobian poles in half.

4.5 The symbol of a transcendental function

In this section we provide a brief introduction to the so-called *symbol* of a transcendental function, an object which, though only recently introduced in the amplitude literature, has gained widespread use there—extending in particular to Section 5.3 of this thesis.

The symbol made its first appearance in the amplitude literature in ref. [49] where it was used to simplify a 17-page expression [50, 51] for the so-called BDS remainder function [52], involving exotic (Goncharov) polylogarithms to a four-line expression involving classical polylogarithms. The basic idea of the symbol is to associate a tensor with a polylogarithm-type function; all the complicated functional equations among polylogarithms are then translated into algebraic relations in the tensor algebra.

As an example, let us consider the identity[11]

$$-\text{Li}_2(z) - \log z \, \log(1-z) = \text{Li}_2(1-z) - \frac{\pi^2}{6}\,. \tag{4.61}$$

[11] This example is taken from a lecture by C. Duhr from the *School of Analytic Computing in Theoretical High-Energy Physics* in Atrani, Italy during October 6-11, 2011.

To prove this identity, recall the definition of the dilogarithm as an iterated integral,

$$\mathrm{Li}_2(z) = -\int_0^z \frac{dt}{t}\log(1-t)\,, \tag{4.62}$$

or equivalently,

$$d\mathrm{Li}_2(z) = -\log(1-z)\,d\log z\,. \tag{4.63}$$

The differential of the other function appearing in the identity (4.61) is

$$d\big[\log(1-z)\log z\big] = \log z\,d\log(1-z) + \log(1-z)\,d\log z\,. \tag{4.64}$$

Let us use these differentials as inspiration to define a linear map,

$$\begin{aligned}\mathscr{S}(\mathrm{Li}_2(z)) &= -\big[(1-z)\otimes z\big] &(4.65)\\ \mathscr{S}(\log z\,\log(1-z)) &= z\otimes(1-z)+(1-z)\otimes z\,, &(4.66)\end{aligned}$$

known as the *symbol*.

Applying the symbol map to the left hand side of eq. (4.61) yields

$$\begin{aligned}-\mathscr{S}(\mathrm{Li}_2(z)) - \mathscr{S}(\log z\,\log(1-z)) &= (1-z)\otimes z - \big[z\otimes(1-z)+(1-z)\otimes z\big]\\ &= -\big[z\otimes(1-z)\big] &(4.67)\\ &= \mathscr{S}(\mathrm{Li}_2(1-z))\,, &(4.68)\end{aligned}$$

equal to the symbol of the right hand side of eq. (4.61), provided that

$$\mathscr{S}(\pi^2) = 0\,. \tag{4.69}$$

What we have shown is that the left and right hand sides of eq. (4.61) are equal, up to addition of terms of the form $\pi\log(z)$ or π^2 times rational functions of z. These terms must then be determined by other means.

More generally, a function of transcendentality n is defined as one which can be written as an n-fold iterated integral,

$$T_n = \int_a^b d\log R_1 \circ\cdots\circ d\log R_n = \int_a^b \left(\int_a^t d\log R_1\circ\cdots\circ d\log R_{n-1}\right) d\log R_n(t)\,. \tag{4.70}$$

Such a function has the associated symbol

$$\mathscr{S}(T_n) = R_1\otimes\cdots\otimes R_n\,. \tag{4.71}$$

For example, from this definition it immediately follows that the classical polylogarithms, iteratively defined by

$$\mathrm{Li}_n(z) = \int_0^z \mathrm{Li}_{n-1}(t)\,d\log t\,, \qquad \mathrm{Li}_1(z) = -\log(1-z)\,, \tag{4.72}$$

have the symbol

$$\mathscr{S}(\mathrm{Li}_n(z)) = -(1-z)\otimes\underbrace{z\otimes\cdots\otimes z}_{n-1\text{ factors}}\,. \tag{4.73}$$

The symbol in eq. (4.73) can be understood concretely in terms of iterated discontinuities as follows. The first entry from the left can be interpreted as the discontinuity of $\mathrm{Li}_k(z)$ across the branch cut $1 < z < \infty$. The analytic continuation of the resulting function $\mathrm{Disc}_{1<z<\infty}\mathrm{Li}_n(z) = \frac{2\pi i}{(n-1)!}(\log z)^{n-1}$ in turn has a discontinuity across the branch cut $-\infty < z < 0$; this corresponds to the second entry of eq. (4.73) (after multiplying this entry by -1, as allowed by eq. (4.75)) etc. This interpretation can be made precise and extended to all functions of the form (4.70) [53].

Moreover, the definition of the symbol in eqs. (4.70)-(4.71) immediately implies the logarithmic behavior

$$\begin{aligned} R_1 \otimes \cdots \otimes (R_a R_b) \otimes \cdots \otimes R_n = R_1 \otimes \cdots \otimes R_a \otimes \cdots \otimes R_n \\ + R_1 \otimes \cdots \otimes R_b \otimes \cdots \otimes R_n \end{aligned} \tag{4.74}$$

$$R_1 \otimes \cdots \otimes cR_j \otimes \cdots \otimes R_n = R_1 \otimes \cdots \otimes R_j \otimes \cdots \otimes R_n\,, \tag{4.75}$$

where c denotes an arbitrary constant and R_i arbitrary rational functions.

As an example of the use of the identities (4.74)-(4.75), let us consider the identity

$$\mathrm{Li}_2(z^2) = 2\mathrm{Li}_2(z) + 2\mathrm{Li}_2(-z)\,. \tag{4.76}$$

At the level of the symbol we have

$$\mathscr{S}(\mathrm{Li}_2(z^2)) = -\big[(1-z^2)\otimes z^2\big] \tag{4.77}$$

$$= -2\big[(1-z)\otimes z + (1+z)\otimes z\big] \tag{4.78}$$

$$= -2\big[(1-z)\otimes z + (1-(-z))\otimes(-z)\big] \tag{4.79}$$

$$= 2\mathscr{S}(\mathrm{Li}_2(z)) + 2\mathscr{S}(\mathrm{Li}_2(-z))\,, \tag{4.80}$$

which proves the identity (4.76), again up to addition of terms of the form $\pi\log(z)$ or π^2 times rational functions of z. The ambiguity of lower transcendental functions (times appropriate factors of π^k or $\zeta(k)$) is an inherent feature of the symbol map: when applied to a functional equation, the symbol only retains information about the leading transcendental part.

5. A basis of IR-finite integrals?

A central question in generalized-unitarity calculations concerns the choice of basis integrals in which amplitudes are expanded. Currently, methods are available to generate integration-by-parts identities [32, 54] at two loops, examples of which were used in Chapter 3. Such identities allow one to reduce any set of tensor integrals produced by the Feynman rules to a basis of one's choosing. However, it remains an open problem to single out one particularly compelling choice of two-loop basis which is universally applicable to *all* gauge theories, in particular QCD.

To guide one's search, reasonable questions to ask are: which features are desirable for the basis integrals to possess? Insisting on such features to be present, is there some systematic way of generating the appropriate integrands? And assuming such integrands can be formed, can the integrals be evaluated in practice?

In this chapter we identify a class of basis integrals which are likely to simplify unitarity calculations substantially at two loops, and moreover analytically evaluate two such integrals at four points. We remark that the presentation in Sections 5.1-5.2 is essentially that of Section 5.2 in Paper III, adding here a few comments. Section 5.3 gives an overview of the analytical evaluation in Section 6 of Paper III, skipping the technical details.

5.1 Motivation

As indicated in the basis decomposition of two-loop amplitudes in eq. (3.2), the integral coefficients are functions of the dimensional regulator ε. But in contrast to the situation at one loop, the $\mathcal{O}(\varepsilon)$ contributions to the coefficients cannot be re-expressed as rational contributions to the amplitude, and these corrections therefore form an inevitable part of the two-loop integral coefficients. The physical significance of these $\mathcal{O}(\varepsilon)$ contributions lies in the fact that in the basis expansion of the two-loop amplitude, they will multiply $\frac{1}{\varepsilon^k}$ singularities in the integrated expressions for the two-loop integrals, thus producing finite contributions to the amplitude. Their extraction therefore poses an important problem. But unfortunately, as we explained in Chapter 3, the $\mathcal{O}(\varepsilon)$ parts of two-loop integral coefficients are not obtainable from four-dimensional cuts. Instead, they must be computed by evaluating cuts in $D = 4 - 2\varepsilon$ dimensions, something which is technically much more involved.

Ideally, one would like to circumvent the need for taking cuts in $D = 4 - 2\varepsilon$ dimensions, or at least limit such computations as much as possible. One way to achieve this would be to expand the two-loop amplitude in a basis that contains as many infrared-finite integrals as possible. Indeed, although the expansion coefficients may still depend on ε, the physically relevant part of the coefficients multiplying IR-finite integrals is purely $\mathcal{O}(\varepsilon^0)$ and may thus be obtained from strictly four-dimensional cuts. Of course, as two-loop amplitudes do have IR divergences of their own (as they necessarily must, to cancel the IR divergences of tree and one-loop amplitudes in the cross-section [55, 56]), any basis of integrals must contain IR-divergent integrals[1]. Nonetheless, it is plausible that by using a basis with a minimal number of IR-divergent integrals one can minimize the work of extracting the physically relevant part of the basis integral coefficients. Focusing our attention to the double-box contributions to two-loop amplitudes, we thus turn to the question: can one find two linearly independent infrared-finite integrals with the double-box topology?

5.2 Chiral integrals

A class of integrals with the property of infrared finiteness was introduced in ref. [6] where they were used to express the integrand of $\mathcal{N} = 4$ super Yang-Mills amplitudes in a strikingly simple form. Here, we wish to investigate whether these so-called chiral numerator integrals can be used as master integrals for two-loop amplitudes in *any* gauge theory.

For four lightlike external momenta there are, up to parity conjugation, two distinct chiral numerator integrals, which we can define as[2]

$$I_{++} \equiv I_{1,1,0,1,1,0}\big[[1|\ell_1|2\rangle\langle 3|\ell_2|4]\big] \quad \times \quad [2\,3]\langle 1\,4\rangle \tag{5.1}$$

$$I_{+-} \equiv I_{1,1,0,1,1,0}\big[[1|\ell_1|2\rangle\langle 4|\ell_2|3]\big] \quad \times \quad [2\,4]\langle 1\,3\rangle \tag{5.2}$$

where we remind the reader of the numerator insertion notation explained in eq. (4.2). Similar definitions can be given for an arbitrary number of external legs, replacing the spinors $[i|$ or $\langle i|$ by their flattened counterparts $[K_i^\flat|$ or $\langle K_i^\flat|$.

This definition has a straightforward physical motivation: the infrared divergences of the massless double-box integral arise from the regions of the

[1] Unless we are prepared to accept integral coefficients with $\frac{1}{\varepsilon^k}$ singularities – which we are not.

[2] We stress that the chiral numerator integrals considered here are not exactly chiral in the sense of ref. [6], in which the general notion of a chiral integral was formulated in terms of the analytic structure of its integrand. There, chiral integrals were defined as integrals which have at most simple-pole singularities on each leading-singularity contour, and whose residues are all equal to either zero, or plus or minus one. In general, such integrals may differ from the chiral numerator integrals $I_{+\pm}$ considered here by the addition of integrals with fewer internal lines, such as triangle-boxes or double-triangles. Since we are not concerned with the latter integrals in this thesis, this distinction will not be of relevance here, however.

loop momentum integrations where a loop momentum is becoming collinear with a massless external leg, $\ell_1 \| k_{1,2}$ or $\ell_2 \| k_{3,4}$. However, in these regions, the numerator insertions $[1|\not{\ell}_1|2\rangle$ etc. approach zero, thereby rendering the integral IR finite. This observation suggests a general strategy for constructing IR-finite integrals: identify IR-dangerous regions of the scalar integral, and construct appropriate numerator insertions that vanish in these regions.

In the notation of eq. (4.50), the maximal cuts of the above integrals take the form

$$I_{++}^{\text{cut}} = \omega_{6,\infty_R} \tag{5.3}$$

$$I_{+-}^{\text{cut}} = \omega_{1\cap 2}\,, \tag{5.4}$$

receiving contributions from a remarkably small number of leading singularities. The vanishing of a large number of leading-singularity residues reflects the absence of infrared singularities in the uncut integrals, as observed in Section 4.2.1. Here, we could of course also have chosen to consider the integrals I_{--} and I_{-+} whose numerator insertions are obtained by parity conjugation $\langle\cdot|\cdot|\cdot] \longleftrightarrow [\cdot|\cdot|\cdot\rangle$ of eqs. (5.1)-(5.2). However, on the solution of the first four constraint equations of (4.53) (which express parity invariance of the contours), one finds that the maximal cuts of parity-conjugate integrals are equal. The largest potentially linearly independent set of chiral double boxes therefore consists, at four points, of two integrals which we choose as those given in eqs. (5.1)-(5.2).

Considering these two integrals, let us now ask: are they linearly independent as master integrals? Equivalently, can one find two distinct contours, satisfying the constraint equations (4.53), each with the property of yielding a nonvanishing maximal cut for precisely one of these integrals?

Remarkably, such master contours do exist: the contours which extract the coefficient of I_{++} and I_{+-} are, respectively,

$$\Omega_{++} = (0,-1,0,0,-1,0,1,1) \quad \text{and} \quad \Omega_{+-} = (1,1,1,1,1,1,0,0)\,. \tag{5.5}$$

Thus the integrals I_{++} and I_{+-} are linearly independent and may be used as master integrals for the double-box contributions to two-loop amplitudes in *any* gauge theory. Incidentally, as a bonus, the contours in eq. (5.5) take a somewhat simpler form than those in eq. (4.56) whose winding numbers display no easily discernible pattern.

The choice of using the chiral numerator integrals as master integrals provides a substantial simplification over other choices (such as that of eqs. (4.54)-(4.55)), as their infrared finiteness allows their expansion coefficients in the two-loop amplitude to be obtained from strictly four-dimensional cuts. But one might worry that the technical difficulty is simply shifted elsewhere, in particular to the analytical evaluation of these integrals. To counter this concern, we present in the next section a detailed analytical evaluation of these integrals and moreover find the result to take a remarkably compact form.

5.3 Analytical evaluation of chiral double boxes

In the previous section we found that the chiral numerator integrals in eqs. (5.1)-(5.2) form a basis of the master integrals with the double-box topology.

In this section we turn to the question of evaluating these integrals analytically. We will focus our attention on obtaining analytical expressions in the special case of four lightlike external momenta, but we are hopeful that many of the ideas presented here will prove applicable for higher numbers of external legs as well. Our aim in this section is to give an overview of the calculation. We refer to Section 6 of Paper III for more details.

Let us start by observing that as a result of the infrared (and also UV) finiteness of our integrals, they can be evaluated in strictly four dimensions, with no need for regularization. Our starting point is the standard Feynman parametrization formula in terms of which our integrals may be written[3]

$$\begin{aligned} I_{++} &= -\chi^2 \left(1 + (1+\chi)\frac{\partial}{\partial\chi}\right) I_1(\chi) \quad \text{and} \\ I_{+-} &= -(1+\chi)^2 \left(1 + \chi\frac{\partial}{\partial\chi}\right) I_1(\chi)\,. \end{aligned} \tag{5.6}$$

with

$$I_1(\chi) = \int \frac{d^3a\, d^3b\, dc\, c\, \delta\big(1-c-\sum_i a_i - \sum_i b_i\big)\Big(\sum_i a_i \sum_i b_i + c\big(\sum_i a_i + \sum_i b_i\big)\Big)^{-1}}{\Big(a_1 a_3\big(c+\sum_i b_i\big) + (a_1 b_4 + a_3 b_6 + a_2 b_5 \chi)c + b_4 b_6\big(c+\sum_i a_i\big)\Big)^2} \tag{5.7}$$

where the integration range of variables a_i, b_i, c is the real interval $[0,1]$ and where we re-introduce the notation $\chi \equiv \frac{t}{s} \equiv \frac{s_{14}}{s_{12}}$ from Chapter 3.

The second step of the calculation is to derive an equivalent form of eq. (5.7) where such high powers of the integration variables do not occur within the denominator. Here, we were inspired by recent work [41] on Mellin space transforms, but the representation of $I_1(\chi)$ below can be obtained without reference to Mellin space. Rather, we only used a series of simple, if rather non-obvious, changes of variables[4]. One finds

$$I_1(\chi) = 6\int_1^\infty dc \int_0^\infty \frac{d^7(a_1 a_2 a_3 a_{\not s} b_1 b_2 b_3 b_{\not s})}{\mathrm{vol(GL(1))}} \frac{1}{(cA^2 + A.B + B^2)^4} \tag{5.8}$$

where $A^2 \equiv a_1 a_3 + a_{\not s}(a_1+a_2+a_3)$, $A.B \equiv b_1 b_3 + a_{\not s}(b_1+b_2+b_3) + b_{\not s}(a_1+a_2+a_3) + a_2 b_2 \chi$ and $B^2 \equiv b_1 b_3 + b_{\not s}(b_1+b_2+b_3)$. The "$1/\mathrm{vol(GL(1))}$" notation is an instruction to set any one of the variables $a_1, \ldots, b_{\not s}$ equal to 1

[3] In this chapter, we use the normalization $I[\cdots] \equiv \int \frac{d^4\ell_1 d^4\ell_2\,(\cdots)}{(i\pi^{D/2})^2(\text{inverse propagators})}$.

[4] Incidentally, these changes of variables, when applied to the double-box integral considered in eq. (8.1) of ref. [41], reproduces that formula exactly, giving an elementary derivation of it.

and integrate over the seven remaining ones; this is also why we wrote "d^7" instead of "d^8". As the notation suggests, the result does not depend on which variable is set to 1, due to the scaling ("GL(1)") symmetry of the integrand.

In principle, the third step of the calculation is now to integrate out the variables in eq. (5.8) one at the time. In reality, this would produce extremely lengthy expressions involving polylogarithms. However, due to the many functional identities between polylogarithms, such expressions can typically be simplified. As we discussed in Section 4.5, this is achieved very efficiently by working at the level of the symbol. Integrating out the variables in eq. (5.8) one at the time at the level of the symbol, we are left with the following symbol

$$\mathscr{S}[I_1(\chi)] = \frac{2}{\chi}\,[\chi\otimes\chi\otimes(1+\chi)\otimes(1+\chi)] - \frac{2}{1+\chi}\,[\chi\otimes\chi\otimes(1+\chi)\otimes\chi]\,. \tag{5.9}$$

Let us note that in attempting to integrate out the variables in eq. (5.8) one at the time, one observes that $I_1(\chi)$ has uniform transcendentality degree 4.

The fourth step of the calculation is now to "integrate" the symbol; that is, to find an appropriate transcendental function with the symbol (5.9). In order to arrive at an unambiguous answer we need to impose a number of constraints on the final result for $I_1(\chi)$. They take the following form.

1. The fact that $I_1(\chi)$ has the uniform transcendentality degree 4, as explained above.

2. The physical requirement that, on all physical sheets (which can be either $-1<\chi<0$, $-\infty<\chi<-1$ or $0<\chi<\infty$, depending on the channel under consideration), the integral is analytic around $\chi=-1$. This is because our integral, being planar, has a vanishing unitarity cut in the u-channel and hence, by the Cutkosky rules[5], cannot have a discontinuity in the u-channel.

3. The asymptotics ("Regge limit")

$$I_1(\chi)\to\frac{\pi^2}{6}\log^2\chi+\left(4\zeta(3)-\frac{\pi^2}{3}\right)\log\chi+\mathscr{O}(1)\quad\text{as}\quad\chi\to 0\qquad\text{and}$$
$$I_1(\chi)\to 6\zeta(3)\frac{\log\chi}{\chi}+\mathscr{O}(\chi^{-1})\quad\text{as}\quad\chi\to\infty \tag{5.10}$$

which is obtained directly from eq. (5.8). For instance, the double logarithm originates from the region where $1\ll a_1\sim b_1\ll a_2\ll 1/\chi$ (and other variables ~ 1). The subleading logarithm originates from the boundaries of that region — explicitly, the three regions $1\sim a_1\ll a_2\ll 1/\chi$, $1\ll a_1\sim a_2\ll 1/\chi$ and $1\ll a_1\ll a_2\sim 1/\chi$. The $\chi\to\infty$ logarithm originates from the $a_2\to 0$ region where the other variables are ~ 1.

[5] See Theorem 1 in Section 2.1.2.

As it turns out, knowing only the symbol (5.9) and imposing these three constraints, it is possible to reconstruct the function $I_1(\chi)$ uniquely. The result can be conveniently expressed in terms of the harmonic polylogarithms [57]

$$H_{-1,-1,0,0}(x) \equiv \int_0^x \frac{dt}{t+1} H_{-1,0,0}(t) \quad \text{and} \quad H_{0,-1,0,0}(x) \equiv \int_0^x \frac{dt}{t} H_{-1,0,0}(t)\,, \tag{5.11}$$

with

$$H_{-1,0,0}(x) \equiv \frac{1}{2}\int_0^x \frac{dt}{t+1}\log^2 t = -\mathrm{Li}_3(-x) + \log x \mathrm{Li}_2(-x) + \frac{1}{2}\log^2 x \log(1+x)\,. \tag{5.12}$$

Plugging the result for $I_1(\chi)$ into eq. (5.6), we then obtain the following complete results for the chiral numerator integrals I_{++} and I_{+-} in eqs. (5.1)-(5.2):

$$\begin{aligned} I_{++}(\chi) &= 2H_{-1,-1,0,0}(\chi) - \frac{\pi^2}{3}\mathrm{Li}_2(-\chi) \\ &\quad + \left(\frac{\pi^2}{2}\log(1+\chi) - \frac{\pi^2}{3}\log\chi + 2\zeta(3)\right)\log(1+\chi) - 6\chi\zeta(3)\,, \end{aligned} \tag{5.13}$$

$$\begin{aligned} I_{+-}(\chi) &= 2H_{0,-1,0,0}(\chi) - \pi^2\mathrm{Li}_2(-\chi) - \frac{\pi^2}{6}\log^2\chi - 4\zeta(3)\log\chi \\ &\quad - \frac{\pi^4}{10} - 6(1+\chi)\zeta(3)\,. \end{aligned} \tag{5.14}$$

These formulas are such that, with the standard branch choice for the polylogarithms, the result is real in the Euclidean region $\chi > 0$. Also, we refer to the footnote below eq. (5.8) for an explanation of our conventions. If desired, these results could be rewritten in terms of classical polylogarithms such as Li_4, but we have not found such rewritings particularly illuminating.

Equations (5.13)-(5.14) contain $\zeta(3)$ terms which violate the uniform transcendentality degree of the other terms, which may be surprising at first sight. We tentatively attribute this to double-triangle integrals present in the difference between our $I_{+\pm}$ and the "true" chiral integrals, as discussed in the footnote below eqs. (5.1)-(5.2). It would be interesting to evaluate the difference explicitly and see if the $\zeta(3)$-terms disappear.

As we were hoping, we have found that the chiral numerator integrals $I_{+\pm}$ admit rather compact analytical expressions. We invite the reader to compare our results against earlier results in the literature for double-box integrals. We refer to eqs. (22)-(25) of ref. [45] for the analytical result for the scalar double box, and to eq. (13) of ref. [46] for the analytical result for the double box with the $(\ell_1 + k_4)^2$ numerator insertion.

6. Loop-level recursion: a numerical check

In this final chapter we turn to two-loop calculations beyond four points. This chapter is intended to provide an overview of Paper II, and we refer to the original paper for further technical details.

Paper II stands somewhat apart in method and purpose from the other papers reviewed in this thesis. It serves to provide a check on a recently developed BCFW-like recursion relation [5, 6] for the (four-dimensional) integrand of $\mathcal{N} = 4$ supersymmetric Yang-Mills theory. Specifically, this paper provides a comparison of the prediction for the two-loop six-gluon maximally helicity violating (MHV) integrand against the result obtained by use of the leading-singularity method. This comparison was performed numerically, for a large number of randomly selected momenta.

The focus of this chapter will be on the use of the leading-singularity approach to obtain the two-loop integrand. In particular to explain how, given a set of randomly generated momenta, the integrand may be evaluated numerically.

6.1 Heptacut constructibility

In our attempt to construct the complete two-loop six-gluon MHV amplitude we are faced with two limitations. One is that the integration-by-parts (IBP) identities that were used in Chapter 3 to determine maximal-cut contours are not fully known at six points. The other is that a two-loop formalism along the lines of Paper I has not yet been developed to treat integrals with less than seven propagators.

The way around both of these obstacles is to expand the two-loop amplitude in an appropriate set of integrals that reflect the loop-momentum power counting of $\mathcal{N} = 4$ SYM. For the latter we choose the integral basis of ref. [21], illustrated for convenience in figure 6.1 below. The use of the word "basis" here is somewhat misleading, and stands in contrast to its use in the previous chapter, as there are linear relations between the integrals in figure 6.1. Moreover, integrals containing subloops with less than four propagators (which would be needed to express lower-supersymmetric and QCD amplitudes) are absent. Nonetheless, for brevity, we will stick to this abuse of terminology in this chapter.

Thus, we expand the two-loop six-gluon MHV amplitude in the basis in figure 6.1,

$$M^{(2)}_{6,\mathrm{MHV}} = \frac{A^{(2)}_{6,\mathrm{MHV}}}{A^{\mathrm{tree}}_{6,\mathrm{MHV}}} = \frac{1}{4} \sum_{\substack{i=1,\ldots,24 \\ j=1,\ldots,12}} r_i c_{i,\sigma_j} I_{i,\sigma_j} \tag{6.1}$$

where for convenience we normalized by the corresponding tree-level amplitude. The dihedral permutations σ_j were listed in eq. (A.37), and the symmetry factors r_i of the integrals can be read off from figure 6.1.

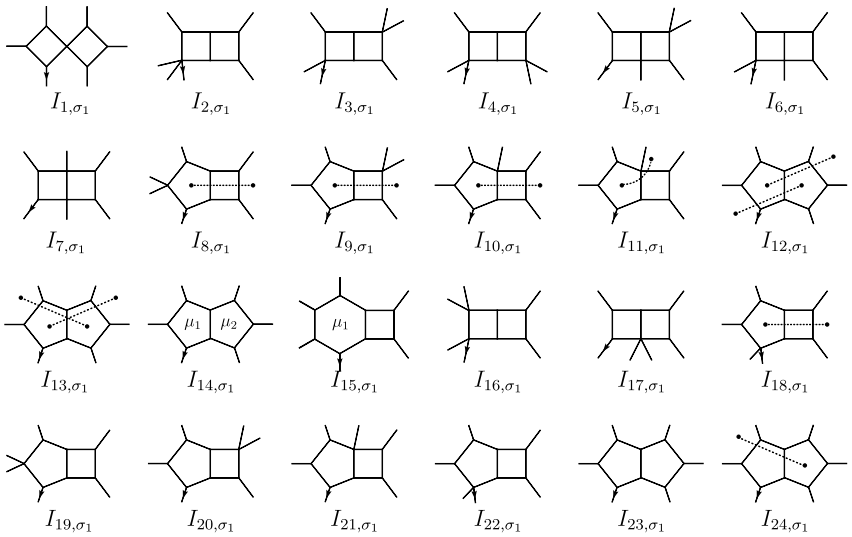

Figure 6.1. The (overcomplete) integral basis in terms of which the two-loop six-gluon amplitude is expressed. The integrals shown here are recorded in the σ_1 permutation where the external momenta are labeled clockwise starting with k_1 at the position of the arrow. The dotted lines appearing, for example, in I_{8,σ_1} denote numerator insertions of loop momenta, specified more explicitly in figure 6.2.

Let us now turn to the two issues raised above. The absence of integrals containing subloops with less than four propagators in the two-loop amplitude can be understood as follows: such integrals admit two-particle cuts that factor out a subtriangle or sub-bubble. Thus, a nonzero coefficient in the decomposition of the two-loop amplitude would require a nonzero coefficient of these triangles and bubbles in the one-loop amplitude isolated by the cut. However, one-loop amplitudes in $\mathcal{N} = 4$ SYM only have box contributions, owing to supersymmetric cancelations. This strongly suggests (but does not rigorously prove) that subtriangle and sub-bubble integrals would appear with zero coefficient if included in the two-loop basis expansion.

Throughout this chapter we will make use of heptacut contours that are not constrained by IBP identities. The fact that this does not produce spurious terms here, unlike in Chapter 3, can be traced back to the loop-momentum

power counting of $\mathcal{N} = 4$ amplitudes. As we argued above, supersymmetric cancelations enforce vanishing coefficients of integrals with less than seven propagators. In fact, even more is true: only the integrals shown in figure 6.1 survive the cancelations.

The fact that, for example, there are no further integrals of the topology of I_{19,σ_1} and I_{8,σ_1} can be shown by setting any seven of their propagators on-shell in eq. (6.1). Partial fractioning the integrand $\prod_{j=1}^{6} A_j^{\text{tree}}(z)$ of the resulting left hand side then reveals terms of the same form as the heptacuts of I_{19,σ_1} and I_{8,σ_1}, but none sharing this topology and containing, e.g., higher powers of loop momenta in the numerator.

In contrast, the sum of Feynman diagrams (after cancelations) of lower supersymmetric or QCD amplitudes would contain the integrals I_{19,σ_1} and I_{8,σ_1}, and in addition integrals of this topology with numerator insertions quadratic (or higher) in the loop momenta. To express these amplitudes in terms of the basis in figure 6.1, IBP identities would be needed to reduce higher numerator powers to the scalar and linear powers of I_{19,σ_1} and I_{8,σ_1}. However, the integrands before and after reduction are only equal up to terms which integrate to zero on $\mathbb{R}^D \times \mathbb{R}^D$; as discussed in Chapter 3, such terms do not necessarily integrate to zero on the T^8-tori defining the heptacut contours. Thus, in the case of $\mathcal{N} < 4$ SYM, avoiding spurious terms requires heptacut contours that respect IBP identities. On the other hand, for $\mathcal{N} = 4$ SYM, as IBP reductions are never used, we are not obliged to have the heptacut contours respect them.

To summarize what has been said so far, the loop-momentum power counting of $\mathcal{N} = 4$ SYM essentially guarantees that the two-loop six-gluon amplitude is contructible entirely by heptacuts. Moreover, when the amplitude is expanded in the basis in figure 6.1, the heptacut contours need not be constrained by IBP relations. This, then, will be our approach to compute the two-loop amplitude.

The use of the basis in figure 6.1 comes at a price, though. As our goal is to compare our result to that of Arkani-Hamed et al. in refs. [5, 6]—which is expressed in terms of a different integral basis—it is not meaningful to check agreement between individual integral coefficients in the two representations.

A quantity that can be meaningfully compared is the two-loop integrand: in general, in the planar limit of any field theory, the loop integrand is a well-defined rational function of the external momenta (which for example can be thought of as being produced by the Feynman rules). In our case, the two-loop integrand is the quantity under the integral sign in eq. (6.1), obtained as the sum of the integrands of the 24 basis integrals I_{i,σ_j}, weighted by the integral coefficients c_{i,σ_j} and symmetry factors r_i, where the summation is taken over all dihedral permutations σ_j of the external momentum labels. Agreement between the two-loop integrand as computed by either method would imply agreement between the integrated expressions; that is, the results for the ampli-

tude.[1] Accordingly, the following two sections will be devoted to explaining how, given a set of randomly generated momenta, the two-loop integrand may be evaluated numerically. In Section 6.2 we show how the integral coefficients c_{i,σ_j} in eq. (6.1) are computed and proceed in Section 6.3 to discuss how the integrands of the basis integrals I_{i,σ_j} are added in a meaningful way to produce the integrand of eq. (6.1).

6.2 Determining integral coefficients

In this section we show how the integral coefficients in eq. (6.1) are determined. As the heptacut contours used to compute them are not constrained by IBP relations, the approach followed in Paper II is essentially that of the leading-singularity method rather than that of Paper I. The results of Paper II thus have some overlap with ref. [21], but differ in that the entire two-loop six-gluon MHV integrand, rather than only the parity-even[2] part, is constructed.

6.2.1 Example: integral coefficients from leading singularities

As an example, let us apply to eq. (6.1) the heptacut illustrated in figure 6.2.

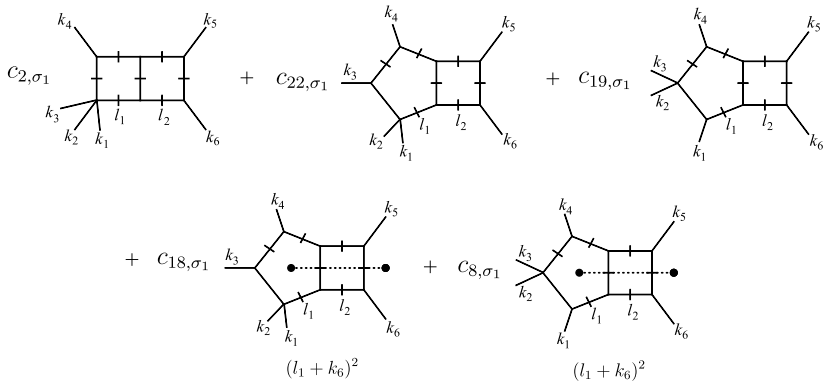

Figure 6.2. The result of applying a particular heptacut to the right hand side of eq. (6.1). The cut propagators are illustrated by the inclusion of an additional orthogonal line. This heptacut isolates the contribution of a unique double-box integral (I_{2,σ_1}), but also receives contributions from the pentagon-box integrals shown here.

[1] More accurately, the object we are comparing is the strictly four-dimensional part of the integrand. Indeed, cf. Section 6.2.2, the μ-integrals $I_{14,\sigma_j}, I_{15,\sigma_j}$ give rise to contributions to the integrand which are $\mathcal{O}(\varepsilon)$ in the dimensional regulator and hence not obtainable from evaluating leading singularities in strictly four dimensions. Thus, our findings of agreement between the integrands should be interpreted as a statement concerning the $\mathcal{O}(\varepsilon^0)$ part exclusively.

[2] The integrand of the normalized two-loop amplitude in eq. (6.1) can be canonically split into two terms, respectively even and odd under parity $\langle a\, b\rangle \longleftrightarrow [a\, b]$.

This turns eq. (6.1) into an equation involving contour integrals in the complex plane,

$$\frac{i}{A^{\text{tree}}_{\text{MHV}}}\sum_{i=1}^{6}\oint_{\Gamma_i} dz J_i(z)\prod_{j=1}^{6}A_j^{\text{tree}}(z)\Big|_{\mathscr{S}_i} \;=\; \frac{1}{4}\sum_{i=1}^{6}\oint_{\Gamma_i} dz J_i(z)K_i(z)\,. \tag{6.2}$$

The subscript $\big(\cdots\big)\big|_{\mathscr{S}_i}$ refers to the six kinematical solutions (essentially illustrated in figure 3.3) of the joint on-shell constraints, and Γ_i denote contours contained in the associated Riemann spheres. The further details of this equation are not necessary for understanding the basic idea of the leading-singularity method and are suppressed here.[3]

The integral coefficients to be determined (in this heptacut, $c_{2,\sigma_1}, c_{22,\sigma_1}$, $c_{19,\sigma_1}, c_{18,\sigma_1}, c_{8,\sigma_1}$) are contained implicitly in the kernels $K_i(z)$. These are functions with poles (specific to the various pentagon-boxes in figure 6.2) at various values of z where the uncut propagators become on-shell. In addition, the Jacobians $J_i(z)$ contain poles common to the double box and the pentagon-boxes. The idea of the leading-singularity method is that by making various choices of the contours Γ_i, eq. (6.2) produces a system of linear equations which can be solved to obtain the integral coefficients.

For example, we can consider the contour $\Gamma_i = \delta_{i,5}C_\varepsilon(P_1)$ which encircles the nonzero Jacobian pole in solution $\mathscr{S}_5$, and no other poles in the remaining Riemann spheres. With this choice of Γ_i, eq. (6.2) reduces to

$$\begin{aligned}\frac{1}{4}\left(c_{2,\sigma_1} - \frac{1}{2}\frac{c_{22,\sigma_1}}{\langle K_2^\flat - |\not{k}_{12}|K_1^\flat -\rangle (P_1-P_2)} - \frac{1}{2}\frac{c_{19,\sigma_1}}{\langle K_2^\flat - |\not{k}_{1}|K_1^\flat -\rangle (P_1-P_3)}\right)\\ = \;\; -2\gamma_1\gamma_2 P_1\langle K_2^\flat - |\not{k}_5|K_1^\flat -\rangle\,.\end{aligned} \tag{6.3}$$

Similar equations may be obtained from eq. (6.2) by making various choices of contours. Solving the resulting system of linear equations (and imposing the "gauge fixing" in eq. (6.4), as explained in the next subsection) then produces unique answers for the integral coefficients.

6.2.2 Overcompleteness and μ-integrals

In attempting to obtain the integral coefficients c_{i,σ_j} in eq. (6.1) from generalized four-dimensional cuts, one encounters two technical issues. The first point is that the basis in figure 6.1 is overcomplete, and the integral coefficients are therefore not uniquely defined. This feature will manifest itself as the appearance of free parameters in the solutions of the linear equations satisfied by the integral coefficients. This in turn means that one has to set a subset of the

[3] Nonetheless, we refer the curious reader to eqs. (4.7), (4.26) and (4.19)-(4.24) in Paper II for the precise form of the Jacobians $J_i(z)$, the cut amplitude $\prod_{j=1}^{6}A_j^{\text{tree}}(z)$ and the kernels $K_i(z)$.

integral coefficients equal to specific values in order to obtain unique solutions for the remaining coefficients. The non-uniqueness of the integral coefficients is accounted for by the existence of various linear relations between the integrals in figure 6.1, as was explained carefully in ref. [21]. In order to obtain unique answers for all integral coefficients, we make the following "gauge choices": we set

$$\left.\begin{aligned} c_{11,\sigma_j} &= s_{\sigma_j(61)} s_{\sigma_j(12)} s_{\sigma_j(123)} \\ c_{12,\sigma_j} &= s_{\sigma_j(456)} \big(s_{\sigma_j(345)} s_{\sigma_j(456)} - s_{\sigma_j(12)} s_{\sigma_j(45)} \big) \\ c_{24,\sigma_j} &= 0 \end{aligned}\right\} \quad \text{for } \; j = 1, \ldots, 12 \tag{6.4}$$

whereby $c^{\text{odd}}_{11,\sigma_j} = c^{\text{odd}}_{12,\sigma_j} = c^{\text{odd}}_{24,\sigma_j} = 0$. We then find unique results for the remaining coefficients with the property that $\text{Re}\, c_{i,\sigma_j} = c^{\text{even}}_{i,\sigma_j}$.

The second point is that the coefficients of the μ-integrals I_{14,σ_1} and I_{15,σ_1} (thus called because their integrands contain factors involving the (-2ε)-dimensional part of the loop momenta) are of $\mathcal{O}(\varepsilon)$ in the dimensional regulator and hence are not obtainable from four-dimensional cuts, as discussed in Section 3.3. As we restrict ourselves to taking four-dimensional generalized cuts here, we shall therefore not be concerned with these integral coefficients.

6.3 Assembling the integrand

Having explained in the previous section how the integral coefficients of eq. (6.1) are obtained, we proceed in this section to discuss how the integrands of the basis integrals I_{i,σ_j} are added in a meaningful way to produce the integrand of eq. (6.1).

Expressed as functions of internal and external momenta, the integrands of the basis integrals cannot be added in any meaningful way as the value of any term would depend on the labeling of the internal lines of the corresponding graph (i.e., which propagators are labeled ℓ_1 and ℓ_2). To remedy this, the integrand must be expressed in terms of dual x-space coordinates, defined by

$$\begin{aligned} x_i - x_{i+1} &= k_i & i &= 1, \ldots, 6 \pmod 6 \\ \left.\begin{aligned} x_{\sigma_j(1)} - x_7 &= \ell_1 \\ x_{\sigma_j(1)} - x_8 &= -\ell_2 \end{aligned}\right\} & j &= 1, \ldots, 6 \\ \left.\begin{aligned} x_{\sigma_j(6)} - x_7 &= -\ell_1 \\ x_{\sigma_j(6)} - x_8 &= \ell_2 \end{aligned}\right\} & j &= 7, \ldots, 12 \\ x_{ij} &\equiv x_i - x_j & i, j &= 1, \ldots, 8, \end{aligned} \tag{6.5}$$

with the additional requirement that, for any given graph, ℓ_1 and ℓ_2 be offset by appropriate translations by external momenta so that all propagators take the form $1/x_{ij}^2$. Finally, the integrand must be symmetrized in x_7 and x_8. Namely, any assignment of these points to a given graph will fail to be invariant under

vertical reflections of the graph; to ensure that the value of the integrand is not dependent on how its contributing graphs happen to be drawn, one must therefore average over the two possible assignments of these points. The integrands of the basis integrals in figure 6.1 are presented in Section A.1 of Paper II.

In summary, given a set of random internal and external momenta, the evaluation of the integrand of eq. (6.1) proceeds in three steps. First, the integral coefficients are obtained by solving the linear equations that follow from taking the leading singularities of eq. (6.1). Second, the integrands of the basis integrals are computed after converting the momenta into the dual x-space (which is achieved by solving eq. (6.5) and choosing, e.g., the base point $x_6 = 0$). Finally, the intermediate results are combined, weighting the contributions by the appropriate symmetry factors r_i of the integrals. This is essentially the procedure followed by the code [58] which is available online. As a simple consistency check of the code, we remark that the results produced for the integrand indeed satisfy crossing symmetry; that is,

$$\text{integrand of } M^{(2)}_{6,\,\text{MHV}}(x_1,\ldots,x_6) = \text{integrand of } M^{(2)}_{6,\,\text{MHV}}(x_{\sigma_j(1)},\ldots,x_{\sigma_j(6)}) \quad \text{for } \sigma_j \in D_6\,. \tag{6.6}$$

We have evaluated the two-loop six-gluon MHV integrand for a large number of randomly selected rational momenta[4] and in all cases find agreement with [5, 6] to high numerical accuracy [59]. In Table 1 below we have provided a few sample points to allow the curious reader to reproduce our results. Further data points can be generated by the `Mathematica` notebook [58] available online.

Finally, one may observe that the assumption that the two-loop amplitude is MHV is only used when evaluating the heptacuts of the left hand side of eq. (6.1). The form of the heptacuts of the right hand side of eq. (6.1) is independent of the external helicities, and the results of Paper II can therefore straightforwardly be extended to obtain the NMHV integrand as well.

[4] To generate n rational momenta which are lightlike in $(+,-,-,-)$ signature, the first $n-2$ can be chosen as arbitrary Pythagorean quadruples (for example, generated by using the parametrization $(m_3^2+m_1^2+m_2^2, m_3^2-m_1^2-m_2^2, 2m_1m_3, 2m_2m_3)$ with $m_i \in \mathbb{Z}$) normalized by their $\|\cdot\|_1$-norm. To ensure that the n-th momentum will be lightlike and satisfy momentum conservation, the $(n-1)$-th momentum is obtained by generating an additional Pythagorean quadruple ξ of unit $\|\cdot\|_1$-norm and then rescaling it by the constant $\alpha = -\frac{\left(\sum_{i=1}^{n-2} k_i\right)^2}{2\xi^\mu \sum_{i=1}^{n-2} k_{\mu i}} \in \mathbb{Q}$ whereby $k_n = -\left(\sum_{i=1}^{n-2} k_i + \alpha\xi\right)$ is lightlike and rational.

$(x_1,\ldots,x_6)$	(x_7,x_8)	integrand of $M^{(2)}_{6,\mathrm{MHV}}$
$\Big(\big(-\frac{1}{2},\frac{1}{2},0,0\big),$ $\big(-\frac{11}{12},\frac{1}{6},\frac{1}{4},0\big),$ $\big(-\frac{4}{3},\frac{5}{12},\frac{7}{12},0\big),$ $\big(-\frac{7}{4},\frac{29}{36},\frac{13}{18},-\frac{1}{18}\big),$ $\big(-\frac{23}{18},\frac{35}{54},\frac{28}{27},-\frac{10}{27}\big),$ $(0,0,0,0)\Big)$	$\Big(\big(\frac{1}{4},\frac{1}{4},2,1\big),$ $(0,0,2,0)\Big)$	$-\frac{31\,230\,748\,253}{22\,094\,130\,240}-\frac{994\,276\,085}{981\,961\,344}i$
$\Big(\big(\frac{3}{8},\frac{7}{24},\frac{1}{6},-\frac{1}{6}\big),$ $\big(\frac{7}{8},-\frac{5}{24},\frac{1}{6},-\frac{1}{6}\big),$ $\big(\frac{157}{120},-\frac{3}{8},-\frac{7}{30},-\frac{1}{6}\big),$ $\big(\frac{69}{40},-\frac{1}{8},-\frac{17}{30},-\frac{1}{6}\big),$ $\big(\frac{73}{90},\frac{5}{54},-\frac{53}{135},\frac{19}{27}\big),$ $(0,0,0,0)\Big)$	$\Big(\big(1,\frac{1}{3},0,2\big),$ $(0,0,1,1)\Big)$	$\frac{4\,777\,009\,838\,357}{201\,230\,662\,913\,280}+\frac{1\,802\,603\,853\,899}{259\,652\,468\,275\,200}i$
$\Big(\big(\frac{5}{12},\frac{1}{3},0,\frac{1}{4}\big),$ $\big(\frac{79}{96},-\frac{1}{24},\frac{1}{8},\frac{5}{32}\big),$ $\big(\frac{59}{48},-\frac{1}{6},\frac{7}{32},-\frac{7}{32}\big),$ $\big(\frac{157}{96},-\frac{13}{24},\frac{1}{8},-\frac{3}{32}\big),$ $\big(\frac{125}{224},\frac{15}{28},\frac{1}{8},-\frac{3}{32}\big),$ $(0,0,0,0)\Big)$	$\Big(\big(\frac{1}{2},\frac{1}{3},\frac{1}{3},0\big),$ $\big(\frac{1}{2},0,0,0\big)\Big)$	$\frac{3\,393\,545\,258\,977\,272}{16\,669\,297\,265}-\frac{43\,045\,877\,862\,533\,664}{183\,362\,269\,915}i$

Table 1: Values of the two-loop six-gluon MHV integrand (normalized with respect to the tree-level amplitude) at three randomly chosen sets of points $(x_1,\ldots,x_6)$ and (x_7,x_8) in dual x-space, respectively encoding external and internal momenta as prescribed by eq. (6.5). The parity-even and odd parts of the integrand of $M^{(2)}_{6,\mathrm{MHV}}$ respectively coincide with its real and imaginary parts. Further data points can be generated by the `Mathematica` notebook [58] available online.

7. Conclusions and outlook

In the papers I-IV reviewed in this thesis we have taken the first steps in developing a new method for computing two-loop amplitudes, based on generalized unitarity. The method does not rely on any assumptions such as supersymmetry and is therefore expected to be applicable to all gauge theories, in particular to QCD.

To put this two-loop method in proper context, let us first recapitulate our review of one-loop unitarity in Chapter 2. The starting point of calculations of one-loop amplitudes within the unitarity framework is to expand the amplitude as a linear combination in a basis of one-loop integrals (illustrated in figure 2.4). The process dependence thereby resides in the integral coefficients, and the goal of the calculation is to express these coefficients as functions of the momenta of the scattering particles. The determination of the coefficients is done by applying to both sides of the basis decomposition of the amplitude a number of so-called cuts. In the basic variant of unitarity, cuts are defined as replacing a pair of propagators by delta functions, thereby (by the Cutkosky rules) computing the branch cut discontinuities across the various kinematic channels. The amplitude, defined by its Feynman diagram expansion, is then turned into a product of tree-level amplitudes (again, by the Cutkosky rules), enabling the computation of one-loop amplitudes from tree-level data. In practice, however, these cuts are shared between several of the integrals in the basis decomposition of the amplitude, and non-trivial algebra is required to disentangle the coefficients of each integral.

One-loop unitarity also exists in a more recent version, called generalized unitarity, in which the operation of taking cuts does not have any known interpretation in terms of branch cut discontinuities. Rather, generalized cuts are defined as a change of the integration range away from the real slice $\mathbb{R}^D$ (where $D = 4 - 2\varepsilon$) into a contour of real dimension 4, embedded in $\mathbb{C}^4$. More concretely, to extract the coefficient of any box integral in figure 2.4, the contour is an average of two tori, each encircling a point in $\mathbb{C}^4$ where all four propagators become on-shell. The integration over this contour, rather than $\mathbb{R}^D$, in figure 2.4 annihilates all integrals on the right hand side but the box, whereas the left hand side becomes a product of four tree amplitudes. The end result is thus a formula (see eq. (2.67)) expressing the box integral coefficient in terms of tree-level data. Similarly, for any particular triangle or bubble integral on the right hand side of figure 2.4, there are known contours which annihilate all remaining integrals, thereby yielding a formula for the associated coefficient purely in terms of tree-level amplitudes.

Maximal unitarity at two loops

In Chapter 3 we have taken the first steps in developing a systematic extension of generalized unitarity to two loops. In this approach, the two-loop amplitude (defined by its Feynman diagram expansion) is expanded in a basis of two-loop integrals. In similarity with one-loop generalized unitarity, the expansion coefficients are then obtained by applying to both sides of the basis composition of the amplitude the maximal number of cuts possible. To be specific, we considered the four-point amplitude with massless external states and restricted our attention to the basis integrals containing the maximal number of propagators, namely the double boxes (illustrated in figure 3.1). With four massless external momenta there turn out to be two linearly independent integrals of this topology. The task is then to find formulas for their coefficients in terms of tree amplitudes.

Double-box integrals have seven propagators that can be cut, whereas the two four-dimensional loop momenta have a total of eight degrees of freedom. Imposing seven on-shell constraints—referred to as taking a *heptacut*—will therefore leave one free parameter. The effect of cutting all available propagators at two loops is therefore different from that at one loop where the quadruple cut used to extract the box coefficient freezes all components of the loop momentum.

As it turns out, however, it is in fact possible to freeze the remaining degree of freedom at two loops as follows. The heptacut is defined as a change of the integration range in the basis decomposition of the amplitude from $\mathbb{R}^D \times \mathbb{R}^D$ into a contour embedded in $\mathbb{C}^8$ of real dimension eight. More specifically, the contour encircles various poles of the integrand. The integration over it will thus immediately freeze seven of the loop momentum variables through the use of a multidimensional version of Cauchy's residue theorem whereby the resulting loop momenta solve the seven on-shell constraints. However, in order to use Cauchy's theorem, one must first perform a change of variables to linearize the denominators of the propagators. This will produce a Jacobian factor which becomes part of the measure of the remaining integration. This measure contains poles known as *composite leading singularities* which the remaining contour may be chosen to encircle.

As the maximal cuts of the double-box basis integrals are contour integrals, the task of finding formulas for their coefficients is turned into the question of finding appropriate integration contours for the remaining degree of freedom. This is not a trivial problem, however, as there is a variety of leading-singularity poles which may all be encircled with some a priori arbitrary winding numbers. For gauge theories with less than maximal supersymmetry (or in particular, no supersymmetry such as QCD), various random choices of contours would produce various different results for the double-box coefficients. The question is then: what principle selects contours that produce correct results for the coefficients?

The selection principle established in Chapter 3 is remarkably simple: the (complete $\mathbb{C}^8$-embedded) contours must annihilate all functions that have vanishing integrations on $\mathbb{R}^D \times \mathbb{R}^D$. This constraint traces back to the definition of the heptacut as a change of the integration range in the basis decomposition of the two-loop amplitude: in the original equation, the integrands on either side are equal up to terms that integrate to zero on $\mathbb{R}^D \times \mathbb{R}^D$. Such terms do not integrate to zero on randomly chosen $\mathbb{C}^8$-embedded contours and would produce spurious contributions—unless the contours are chosen in such a way as to annihilate them.

The use of composite leading singularities to freeze loop integrations to points in $\mathbb{C}^8$ is common to the approach in Chapter 3 and that of the leading-singularity method, and it is worth explaining the difference between these two approaches. The leading-singularity method has notably only been explored for $\mathscr{N} = 4$ supersymmetric Yang-Mills (SYM) theory. It employs purely *integrand-level* reductions to the Feynman-diagram expansion defining the amplitude. As the integrands on either side of the reduction equation are equal, one may choose *any* linear combination of leading-singularity contours to determine integral coefficients.

In contrast, the approach in Chapter 3 makes use of additional reductions coming from integration-by-parts (IBP) identities. This has the virtue of producing an extremely compact result for the amplitude. For example, for four massless external states, the Feynman rules for gauge theory produce 22 double-box integrals with various powers of the loop momenta in the integrand numerator. Through IBP relations, these are reduced to two linearly independent double boxes. Similarly, for five massless states, the 76 pentagon-boxes produced by the Feynman rules are reduced via IBP's (and two Gram determinant constraints) to a single pentagon-box integral. Thus, the use of IBP reductions leads to somewhat remarkable simplifications, yielding in some sense a minimal representation of the amplitude. However, as the reduction equation for the two-loop amplitude no longer holds at the level of the integrand, to avoid contamination from spurious terms, one is now obliged to choose linear combinations of leading-singularity contours that respect the IBP (and possibly Gram determinant) constraints.

In the case of four massless external states considered in Chapter 3, there turn out to be four constraints arising from the vanishing integrations of double boxes whose numerators involve Levi-Civita contractions of the loop momenta. Moreover, the 20 IBP relations turn out to provide only two additional constraints on the contours, yielding a total of six constraints. As mentioned above, the IBP relations leave two linearly independent double-box integrals at four points, referred to as master double boxes. Among the linear combinations of leading-singularity contours that satisfy all six constraints there are contours which moreover set the heptacuts of the two master double boxes equal to respectively one and zero, or vice versa. Since they extract the co-

efficient of a unique double-box integral in the basis decomposition of the amplitude, we refer to them as *master contours*.

Our final prescription for determining the double-box coefficients of the two-loop amplitude is thus to integrate a product of tree-level amplitudes (resulting from applying heptacuts to the sum over Feynman diagrams) over specific contours in the complex plane, subject to consistency conditions. Different contours produce different integral coefficients. The formalism is summarized in eqs. (3.52)-(3.53). Examples of the master contours P_1 and P_2 are illustrated in figure 3.4.

We have applied this formalism to obtain the double-box coefficients of the four-gluon amplitudes in $\mathcal{N} = 4, 2, 1$ SYM theory, finding agreement with unpublished results supplied to us by Lance Dixon [37]. We emphasize that though we have only given explicit results for supersymmetric theories, the method can also be applied to find the double-box coefficients of QCD amplitudes. The only required change in the calculation is that the tree-level data fed into the master formulas in eqs. (3.52)-(3.53) should be computed for QCD instead.

Uniqueness of two-loop master contours

In Chapter 4 we explain a puzzling feature of the (double-box) master contours obtained in the preceding chapter, namely that the contours appear to depend on six free parameters. This stands in contrast to the situation in generalized unitarity at one loop where the master contours associated with boxes, triangles etc. are uniquely defined, containing no free parameters. From the point of view of the contour selection principle of Chapter 3, the six free parameters seem to suggest that we have overlooked six constraints on the contours. Their origin turns out to have a much simpler explanation, however: the composite leading singularities encircled by the master contours are in fact shared between the different kinematical solutions to the heptacut constraints, resulting in a double-counting of these poles in Chapter 3. Eliminating the ensuing redundancy of variables, the two-loop master contours associated with double-box master integrals are found to be uniquely defined, in perfect analogy with the situation at one loop. Said differently, we find that the double-box master integrals in the two-loop basis are each associated with a unique contour producing their coefficient in the basis decomposition of the amplitude. This strongly suggests that the contour selection principle of Chapter 3 is sufficient to completely determine the contours defining maximal cuts at two loops.

The sharing of the composite leading singularities between different kinematical solutions leads to an appealing physical interpretation of these poles. Indeed, the different solutions to the heptacut constraints are distinguished by the loop momenta satisfying different collinearity conditions at the three-point vertices of the double-box graph (e.g., see figure 3.3). When the loop momenta are evaluated at the composite leading singularities, one of the momenta must then satisfy two collinearity conditions simultaneously, forcing this mo-

mentum to become collinear with whichever lightlike external momenta are attached to the respective vertices of the double box. In the original uncut double-box integral, the regions of loop-momentum integration that produce infrared divergences are precisely those where a loop momentum is becoming collinear with external lightlike momenta. In this sense, two-loop composite leading singularities are naturally associated with the infrared divergences of the original loop integral.

In Chapter 4 we also give a complete classification of the kinematical solutions to the heptacut constraints associated with the general double-box integral. As discussed above, these constraints leave one free parameter which must necessarily be complex, $z \in \mathbb{C}$, in order to satisfy the constraints. This degree of freedom naturally parametrizes Riemann surfaces where, for a given double-box integral, each surface corresponds to a particular kinematical solution. These Riemann surfaces are not disjoint, but rather have intersections at points which, as noted above, coincide with the composite leading singularities.

Our classification of the kinematical solutions is given in terms of three-point vertices. Depending on whether all, exactly two, exactly one or none of the vertical lines in the double-box graph in figure 4.1 are part of some three-point vertex, one finds respectively six, four or two distinct Riemann spheres, intersecting in points and linked into a chain; and, ultimately, an elliptic curve (see figures 4.3, 4.4, 4.5, 4.7). In all cases involving spheres there is a total of eight independent leading-singularity poles, distributed in various ways over the spheres. For the elliptic curve we find a total of nine independent leading-singularity cycles. Finally, we tentatively relate the appearance of an elliptic curve in the heptacut to the appearance of non-polylogarithm type functions in the integrated expression for the 10-point integral in figure 4.6.

Ideal two-loop integral bases

A central question in generalized-unitarity calculations concerns the choice of basis integrals in which amplitudes are expanded. So far, it remains an open problem to single out one particularly compelling choice of two-loop basis which is universally applicable to *all* gauge theories, in particular QCD. In Chapter 5 we pointed out that a basis containing as many infrared-finite integrals as possible is likely to simplify unitarity calculations substantially at two loops.

The point is that when the two-loop amplitude is expanded in a basis of two-loop integrals, there will inevitably be $\mathcal{O}(\varepsilon)$ corrections to the expansion coefficients. These corrections cannot be obtained from cuts in strictly four dimensions, but rather require taking cuts in $D = 4 - 2\varepsilon$ dimensions, something which is technically much more involved. The knowledge of these corrections is important when expanding in a generic basis, as they will multiply $\frac{1}{\varepsilon^k}$ singularities in the integrated expressions for the two-loop integrals, thereby producing finite contributions to the amplitude. In contrast, when expanding

in a basis of finite integrals, $\mathcal{O}(\varepsilon)$ corrections are still present, but become physically irrelevant. Of course, as two-loop amplitudes necessarily have infrared divergences, it is impossible to expand them in a basis consisting entirely of infrared-finite integrals. Nevertheless, it is plausible that by using a basis with a minimal number of IR-divergent integrals, one can minimize the work needed to compute the physically relevant part of the expansion coefficients.

More concretely, we pointed out that the chiral integrals introduced by Arkani-Hamed et al. can be used as master integrals for the double-box contributions to the four-point amplitudes in *any* gauge theory, including QCD. The infrared finiteness of these integrals can be easily understood. Namely, their integrands contain factors that vanish in the regions where the loop momenta become collinear with lightlike external momenta, thereby quenching the source of IR divergences.

We then evaluated the chiral double-box integrals analytically at four points, obtaining remarkably compact results. Our calculation proceeded in four steps. First, we write the integrals in terms of their Feynman parametrization. Second, we rewrite the Feynman-parametrized form as an integral over projective space, a form which is particularly amenable to analytic evaluation. In the third step, we integrate out the variables in the projectivized representation one at the time. However, we only carry out these integrations at the level of the so-called symbol of transcendental functions. We do so to ensure that the polylogarithmic expressions produced by the integrations are written in the most compact form possible. In the last step we reconstruct the analytic expressions for the chiral integrals from the symbol along with three constraints on the integrated expression. Our results are expressed in terms of harmonic polylogarithms and given in eqs. (5.13)-(5.14).

Loop-level recursion: a numerical check

In Chapter 6 we considered two-loop calculations beyond four points. Here we have provided a check on a recently developed BCFW-like recursion relation [5, 6] for the (four-dimensional) integrand of the amplitudes of $\mathcal{N} = 4$ SYM theory. Specifically, we have provided a comparison of the prediction for the two-loop six-gluon maximally helicity violating (MHV) integrand against the result obtained by use of the leading-singularity method. The comparison is performed numerically for a large number of randomly selected momenta and in all cases finds agreement between the two results to high numerical accuracy. Equivalently, assuming the validity of refs. [5, 6], one can view the analysis carried out in this chapter as a check that the leading singularities of the $\mathcal{N} = 4$ SYM integrand evaluated in strictly four dimensions (as opposed to in $D = 4 - 2\varepsilon$ dimensions) are sufficient to detect the parity-odd[1] part of

[1] We refer to the footnote below figure 6.2 for a definition of the parity-even and odd parts of the integrand.

the integrand. In Table 1 we have provided the values of the two-loop six-gluon MHV integrand at three randomly chosen sets of internal and external momenta.

Future research

The work presented in this thesis opens many directions for future research.

Among the more urgent open problems is to extend the method of Paper I to allow calculations of complete two-loop amplitudes. This requires capturing the contributions from all integrals in a two-loop basis. In addition to double boxes, such a basis will contain integrals with less than seven propagators. Extracting their coefficients by use of maximal unitarity thus requires examination of hexacuts, pentacuts etc. Two-loop integrals whose subloops contain at least three propagators all admit T^8-integration contours (analogous to those in eq. (3.24)) that appropriately define such cuts. Moreover, the cut integrand is a holomorphic function, and the contour integrations can thus be performed directly by means of a multidimensional version of Cauchy's residue theorem, localizing the integration to points in $\mathbb{C}^8$. In contrast, two-loop integrals with bubble-subloops do not admit T^8 contours: for example, the box-bubble integral rather admits a $T^6 \times S^2$ contour which does not immediately localize to points in $\mathbb{C}^8$. Nevertheless, as shown by Mastrolia in ref. [60], the S^2 integration associated with bubble integrals at one loop can effectively be localized through the use of Stokes' theorem, and the bubble coefficients directly extracted. A related approach is that of Arkani-Hamed et al. in ref. [61]. To summarize, the integrals in a two-loop basis are associated with a variety of $T^8, T^6 \times S^2$ and also $T^4 \times S^2 \times S^2$ contours encircling the poles that come from the measure of the cut integrals, or from propagators going on-shell.

Developing a formalism for extracting the coefficients of all the integrals in a two-loop basis therefore requires two steps. The first is a systematic way of uncovering and enumerating all such contours. The second is to construct appropriate linear combinations of these contours which annihilate all functions that have vanishing $\mathbb{R}^D \times \mathbb{R}^D$ integrations, such as those arising from integration by parts. It would be extremely interesting to carry out these steps and to examine whether the uniqueness of master contours, observed for double boxes in Papers III and IV, continues to hold.

To be more accurate, the above considerations only suffice to determine integral coefficients to $\mathcal{O}(\varepsilon^0)$ in the dimensional regulator. As discussed above, the knowledge of higher order corrections requires taking cuts beyond strictly four dimensions; but this knowledge would only be needed for a few integrals if the amplitude is expanded in a "maximally IR-finite" basis. It would be very interesting to construct such a basis in practice. Moreover, to calculate the coefficients of IR-divergent integrals to higher orders, it may be possible to take cuts in $D = 6$ dimensions rather than in $D = 4 - 2\varepsilon$ dimensions, extending the one-loop analysis of Davies [62]. Investigating this more closely would also be intriguing.

Interesting applications of the formalism would be to compute two-loop QCD amplitudes relevant to precision LHC phenomenology; in particular, the amplitudes of the four-particle processes $q\bar{q} \to W^{\pm}\gamma$, $q\bar{q} \to Z^0\gamma$ and $H \to 3$ partons as well as five-particle processes such as $gg \to q\bar{q}V$. One could also imagine applying the ideas presented here to examine the UV properties of supergravity theories, such as the no-triangle hypothesis.

It would also be very interesting to see if the techniques of Chapter 5 used to evaluate the chiral double-box integrals at four points can be extended to compute higher-point integrals at two loops. Other open questions are how to augment the formalism to tackle non-planar integrals and, looking further ahead, how it may ultimately be implemented in a numerical routine such as BLACKHAT in an efficient and numerically stable way.

Let us end this thesis on an inquisitive note. So far, we have no deep understanding of what the IBP constraints on the maximal-cut contours are trying to tell us. Clearly, from a computational viewpoint it would be desirable if these constraints could be understood more transparently, perhaps making the knowledge of IBP relations unnecessary. From a more philosophical viewpoint, the immediate goal of building a bestiary of master contours may not necessarily be the final word. Rather, one would hope that the contours can ultimately be understood in a more unified way, perhaps in terms of a deeper underlying principle yet to be uncovered.

Perhaps the IBP relations themselves can be trivialized by an appropriate representation of the loop integrals. This is turn might give a clue as to what is the right language in which to phrase the constraints. Or perhaps it is possible to understand the constraints directly, without reference to IBP relations, in terms of a purely geometric picture. In fact, we have already seen that the Levi-Civita constraints simply state that the master contours are invariant under 180° rotations of the chains of Riemann spheres in Chapter 4. Maybe this is a hint that there are simple geometric rules at work. It will be fascinating to see if future investigations will shed light on these questions.

A. Notation and conventions

In this appendix we specify conventions and notation used throughout the thesis.

The spacetime signature is $\eta^{\mu\nu} = \mathrm{diag}(1,-1,-1,-1)$. All external momenta in an amplitude are outgoing and will be denoted by k_i. We will make use of the spinor helicity formalism [14, 63–69] in which a given lightlike four-dimensional momentum is written as a tensor product of two massless Weyl spinors,

$$k_i^\mu \;=\; \big(\overline{u_-(k_i)}\big)^a \sigma^\mu_{a\dot{a}} u_-^{\dot{a}}(k_i) \;+\; \big(\overline{u_+(k_i)}\big)^{\dot{a}} \sigma^\mu_{a\dot{a}} u_+^a(k_i) \tag{A.1}$$

where $a, \dot{a} = 1,2$. The spinors are often denoted as

$$\lambda_i^a = u_+^a(k_i)\,, \qquad \widetilde{\lambda}_i^{\dot{a}} = u_-^{\dot{a}}(k_i)\,. \tag{A.2}$$

One can form the following Lorentz invariant inner products out of the spinors,

$$\langle i\,j\rangle \equiv \langle i^-|j^+\rangle \equiv \varepsilon_{ab}\lambda_i^a\lambda_j^b = \big(\overline{u_-(k_i)}\big)^a u_+(k_j)_a\,, \tag{A.3}$$

$$[i\,j] \equiv \langle i^+|j^-\rangle \equiv \varepsilon_{\dot{b}\dot{a}}\widetilde{\lambda}_i^{\dot{a}}\widetilde{\lambda}_j^{\dot{b}} = \big(\overline{u_+(k_i)}\big)_{\dot{a}} u_-(k_j)^{\dot{a}} \tag{A.4}$$

which satisfy

$$\langle i\,j\rangle[j\,i] = 2k_i\cdot k_j\,. \tag{A.5}$$

To give a useful representation of the spinors, it is convenient to use the following representation of the gamma matrices,

$$\begin{aligned}
&\gamma^0 = \begin{pmatrix} 0 & i\sigma^2 \\ -i\sigma^2 & 0 \end{pmatrix}, \quad \gamma^1 = \begin{pmatrix} 0 & \sigma^3 \\ -\sigma^3 & 0 \end{pmatrix} \\
&\gamma^2 = -i\begin{pmatrix} 0 & I \\ I & 0 \end{pmatrix}, \qquad \gamma^3 = \begin{pmatrix} 0 & \sigma^1 \\ -\sigma^1 & 0 \end{pmatrix} \\
&\gamma_5 = -i\gamma^0\gamma^1\gamma^2\gamma^3
\end{aligned} \tag{A.6}$$

which may be obtained by matrix conjugation of the Weyl representation, $\gamma^\mu = R^{-1}\gamma^\mu_{\mathrm{Weyl}}R$ with

$$R = \begin{pmatrix} 1 & 0 & 0 & 0 \\ 0 & -1 & 0 & 0 \\ 0 & 0 & 0 & 1 \\ 0 & 0 & 1 & 0 \end{pmatrix}. \tag{A.7}$$

In the representation (A.6), the spinors defined out of a lightlike four-vector $p_\mu = (p_0, p_1, p_2, p_3)$ take the following form

$$\langle p| \equiv \langle p^-| \equiv \overline{u_-(p)} = \frac{1}{\sqrt{p_0+p_3}} \begin{pmatrix} p_1+ip_2 \\ p_0+p_3 \\ 0 \\ 0 \end{pmatrix} \tag{A.8}$$

$$|p\rangle \equiv |p^+\rangle \equiv u_+(p) = \frac{1}{\sqrt{p_0+p_3}} \begin{pmatrix} p_0+p_3 \\ -p_1-ip_2 \\ 0 \\ 0 \end{pmatrix} \tag{A.9}$$

and

$$[p| \equiv \langle p^+| \equiv \overline{u_+(p)} = \frac{1}{\sqrt{p_0+p_3}} \begin{pmatrix} 0 \\ 0 \\ p_1-ip_2 \\ p_0+p_3 \end{pmatrix} \tag{A.10}$$

$$|p] \equiv |p^-\rangle \equiv u_-(p) = \frac{1}{\sqrt{p_0+p_3}} \begin{pmatrix} 0 \\ 0 \\ -p_0-p_3 \\ p_1-ip_2 \end{pmatrix} \tag{A.11}$$

where we included two auxiliary zero-entries for the holomorphic spinors in eqs. (A.8)-(A.9) as well as for the antiholomorphic spinors in eqs. (A.10)-(A.11).

In terms of the notation introduced in eqs. (A.8)-(A.11), one can rewrite eq. (A.1) as

$$\not{p} = p_\mu \gamma^\mu = |p\rangle[p| + |p]\langle p| = |p^+\rangle \otimes \langle p^+| \;+\; |p^-\rangle \otimes \langle p^-| \,. \tag{A.12}$$

Moreover, in the representation (A.8)-(A.11) of the spinors, the inner products in eq. (A.4) take the form

$$\langle p\, q\rangle = \langle p^-|q^+\rangle = \frac{\sqrt{q_0+q_3}}{\sqrt{p_0+p_3}}(p_1+ip_2) - \frac{\sqrt{p_0+p_3}}{\sqrt{q_0+q_3}}(q_1+iq_2) \tag{A.13}$$

and

$$[p\, q] = \langle p^+|q^-\rangle = \frac{\sqrt{q_0+q_3}}{\sqrt{p_0+p_3}}(-p_1+ip_2) + \frac{\sqrt{p_0+p_3}}{\sqrt{q_0+q_3}}(q_1-iq_2) \,. \tag{A.14}$$

For real momenta p, q, the angle and square spinor products (A.13)-(A.14) are related by complex conjugation as follows

$$\langle p\, q\rangle^* = -[p\, q] \,. \tag{A.15}$$

The inner products in eqs. (A.13)-(A.14) can also be used in the situation when the momenta p,q are complex. In particular, the following useful identities hold true for arbitrary lightlike momenta k_i, k_j,

$$\text{Gordon identity:} \qquad \langle i^{\pm}|\gamma^{\mu}|i^{\pm}\rangle = 2k_i^{\mu} \tag{A.16}$$

$$\text{projection operator:} \qquad |i^{\pm}\rangle\langle i^{\pm}| = \tfrac{1}{2}(1\pm\gamma_5)\not{k}_i \tag{A.17}$$

$$\text{antisymmetry:} \qquad \langle i\,j\rangle = -\langle j\,i\rangle\,, \quad [i\,j] = -[j\,i] \tag{A.18}$$

$$\text{Fierz rearrangement:} \qquad \langle i^{+}|\gamma^{\mu}|j^{+}\rangle\langle k^{+}|\gamma_{\mu}|l^{+}\rangle = 2[i\,k]\langle l\,j\rangle \tag{A.19}$$

$$\text{charge conjugation:} \qquad \langle i^{+}|\gamma^{\mu}|j^{+}\rangle = \langle j^{-}|\gamma^{\mu}|i^{-}\rangle \tag{A.20}$$

$$\text{Schouten identity:} \qquad \langle i\,j\rangle\langle k\,l\rangle = \langle i\,k\rangle\langle j\,l\rangle + \langle i\,l\rangle\langle k\,j\rangle\,. \tag{A.21}$$

Spinor strings are defined as follows

$$\langle K_i^{-}|\not{P}+\not{Q}|K_j^{-}\rangle = \langle K_i^{-}|\not{P}|K_j^{-}\rangle + \langle K_i^{-}|\not{Q}|K_j^{-}\rangle \tag{A.22}$$

$$\langle K_i^{-}|\not{P}|K_j^{-}\rangle = \langle K_i\,P\rangle[P\,K_j] \qquad \text{if} \quad P^2=0\,. \tag{A.23}$$

We use the following normalizations for expressions involving Levi-Civita contractions of momenta

$$\varepsilon(1,2,3,4) = \varepsilon^{\mu\nu\rho\sigma}k_{1\mu}k_{2\nu}k_{3\rho}k_{4\sigma} \tag{A.24}$$

$$= \sum_{\sigma\in S_4}(\operatorname{sgn}\sigma)k_{1,\sigma(0)}k_{2,\sigma(1)}k_{3,\sigma(2)}k_{4,\sigma(3)} \tag{A.25}$$

$$= -\frac{i}{4}\operatorname{Tr}(\gamma_5\not{k}_1\not{k}_2\not{k}_3\not{k}_4) \tag{A.26}$$

$$= -\frac{i}{4}\big([1\,2]\langle 2\,3\rangle[3\,4]\langle 4\,1\rangle - \langle 1\,2\rangle[2\,3]\langle 3\,4\rangle[4\,1]\big)\,. \tag{A.27}$$

We will use the following notation for sums and invariant masses of external momenta,

$$k_{i_1\cdots i_n} \equiv k_{i_1}+\cdots+k_{i_n} \tag{A.28}$$

$$s_{i_1\cdots i_n} \equiv (k_{i_1}+\cdots+k_{i_n})^2 \tag{A.29}$$

$$S_i \equiv K_i^2\,. \tag{A.30}$$

In Chapters 4-6 we make use of the "flattened" momenta introduced in refs. [30, 70]: for a pair of momenta K_1, K_2, define the quantity

$$\gamma_{1\pm} = (K_1\cdot K_2) \pm \sqrt{\Delta_1}\,, \qquad \Delta_1 = (K_1\cdot K_2)^2 - K_1^2K_2^2 \tag{A.31}$$

which can take two different values if both momenta are massive (i.e., if $S_1S_2\neq 0$). For a given value of γ_1 one defines a pair of massless "flattened" momenta as follows

$$K_{1\pm}^{\flat} = \frac{K_1-(S_1/\gamma_{1\pm})K_2}{1-S_1S_2/\gamma_{1\pm}^2}\,, \qquad K_{2\pm}^{\flat} = \frac{K_2-(S_2/\gamma_{1\pm})K_1}{1-S_1S_2/\gamma_{1\pm}^2}\,. \tag{A.32}$$

If one of the momenta K_1 or K_2 is massless, $\gamma_{1\pm}$ can only take one value, and we use the following abbreviated notation:

$$S_1 S_2 = 0 \quad \Longrightarrow \quad \begin{cases} \gamma_1 = 2K_1 \cdot K_2 \\ K_1^\flat = K_1 - (S_1/\gamma_1)K_2 \\ K_2^\flat = K_2 - (S_2/\gamma_1)K_1 \,. \end{cases} \tag{A.33}$$

Similarly, we use the notation

$$\gamma_{2\pm} = (K_4 \cdot K_5) \pm \sqrt{\Delta_2}\,, \qquad \Delta_2 = (K_4 \cdot K_5)^2 - K_4^2 K_5^2 \tag{A.34}$$

$$K_{4\pm}^\flat = \frac{K_4 - (S_4/\gamma_{2\pm})K_5}{1 - S_4 S_5/\gamma_{2\pm}^2}\,, \qquad K_{5\pm}^\flat = \frac{K_5 - (S_5/\gamma_{2\pm})K_4}{1 - S_4 S_5/\gamma_{2\pm}^2}\,. \tag{A.35}$$

$$S_4 S_5 = 0 \quad \Longrightarrow \quad \begin{cases} \gamma_2 = 2K_4 \cdot K_5 \\ K_4^\flat = K_4 - (S_4/\gamma_2)K_5 \\ K_5^\flat = K_5 - (S_5/\gamma_2)K_4 \,. \end{cases} \tag{A.36}$$

In Chapter 6 we denote make use of the dihedral group D_6 whose elements are labeled as follows,

$$\begin{array}{lll} \sigma_1 = (1,2,3,4,5,6) & \sigma_2 = (2,3,4,5,6,1) & \sigma_3 = (3,4,5,6,1,2) \\ \sigma_4 = (4,5,6,1,2,3) & \sigma_5 = (5,6,1,2,3,4) & \sigma_6 = (6,1,2,3,4,5) \\ \sigma_7 = (6,5,4,3,2,1) & \sigma_8 = (5,4,3,2,1,6) & \sigma_9 = (4,3,2,1,6,5) \\ \sigma_{10} = (3,2,1,6,5,4) & \sigma_{11} = (2,1,6,5,4,3) & \sigma_{12} = (1,6,5,4,3,2)\,. \end{array} \tag{A.37}$$

We use a standard color decomposition of the L-loop n-point amplitude to disentangle color from kinematics,

$$\mathscr{A}_n^{(L)} = \sum_{\sigma \in S_n/Z_n} \mathrm{Tr}(T^{a_{\sigma(1)}} T^{a_{\sigma(2)}} \cdots T^{a_{\sigma(n)}}) A_n^{(L)}(\sigma(1), \sigma(2), \ldots, \sigma(n))\,, \tag{A.38}$$

where $A_n^{(L)}$ is an L-loop color-ordered partial amplitude. Throughout the thesis we restrict our attention to the leading-color (planar) partial amplitudes.

Finally, the Parke-Taylor formula for the tree-level n-gluon maximally helicity violating (MHV) amplitude is

$$A_{n,\,\mathrm{MHV}}^{\mathrm{tree}}(i^-, j^-) \;=\; \frac{i\langle i\, j\rangle^4}{\langle 1\,2\rangle\langle 2\,3\rangle \cdots \langle n\,1\rangle}\,, \tag{A.39}$$

and for the $\overline{\mathrm{MHV}}$ amplitude,

$$A_{n,\,\overline{\mathrm{MHV}}}^{\mathrm{tree}}(i^+, j^+) \;=\; (-1)^n \frac{i[i\, j]^4}{[1\,2][2\,3] \cdots [n\,1]}\,. \tag{A.40}$$

Acknowledgments

Above all, I am deeply grateful to my academic advisor David Kosower. Thanks for your guidance, for successful collaboration and for setting ambitious goals for research. I feel privileged to have worked on such an interesting project during my PhD.

Also a sincere thanks to my advisors in Uppsala, Lisa Freyhult and Joseph Minahan, for your encouragement and for giving me the opportunity to carry out research at the CEA Saclay institute while enrolled as a graduate student at Uppsala University.

It is a pleasure to thank my brilliant collaborators: thanks to Simon Caron-Huot for contributing your creativity and enthusiasm and for wonderful hospitality in Princeton, and to Henrik Johansson for mentoring me and for sharing your knowledge and insights through countless discussions. I am proud to have worked with both of you.

Another collaborator to whom I owe a special gratitude is Rutger Boels. Thank you for introducing me to the fascinating world of scattering amplitudes and for patiently teaching me the ropes.

Having had a dual academic affiliation and having traveled a lot during my time as a graduate student, I have benefited from interactions with so many people that it is impossible to list them all. Let me take this opportunity to thank all faculty members, postdocs and graduate students at the CEA Saclay Institute and at Uppsala University not explicitly mentioned here.

Many people have contributed to the warm and stimulating atmosphere of the CEA Saclay institute during my time there. One person I would like to thank in particular is Gregory Korchemsky for sharing his deep knowledge of quantum field theory over many discussions and lunches. I would also like to thank Ruth Britto for useful discussions, Bertrand Duplantier for many fun discussions over green tea, Mathias Ritzmann for explaining me the latest LHC results and for acting as courier of Swiss chocolate, and Emery Sokatchev for spirited debates about classical music. Thanks also to Giovanni Diana, Edoardo Mirabella and Alexander Otchirov for great company during lunch.

Among my fellow graduate students in Uppsala, I would in particular like to thank Johan Källén for all the great time spent together, and Martin Lundgren and Sergey Slizovskiy for many interesting discussions. And thanks to Till Bargheer and Gabriele Tartaglino-Mazzucchelli for excellent company during lunch and midsommarfirande at Skansen. Also, thanks are due to Wladimir Lyra, Anna Malmstedt, Jian Qiu, Astrid Wachter and Stefan Zieme for keeping me company during my initial time as a graduate student.

I have enjoyed the teaching opportunities given to me in Uppsala and am happy to thank Thomas Klose, Ulf Lindström and Joseph Minahan for pleasant collaboration.

I am delighted to thank Nima Arkani-Hamed, Zvi Bern, Bernd Kniehl and Robert Schabinger for encouraging remarks on my work, and Lance Dixon for providing valuable insight and unpublished results. Thanks also to Janusz Gluza for illuminating discussions and sharing unpublished results.

I would like to thank the Institute for Advanced Study in Princeton for its generosity, allowing me to stay for a total of five weeks. Many thanks to Johannes Henn for inspiring discussions, Benjamin Matschke for initial collaboration, and Adam Rej for pointers on New York. Also, I would like to acknowledge the hospitality of the Niels Bohr Institute which I have frequently visited. Many thanks to Simon Badger, Charlotte Kristjansen, Ricardo Monteiro, Niels Obers, Donal O'Connell and Costas Zoubos for always making it worthwhile to visit Copenhagen.

I am grateful for seminar invitations to CERN, DESY, the IAS in Princeton, Nordita and the University of Zurich where part of the work in this thesis was presented. Moreover, I would like to thank the participants of these seminars for their comments and for discussions.

I would like to thank the excellent administrative staff at CEA Saclay, in particular Catherine Cataldi for organizing the paperwork and for her infinite patience with me, and Laure Sauboy and Sylvie Zaffanella for their helpfulness and cheerful nature. Likewise, I want to thank the administrative staff at the Theoretical Physics Department in Uppsala, especially Inger Ericson for her helpfulness and good humor.

I owe a special gratitude to the Fondation Danoise, my home in Paris for nearly two years. I am grateful to Karl Ejby Poulsen, who sadly passed away in the summer of 2011, for giving me the opportunity to live here. A warm thanks to Marianne Bak Papiau for always finding a room for me, for organizing wonderful *soirées* with chamber music and jazz, and for her general patience with my many requests. I feel very privileged to have lived for such a long time in Paris, this metropolis of magnificent beauty and culture, with its outstanding museums, rich and vibrant concert life and excellent dining. I have enjoyed my time here immensely. *Merci pour avoir enrichi ces années de ma vie, Paris!*

Finally, I want to send my thanks to friends and family in Copenhagen. Thank you for all the enjoyable time spent together and for your support.

Summary in Swedish

Den, av ATLAS och CMS experimenten, annonserade upptäckten av en Higgsboson-liknande partikel med en massa runt 125-126 GeV den 4 juli 2012 gör detta till en spännande tid att arbeta inom partikelfysik. Spännande är också de möjliga tecknen på ny fysik i och med överskottet av två-fotonsönderfall av Higgskandidaten som observerats av de båda grupperna.

Åtminstone tills helt nyligen har standardmodellen för partikelfysik varit en extremt framgångsrik teori som förklarar alla observationer gjorda i experiment med partikelacceleratorer. Enligt standardmodellen är all materia uppbyggd av kvarkar (byggstenarna för protoner och neutroner) och leptoner (såsom elektroner och neutriner) som växelverkar genom tre fundamentala krafter: den elektromagnetiska, den svaga och den starka kraften. Krafterna beskrivs med hjälp av två kvantfältteorier, den elektrosvaga teorin och kvantkromodynamik.

Den elektrosvaga teorin förenar den elektromagnetiska och den svaga kraften i en teori. Denna har en $SU(2) \times U(1)$ gaugesymmetri associerad med de fyra partiklar, γ, $W^{\pm}$ och Z^0, som förmedlar växelverkan mellan elementarpartiklar. Vid energier under omkring 250 GeV är $SU(2) \times U(1)$ gauge symmetrin bruten till $U(1)$ genom Higgsmekanismen, vilket ger massa åt den svaga kraftens kraftpartiklar, $W^{\pm}$ och Z^0, medan fotonen, γ, kraftpartikeln för den elektromagnetiska kraften, förblir masslös. Higgsmekanismen ger därutöver massa till alla elementarpartiklar.

Kvantkromodynamik (QCD) är teorin för växelverkningar mellan protonen och neutronens beståndsdelar, kvarkarna. Växelverkan överförs med hjälp av åtta olika partiklar kallade gluoner, g, associerade med gaugegruppen $SU(3)$. I motsats till fotoner kan gluoner växelverka med sig själva vilket ger upphov till intressanta fenomen, som att när man försöker dra isär kvarkarna i en proton så ökar styrkan hos attraktionskraften mellan dem snabbt vilket håller kvarkarna bundna till varandra på ett avstånd runt 10^{-15} m.

Trots dess framgångar är det tydligt att standardmodellen inte kan vara en komplett teori för partikelfysik. Skillnader mellan observerade hastigheter hos stjärnor i galaktiska omloppsbanor och hastigheter beräknade baserat på mängden av direkt observerbar materia indikerar existensen av en icke-observerad mörk materia, uppskattad till att utgöra 84% av materien i universum. Eftersom ingen av partiklarna i standardmodellen utgör kandidater för mörk materia så är en utvidgning av modellen nödvändig.

En mer spekulativ, men icke desto mindre attraktiv, idé är den om en förening av krafterna där teorierna för elektrosvag och stark växelverkan vid lämplig

energiskala utgör delar av en storförenad teori (GUT) med en större symmetrigrupp, exempelvis $SU(5)$. Mekanismen för att bryta den större symmetrin till standardmodellens gaugesymmetri, $SU(3) \times SU(2) \times U(1)$, tros likna Higgsmekanismen. Förutom att elegant förena de fundamentala krafterna i en enda teori förklarar $SU(5)$ GUT kvarkarnas icke-heltaliga elektriska laddning som beroende av deras laddning under $SU(3)$: i ett nötskal, kvarkar har 1/3 av leptonladdningen eftersom de har tre färger. GUT teorier kan också förklara varför neutrinomassorna är så små genom den såkallade gungbrädemekanismen. En förening av den elektromagnetiska, svaga och starka kopplingskonstanten är dock bara approximativ inom standardmodellen.

Ett särskilt elegant scenario beskrivs av supersymmetriska utvidgningar av standardmodellen. Sådana utvidgningar innehåller kandidater för mörk materia, åstadkommer en förening av de fundamentala krafterna samt stabiliserar Higgsmassan mot stora radiativa korrektioner. Dessutom verkar supersymmetri (SUSY) att vara en viktig ingrediens i ändliga teorier för kvantgravitation. Ett speciellt paradigm inom supersymmetriskt modellbyggande, som inte tycks hotat av aktuell data från LHC, är "split supersymmetry". För dessa modeller är skalan för brott av SUSY hög, runt GUT-skalan på 10^{16} GeV, och alla supersymmetriska skalärer mycket tunga. Detta undertrycker på ett naturligt sätt oönskade sidoeffekter såsom protonsönderfall och "flavour-changing neutral currents" vilka skulle förmedlats via dessa skalärer. Supersymmetriska fermioner kan å andra sidan förbli lätta då de skyddas av chiral symmetri. Bland dessa fermioner kan de lättaste elektriskt neutrala utgöra kandidater för mörk materia medan de lättaste elektriskt laddade kan koppla till fotoner som produceras i Higgssönderfall, och leda till ett överskott av dessa. En analys gjord nyligen visar att om överskottet av två-fotonssönderfall visar sig korrekt så kräver split SUSY existensen av en ny laddad fermion runt 115-150 GeV.

Det kan mycket väl visa sig att idéerna ovan inte har något med naturen att göra, anledningen att vi beskriver dem här är för att visa att ny fysik kan vara inom räckhåll för LHC. Syftet med LHC är dubbelt. Ett syfte, som i skrivande stund mycket troligt har uppfyllts, är att upptäckta Higgsbosonen. Det andra är att upptäcka ny fysik bortom standardmodellen.

I LHC kolliderar hadroner. Detta betyder att QCD-bakgrunden är stor i experimenten, den svarar för över 99% av händelserna. Att identifiera den signal man söker efter kräver därför en kvantitativ förståelse av bakgrunden vilken, i viss mening, måste subtraheras från den insamlade datamängden. Figur 7.1 illustrerar typiska exempel på signal- respektive bakgrundsprocesser.

En förståelse av QCD-bakgrunden kräver en förståelse av tvärsnitten hos alla relevanta processer i standardmodellen med tillräckligt god precision. En viktig ingrediens, om ej alls den enda, för att beräkna tvärsnitt är spridningsamplituder för processerna.

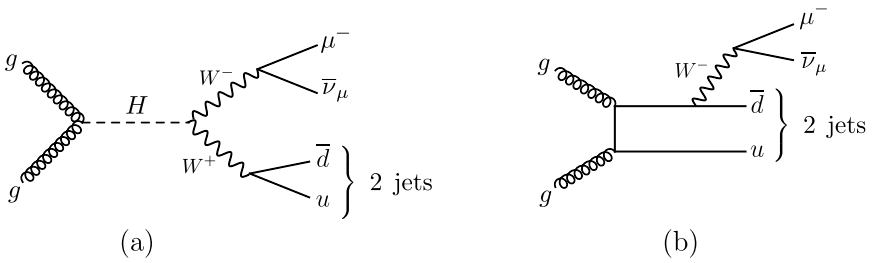

Figure 7.1. Ett exempel på (a) en signalprocess och (b) en bakgrundsprocess.

Traditionellt sett har spridningsamplituder beräknats med hjälp av Feynmandiagram, och mycket imponerande beräkningar har gjorts på detta sätt. Trots detta blir detta angreppssätt vid en viss punkt ohanterligt då antalet och komplexiteten hos de Feynmandiagram som ingår i amplituderna ökar explosionsartat. Effektiva metoder för att beräkna amplituder på träd-nivå har utvecklas under den senare tiden, dessa inkluderar bland annat BCFW-rekursionsrelationerna.

Mer effektiva metoder för att beräkna amplituder på loop-nivå utvecklades under mitten av 1990-talet genom att utnyttja unitariteten hos S-matrisen tillsammans med en ansats för 1-loopsamplituden i termer av enklare integraler än de som är involverade i Feynmandiagramberäknarna. Genom att utnyttja den analytiska strukturen hos 1-loopsintegranden blev det möjligt att bestämma koefficienterna framför dessa integraler i termer av träd-nivå amplituder. Detta tillvägagångssätt kallas för unitaritetsmetoden. Metoden har visat sig effektiv vid en loop där den lett till att ett antal amplituder framgångsrikt har kunnat beräknas, speciellt för processer med många partoner i sluttillståndet. 1-loopsunitaritet finns även i en mer modern form, kallad generaliserad unitaritet. Här används ett större antal on-shell villkor på loopintegranden vilket leder till formler för integralkoefficienterna i termer av trädamplituder utan att algebra behövs i mellanstegen.

Ämnet för den här avhandligen är utvecklandet av ett systematiskt tillvägagångssätt för att beräkna två-loopsamplituder genom generaliserad unitaritet. En sådan utvidgning av unitaritetsmetoden är nödvändig för en effektiv numerisk implementation men det är också troligt att denna typ av formalism kommer att resultera i kompakta analytiska uttryck för spridningsamplituder, resultat som uppnåtts på enkel och rättfram väg. Det bör påpekas att generaliserad unitaritet har används tidigare bortom en loop, primärt för att beräkna amplituder för $\mathcal{N} = 4$ supersymmetrisk Yang-Mills (SYM) teori och $\mathcal{N} = 8$ supergravitation. I dessa beräkningar har det första steget varit att konstruera en ansats genom att omsorgsfullt välja ut ett antal lämpliga integraler. Det har därför inte tidigare funnits något *systematiskt* sätt att använda generaliserad unitaritet bortom en loop.

Två-loopsamplituder behövs för att kunna göra kvantitativa uppskattningar av QCD-bakgrunden vid LHC. Som exempel kan nämnas processer (såsom $gg \to \gamma\gamma$ och $gg \to W^+W^-$) vars amplituder börjar vid en loop och vars differentiella tvärsnitt därför inte börjar som $\mathcal{O}(\alpha_s^0)$ utan istället $\mathcal{O}(\alpha_s^2)$. Tvärsnittet till näst-till-ledande ordning (NLO) får därför bidrag från interferensen mellan 1- och 2-loopsamplituder. (Processen $gg \to \gamma\gamma$ är effektivt sett NLO eftersom de extra faktorerna av α_s jämfört med $q\bar{q} \to \gamma\gamma$ kompenseras av den höga densiteten av gluoner för små x.) Vidare så kräver alla beräkningar vid NNLO två-loopsamplituder som input. NNLO-beräkningar utgör den teoretiska grunden för precisionsmätningar (utöver processerna $e^+e^- \to 3$ jets, $gg \to H$ och W,Z produktion vilka redan har beräknats), används för att uppskatta onoggrannheten hos NLO-beräkningar samt för att minska beroendet av renormaliseringsskalan ytterligare, exempelvis för $gg \to W + n$ jets.

Även om det inte är ämnet för den här avhandlingen är det värt att nämna att stora framsteg har gjorts under de senaste 8-9 åren för amplituder i $\mathcal{N} = 4$ SYM, med upptäckter som dualiteter med Wilson-loopar och korrelationsfunktioner för lokala operatorer; en integrabel struktur som lett till en lösning till alla loopordningar; och en rekursionsrelation för integranden till alla loopordningar à la BCFW. Minst lika spektakulär är omformuleringen av teorins S-matris som en konturintegral på en Grassmannmångfald vilket gör en formulering av partikelspridning utan en manifest rumtid möjlig. Förhoppningen är att man genom att studera spridningsamplituder kan lära sig något fundamentalt nytt om kvantfältteorier, eller till och med om själva rumtiden.

Artiklar

I artikel I tar vi första steget mot att utveckla en systematisk generalisering av generaliserad unitaritet till två loopar. Enligt detta tillvägagångssätt utvecklas två-loopsamplituden i en bas av integraler. Expansionskoefficienterna fås genom att integrera produkter av träd-amplituder längs konturer i det komplexa planet. Vi beskriver en urvalsprincip för att bestämma konturerna som garanterar ett korrekt resultat för amplituder i vilken gaugeteori som helst, QCD exempelvis.

I artiklarna III och IV beskriver vi hur dubbel-lådeintegralerna i två-loopsintegralbasen var och en är associerad med en unikt definierad kontur som ger dess koefficient. Dessutom identifierar vi en klass av basintegraler som högst troligt i hög grad förenklar unitaritetsberäkningarna vid två loopar. Slutligen beräknar vi två sådana integraler analytiskt för fyra punkter.

I artikel II kontrollerar vi en nyligen utvecklad BCFW-lik rekursionsrelation för integranden av $\mathcal{N} = 4$ SYM amplituder genom att undersöka 2-loop 6-gluon MHV-integranden.

References

[1] ATLAS Collaboration, G. Aad *et al.*, (2012), 1207.7214.
[2] CMS Collaboration, S. Chatrchyan *et al.*, Phys.Lett.B (2012), 1207.7235.
[3] N. Arkani-Hamed, K. Blum, R. T. D'Agnolo, and J. Fan, (2012), 1207.4482.
[4] R. Britto, F. Cachazo, B. Feng, and E. Witten, Phys. Rev. Lett. **94**, 181602 (2005), hep-th/0501052.
[5] N. Arkani-Hamed, J. L. Bourjaily, F. Cachazo, S. Caron-Huot, and J. Trnka, JHEP **01**, 041 (2011), 1008.2958.
[6] N. Arkani-Hamed, J. L. Bourjaily, F. Cachazo, and J. Trnka, (2010), 1012.6032.
[7] M. E. Peskin and D. V. Schroeder, (1995).
[8] Z. Bern, J. J. Carrasco, L. J. Dixon, H. Johansson, and R. Roiban, Fortsch.Phys. **59**, 561 (2011), 1103.1848.
[9] Z. Bern, L. J. Dixon, D. C. Dunbar, and D. A. Kosower, Nucl. Phys. **B425**, 217 (1994), hep-ph/9403226.
[10] Z. Bern, L. J. Dixon, D. C. Dunbar, and D. A. Kosower, Nucl. Phys. **B435**, 59 (1995), hep-ph/9409265.
[11] Z. Bern, L. J. Dixon, and D. A. Kosower, Ann. Rev. Nucl. Part. Sci. **46**, 109 (1996), hep-ph/9602280.
[12] Z. Bern, L. J. Dixon, D. C. Dunbar, and D. A. Kosower, Phys. Lett. **B394**, 105 (1997), hep-th/9611127.
[13] Z. Bern, L. J. Dixon, and D. A. Kosower, Nucl. Phys. **B513**, 3 (1998), hep-ph/9708239.
[14] L. J. Dixon, (1996), hep-ph/9601359.
[15] M. T. Grisaru and H. N. Pendleton, Nucl. Phys. B **124**, 81 (1977).
[16] V. Nair, Phys. Lett. B **214**, 215 (1988).
[17] R. Britto, F. Cachazo, and B. Feng, Nucl. Phys. **B725**, 275 (2005), hep-th/0412103.
[18] N. E. J. Bjerrum-Bohr, D. C. Dunbar, and W. B. Perkins, JHEP **04**, 038 (2008), 0709.2086.
[19] F. Cachazo and D. Skinner, (2008), 0801.4574.
[20] F. Cachazo, (2008), 0803.1988.
[21] F. Cachazo, M. Spradlin, and A. Volovich, Phys. Rev. **D78**, 105022 (2008), 0805.4832.
[22] E. Witten, Commun.Math.Phys. **252**, 189 (2004), hep-th/0312171.
[23] R. Roiban, M. Spradlin, and A. Volovich, Phys. Rev. **D70**, 026009 (2004), hep-th/0403190.
[24] C. Vergu, Phys. Rev. **D75**, 025028 (2007), hep-th/0612250.
[25] C. Anastasiou, R. Britto, B. Feng, Z. Kunszt, and P. Mastrolia, Phys. Lett. **B645**, 213 (2007), hep-ph/0609191.
[26] C. Anastasiou, R. Britto, B. Feng, Z. Kunszt, and P. Mastrolia, JHEP **03**, 111 (2007), hep-ph/0612277.

[27] W. T. Giele, Z. Kunszt, and K. Melnikov, JHEP **04**, 049 (2008), 0801.2237.
[28] S. D. Badger, JHEP **01**, 049 (2009), 0806.4600.
[29] H. Elvang, D. Z. Freedman, and M. Kiermaier, JHEP **0904**, 009 (2009), 0808.1720.
[30] D. Forde, Phys. Rev. **D75**, 125019 (2007), 0704.1835.
[31] R. Britto and E. Mirabella, JHEP **1101**, 135 (2011), 1011.2344.
[32] J. Gluza, K. Kajda, and D. A. Kosower, Phys. Rev. **D83**, 045012 (2011), 1009.0472.
[33] E. I. Buchbinder and F. Cachazo, JHEP **11**, 036 (2005), hep-th/0506126.
[34] Z. Bern, L. J. Dixon, and D. A. Kosower, JHEP **01**, 027 (2000), hep-ph/0001001.
[35] Z. Bern, J. S. Rozowsky, and B. Yan, Phys. Lett. **B401**, 273 (1997), hep-ph/9702424.
[36] Z. Bern, J. Carrasco, H. Ita, H. Johansson, and R. Roiban, Phys.Rev. **D80**, 065029 (2009), 0903.5348.
[37] L. Dixon, private communication. .
[38] Z. Bern, A. De Freitas, and L. J. Dixon, JHEP **03**, 018 (2002), hep-ph/0201161.
[39] J. Milne, *Elliptic Curves* (BookSurge Publishers, 2006).
[40] A. Hodges, (2010), 1004.3323.
[41] M. F. Paulos, M. Spradlin, and A. Volovich, (2012), 1203.6362.
[42] S. Caron-Huot.
[43] S. Laporta and E. Remiddi, Nucl. Phys. **B704**, 349 (2005), hep-ph/0406160.
[44] S. Muller-Stach, S. Weinzierl, and R. Zayadeh, (2011), 1112.4360.
[45] V. A. Smirnov, Phys. Lett. **B460**, 397 (1999), hep-ph/9905323.
[46] C. Anastasiou, J. B. Tausk, and M. E. Tejeda-Yeomans, Nucl. Phys. Proc. Suppl. **89**, 262 (2000), hep-ph/0005328.
[47] V. A. Smirnov and O. L. Veretin, Nucl. Phys. **B566**, 469 (2000), hep-ph/9907385.
[48] C. Anastasiou, E. W. N. Glover, and C. Oleari, Nucl. Phys. **B565**, 445 (2000), hep-ph/9907523.
[49] A. B. Goncharov, M. Spradlin, C. Vergu, and A. Volovich, Phys.Rev.Lett. **105**, 151605 (2010), 1006.5703.
[50] V. Del Duca, C. Duhr, and V. A. Smirnov, JHEP **1003**, 099 (2010), 0911.5332.
[51] V. Del Duca, C. Duhr, and V. A. Smirnov, JHEP **1005**, 084 (2010), 1003.1702.
[52] Z. Bern, L. J. Dixon, and V. A. Smirnov, Phys. Rev. **D72**, 085001 (2005), hep-th/0505205.
[53] D. Gaiotto, J. Maldacena, A. Sever, and P. Vieira, JHEP **1112**, 011 (2011), 1102.0062.
[54] R. M. Schabinger, JHEP **1201**, 077 (2012), 1111.4220.
[55] T. Kinoshita, J.Math.Phys. **3**, 650 (1962).
[56] T. Lee and M. Nauenberg, Phys.Rev. **133**, B1549 (1964).
[57] E. Remiddi and J. Vermaseren, Int.J.Mod.Phys. **A15**, 725 (2000), hep-ph/9905237.
[58] See the ancillary file for the arXiv version of Paper II. .
[59] S. Caron-Huot, private communication. .
[60] P. Mastrolia, Phys.Lett. **B678**, 246 (2009), 0905.2909.

[61] N. Arkani-Hamed, F. Cachazo, and J. Kaplan, JHEP **1009**, 016 (2010), 0808.1446.
[62] S. Davies, Phys.Rev. **D84**, 094016 (2011), 1108.0398.
[63] F. Berends, R. Kleiss, P. De Causmaecker, R. Gastmans, and T. T. Wu, Phys. Lett. B **103**, 124 (1981).
[64] P. De Causmaecker, R. Gastmans, W. Troost, and T. T. Wu, Nucl. Phys. B **206**, 53 (1982).
[65] Z. Xu, D.-H. Zhang, and L. Chang, TUTP-84/3-TSINGHUA (1984).
[66] R. Kleiss and W. J. Stirling, Nucl. Phys. B **262**, 235 (1985).
[67] J. F. Gunion and Z. Kunszt, Phys. Lett. B **161**, 333 (1985).
[68] Z. Xu, D.-H. Zhang, and L. Chang, Nucl. Phys. B **291**, 392 (1987).
[69] M. L. Mangano and S. J. Parke, Phys. Rept. **200**, 301 (1991).
[70] G. Ossola, C. G. Papadopoulos, and R. Pittau, Nucl. Phys. **B763**, 147 (2007), hep-ph/0609007.
[71] S. Caron-Huot and K. J. Larsen, unpublished .
[72] M. Spradlin, A. Volovich, and C. Wen, Phys. Rev. **D78**, 085025 (2008), 0808.1054.
[73] C. Vergu, (2009), 0908.2394.
[74] N. Arkani-Hamed, F. Cachazo, C. Cheung, and J. Kaplan, JHEP **03**, 020 (2010), 0907.5418.
[75] L. J. Mason and D. Skinner, JHEP **11**, 045 (2009), 0909.0250.
[76] N. Arkani-Hamed, F. Cachazo, and C. Cheung, JHEP **03**, 036 (2010), 0909.0483.
[77] M. Bullimore, L. J. Mason, and D. Skinner, JHEP **03**, 070 (2010), 0912.0539.
[78] J. Kaplan, JHEP **03**, 025 (2010), 0912.0957.
[79] N. Arkani-Hamed, J. Bourjaily, F. Cachazo, and J. Trnka, JHEP **01**, 049 (2011), 0912.4912.
[80] J. L. Bourjaily, J. Trnka, A. Volovich, and C. Wen, JHEP **01**, 038 (2011), 1006.1899.
[81] M. Bullimore, JHEP **01**, 055 (2011), 1008.3110.
[82] N. Arkani-Hamed, J. L. Bourjaily, F. Cachazo, A. Hodges, and J. Trnka, (2010), 1012.6030.
[83] Z. Bern and A. G. Morgan, Nucl. Phys. **B467**, 479 (1996), hep-ph/9511336.
[84] R. Britto, F. Cachazo, and B. Feng, Phys. Rev. **D71**, 025012 (2005), hep-th/0410179.
[85] S. J. Bidder, N. E. J. Bjerrum-Bohr, L. J. Dixon, and D. C. Dunbar, Phys. Lett. **B606**, 189 (2005), hep-th/0410296.
[86] S. J. Bidder, N. E. J. Bjerrum-Bohr, D. C. Dunbar, and W. B. Perkins, Phys. Lett. **B612**, 75 (2005), hep-th/0502028.
[87] S. J. Bidder, D. C. Dunbar, and W. B. Perkins, JHEP **08**, 055 (2005), hep-th/0505249.
[88] Z. Bern, N. E. J. Bjerrum-Bohr, D. C. Dunbar, and H. Ita, JHEP **11**, 027 (2005), hep-ph/0507019.
[89] Z. Bern, L. J. Dixon, and D. A. Kosower, Phys. Rev. **D73**, 065013 (2006), hep-ph/0507005.
[90] R. Britto, E. Buchbinder, F. Cachazo, and B. Feng, Phys. Rev. **D72**, 065012 (2005), hep-ph/0503132.

[91] R. Britto, B. Feng, and P. Mastrolia, Phys. Rev. **D73**, 105004 (2006), hep-ph/0602178.
[92] P. Mastrolia, Phys. Lett. **B644**, 272 (2007), hep-th/0611091.
[93] A. Brandhuber, S. McNamara, B. J. Spence, and G. Travaglini, JHEP **10**, 011 (2005), hep-th/0506068.
[94] Z. Bern, L. J. Dixon, and D. A. Kosower, Annals Phys. **322**, 1587 (2007), 0704.2798.
[95] R. Britto and B. Feng, Phys. Rev. **D75**, 105006 (2007), hep-ph/0612089.
[96] R. Britto and B. Feng, JHEP **02**, 095 (2008), 0711.4284.
[97] R. Britto, B. Feng, and P. Mastrolia, Phys. Rev. **D78**, 025031 (2008), 0803.1989.
[98] R. Britto, B. Feng, and G. Yang, JHEP **09**, 089 (2008), 0803.3147.
[99] C. F. Berger and D. Forde, Ann. Rev. Nucl. Part. Sci. **60**, 181 (2010), 0912.3534.
[100] Z. Bern, J. J. Carrasco, T. Dennen, Y.-t. Huang, and H. Ita, Phys. Rev. **D83**, 085022 (2011), 1010.0494.
[101] D. A. Kosower and K. J. Larsen, Phys. Rev. **D85**, 045017 (2012), 1108.1180.
[102] Z. Bern, J. J. M. Carrasco, and H. Johansson, Phys. Rev. **D78**, 085011 (2008), 0805.3993.
[103] Z. Bern, J. J. M. Carrasco, and H. Johansson, Phys. Rev. Lett. **105**, 061602 (2010), 1004.0476.
[104] J. J. M. Carrasco and H. Johansson, J. Phys. **A44**, 454004 (2011), 1103.3298.
[105] A. Brandhuber, P. Heslop, and G. Travaglini, Nucl. Phys. **B794**, 231 (2008), 0707.1153.
[106] G. Korchemsky, J. Drummond, and E. Sokatchev, Nucl.Phys. **B795**, 385 (2008), 0707.0243.
[107] J. M. Drummond, J. Henn, G. P. Korchemsky, and E. Sokatchev, Nucl. Phys. **B795**, 52 (2008), 0709.2368.
[108] J. M. Drummond, J. Henn, G. P. Korchemsky, and E. Sokatchev, Nucl. Phys. **B826**, 337 (2010), 0712.1223.
[109] J. M. Drummond, J. Henn, G. P. Korchemsky, and E. Sokatchev, Phys. Lett. **B662**, 456 (2008), 0712.4138.
[110] J. M. Drummond, J. Henn, G. P. Korchemsky, and E. Sokatchev, Nucl. Phys. **B815**, 142 (2009), 0803.1466.
[111] C. Anastasiou *et al.*, JHEP **05**, 115 (2009), 0902.2245.
[112] J. M. Henn, Fortsch. Phys. **57**, 729 (2009), 0903.0522.
[113] A. Brandhuber, P. Heslop, V. V. Khoze, and G. Travaglini, JHEP **01**, 050 (2010), 0910.4898.
[114] P. Heslop and V. V. Khoze, JHEP **06**, 037 (2010), 1003.4405.
[115] A. Brandhuber *et al.*, JHEP **07**, 080 (2010), 1004.2855.
[116] P. Heslop and V. V. Khoze, JHEP **11**, 035 (2010), 1007.1805.
[117] L. J. Mason and D. Skinner, JHEP **12**, 018 (2010), 1009.2225.
[118] S. Caron-Huot, JHEP **07**, 058 (2011), 1010.1167.
[119] M. Bullimore and D. Skinner, (2011), 1101.1329.
[120] P. Heslop and V. V. Khoze, JHEP **11**, 152 (2011), 1109.0058.
[121] N. Beisert and C. Vergu, (2012), 1203.0525.
[122] N. Beisert, S. He, B. U. W. Schwab, and C. Vergu, (2012), 1203.1443.

[123] L. F. Alday, B. Eden, G. P. Korchemsky, J. Maldacena, and E. Sokatchev, JHEP **09**, 123 (2011), 1007.3243.
[124] B. Eden, G. P. Korchemsky, and E. Sokatchev, JHEP **12**, 002 (2011), 1007.3246.
[125] B. Eden, G. P. Korchemsky, and E. Sokatchev, Phys. Lett. **B709**, 247 (2012), 1009.2488.
[126] A. V. Belitsky, G. P. Korchemsky, and E. Sokatchev, Nucl. Phys. **B855**, 333 (2012), 1103.3008.
[127] B. Eden, P. Heslop, G. P. Korchemsky, and E. Sokatchev, (2011), 1103.3714.
[128] T. Adamo, M. Bullimore, L. Mason, and D. Skinner, JHEP **08**, 076 (2011), 1103.4119.
[129] B. Eden, P. Heslop, G. P. Korchemsky, and E. Sokatchev, (2011), 1103.4353.
[130] B. Eden, P. Heslop, G. P. Korchemsky, and E. Sokatchev, (2011), 1108.3557.
[131] B. Eden, P. Heslop, G. P. Korchemsky, and E. Sokatchev, (2012), 1201.5329.
[132] J. M. Drummond, J. Henn, G. P. Korchemsky, and E. Sokatchev, Nucl. Phys. **B828**, 317 (2010), 0807.1095.
[133] N. Berkovits and J. Maldacena, JHEP **09**, 062 (2008), 0807.3196.
[134] N. Beisert, R. Ricci, A. A. Tseytlin, and M. Wolf, Phys. Rev. **D78**, 126004 (2008), 0807.3228.
[135] J. M. Drummond, J. M. Henn, and J. Plefka, JHEP **05**, 046 (2009), 0902.2987.
[136] T. Bargheer, N. Beisert, W. Galleas, F. Loebbert, and T. McLoughlin, JHEP **11**, 056 (2009), 0905.3738.
[137] A. Brandhuber, P. Heslop, and G. Travaglini, JHEP **08**, 095 (2009), 0905.4377.
[138] G. P. Korchemsky and E. Sokatchev, Nucl. Phys. **B832**, 1 (2010), 0906.1737.
[139] A. Sever and P. Vieira, (2009), 0908.2437.
[140] L. F. Alday, D. Gaiotto, and J. Maldacena, JHEP **09**, 032 (2011), 0911.4708.
[141] N. Beisert, J. Henn, T. McLoughlin, and J. Plefka, JHEP **04**, 085 (2010), 1002.1733.
[142] L. F. Alday and J. M. Maldacena, JHEP **0706**, 064 (2007), 0705.0303.
[143] L. F. Alday, J. Maldacena, A. Sever, and P. Vieira, J. Phys. **A43**, 485401 (2010), 1002.2459.
[144] J. M. Drummond and L. Ferro, JHEP **12**, 010 (2010), 1002.4622.
[145] G. P. Korchemsky and E. Sokatchev, Nucl. Phys. **B839**, 377 (2010), 1002.4625.
[146] L. F. Alday, D. Gaiotto, J. Maldacena, A. Sever, and P. Vieira, JHEP **04**, 088 (2011), 1006.2788.
[147] J. M. Henn, J. Phys. **A44**, 454011 (2011), 1103.1016.
[148] M. Bullimore and D. Skinner, (2011), 1112.1056.
[149] S. Caron-Huot and S. He, (2011), 1112.1060.
[150] C. Anastasiou, Z. Bern, L. J. Dixon, and D. A. Kosower, Phys. Rev. Lett. **91**, 251602 (2003), hep-th/0309040.
[151] Z. Bern, M. Czakon, D. A. Kosower, R. Roiban, and V. A. Smirnov, Phys. Rev. Lett. **97**, 181601 (2006), hep-th/0604074.
[152] Z. Bern, M. Czakon, L. J. Dixon, D. A. Kosower, and V. A. Smirnov, Phys. Rev. **D75**, 085010 (2007), hep-th/0610248.
[153] Z. Bern *et al.*, Phys. Rev. Lett. **98**, 161303 (2007), hep-th/0702112.

[154] Z. Bern, J. J. M. Carrasco, H. Johansson, and D. A. Kosower, Phys. Rev. **D76**, 125020 (2007), 0705.1864.
[155] Z. Bern, J. J. Carrasco, D. Forde, H. Ita, and H. Johansson, Phys. Rev. **D77**, 025010 (2008), 0707.1035.
[156] Z. Bern *et al.*, Phys. Rev. **D78**, 045007 (2008), 0803.1465.
[157] Z. Bern, J. J. M. Carrasco, L. J. Dixon, H. Johansson, and R. Roiban, Phys. Rev. **D78**, 105019 (2008), 0808.4112.
[158] Z. Bern, J. J. Carrasco, L. J. Dixon, H. Johansson, and R. Roiban, Phys. Rev. Lett. **103**, 081301 (2009), 0905.2326.
[159] Z. Bern, J. J. M. Carrasco, L. J. Dixon, H. Johansson, and R. Roiban, Phys. Rev. **D82**, 125040 (2010), 1008.3327.
[160] D. A. Kosower, R. Roiban, and C. Vergu, Phys. Rev. **D83**, 065018 (2011), 1009.1376.
[161] J. J. Carrasco and H. Johansson, Phys. Rev. **D85**, 025006 (2012), 1106.4711.
[162] Z. Bern, C. Boucher-Veronneau, and H. Johansson, Phys. Rev. **D84**, 105035 (2011), 1107.1935.
[163] Z. Bern, J. J. M. Carrasco, L. J. Dixon, H. Johansson, and R. Roiban, (2012), 1201.5366.
[164] Z. Bern, A. De Freitas, and L. J. Dixon, JHEP **09**, 037 (2001), hep-ph/0109078.
[165] Z. Bern, A. De Freitas, L. J. Dixon, and H. L. Wong, Phys. Rev. **D66**, 085002 (2002), hep-ph/0202271.
[166] Z. Bern, A. De Freitas, and L. J. Dixon, JHEP **06**, 028 (2003), hep-ph/0304168.
[167] Z. Bern, L. J. Dixon, and D. A. Kosower, JHEP **08**, 012 (2004), hep-ph/0404293.
[168] A. De Freitas and Z. Bern, JHEP **09**, 039 (2004), hep-ph/0409007.
[169] F. Tkachov, Physics Letters B **100**, 65 (1981).
[170] K. Chetyrkin and F. Tkachov, Nuclear Physics B **192**, 159 (1981).
[171] S. Laporta, Phys. Lett. **B504**, 188 (2001), hep-ph/0102032.
[172] S. Laporta, Int. J. Mod. Phys. **A15**, 5087 (2000), hep-ph/0102033.
[173] T. Gehrmann and E. Remiddi, Nucl. Phys. **B580**, 485 (2000), hep-ph/9912329.
[174] R. N. Lee, JHEP **07**, 031 (2008), 0804.3008.
[175] C. Anastasiou and A. Lazopoulos, JHEP **07**, 046 (2004), hep-ph/0404258.
[176] A. V. Smirnov, JHEP **10**, 107 (2008), 0807.3243.
[177] C. Studerus, Comput. Phys. Commun. **181**, 1293 (2010), 0912.2546.
[178] A. V. Smirnov and A. V. Petukhov, Lett. Math. Phys. **97**, 37 (2011), 1004.4199.
[179] L. M. Brown and R. P. Feynman, Phys. Rev. **85**, 231 (1952).
[180] L. M. Brown, Nuovo Cim. **21**, 3878 (1961).
[181] B. Petersson, J. Math. Phys. **6**, 1955 (1965).
[182] G. Källén and J. Toll, J. Math. Phys. **6**, 299 (1965).
[183] D. B. Melrose, Nuovo Cim. **40**, 181 (1965).
[184] G. Passarino and M. J. G. Veltman, Nucl. Phys. B **160**, 151 (1979).
[185] W. van Neerven and J. Vermaseren, Phys. Lett. B **137**, 241 (1984).
[186] G. J. van Oldenborgh and J. Vermaseren, Z. Phys. C **46**, 425 (1990).

[187] H. Elvang, D. Z. Freedman, and M. Kiermaier, JHEP **10**, 103 (2010), 0911.3169.
[188] D. Kosower, private communication. .
[189] R. Britto, F. Cachazo, and B. Feng, Nucl. Phys. **B715**, 499 (2005), hep-th/0412308.
[190] M. Caffo, H. Czyz, S. Laporta, and E. Remiddi, Nuovo Cim. **A111**, 365 (1998), hep-th/9805118.
[191] F. Brown and O. Schnetz, (2010), 1006.4064.
[192] A. Hodges, (2009), 0905.1473.
[193] L. J. Dixon, J. M. Drummond, and J. M. Henn, JHEP **1111**, 023 (2011), 1108.4461.
[194] L. J. Dixon, J. M. Drummond, and J. M. Henn, JHEP **1201**, 024 (2012), 1111.1704.
[195] C. Duhr, H. Gangl, and J. R. Rhodes, (2011), 1110.0458.
[196] A. Gehrmann-De Ridder, T. Gehrmann, E. Glover, and G. Heinrich, JHEP **0711**, 058 (2007), 0710.0346.
[197] S. Weinzierl, Phys.Rev.Lett. **101**, 162001 (2008), 0807.3241.
[198] G. Dissertori *et al.*, JHEP **0908**, 036 (2009), 0906.3436.
[199] G. Dissertori *et al.*, Phys.Rev.Lett. **104**, 072002 (2010), 0910.4283.
[200] S. Badger, H. Frellesvig, and Y. Zhang, JHEP **1204**, 055 (2012), 1202.2019.
[201] P. Mastrolia and G. Ossola, JHEP **1111**, 014 (2011), 1107.6041.
[202] T. Gehrmann, M. Jaquier, E. Glover, and A. Koukoutsakis, JHEP **1202**, 056 (2012), 1112.3554.

Acta Universitatis Upsaliensis

Digital Comprehensive Summaries of Uppsala Dissertations from the Faculty of Science and Technology 952

Editor: The Dean of the Faculty of Science and Technology

A doctoral dissertation from the Faculty of Science and Technology, Uppsala University, is usually a summary of a number of papers. A few copies of the complete dissertation are kept at major Swedish research libraries, while the summary alone is distributed internationally through the series Digital Comprehensive Summaries of Uppsala Dissertations from the Faculty of Science and Technology.

Distribution: publications.uu.se
urn:nbn:se:uu:diva-179203

ACTA
UNIVERSITATIS
UPSALIENSIS
UPPSALA
2012